

THE UNIVERSITY OF HULL

BIOMECHANICAL FUNCTION OF THE PERIODONTAL LIGAMENT
IN BITING AND ORTHODONTIC TOOTH MOVEMENT

being a Thesis submitted for the Degree of Doctor of Philosophy

in the University of Hull

by

Steven William McCormack, MEng (Hons)

March 2016

Abstract

Alveolar bone remodelling is vital for the success of dental implants and orthodontic treatments. However, the underlying biomechanical mechanisms, in particular the function of the periodontal ligament (PDL) in bone remodelling, are not well understood. The PDL is a soft fibrous connective tissue that joins the tooth root to the alveolar bone and plays a critical role in the transmission of loads from the teeth to the surrounding bone. However, due to its complex structure, small size and location within the tooth socket it is difficult to study *in vivo*. Finite element analysis (FEA) is an ideal tool with which to investigate the role of the PDL, but inclusion of the PDL in FE models is complex and time consuming and most FE models that include teeth do not consider the PDL. The aim of this study was to investigate the effects of including the PDL and its fibrous structure in mandibular finite element models.

This research involved the development of a novel method to include the fibres of the PDL in FE models. A simplified single tooth model was developed to assess the effects of modelling fibrous PDL compared to the traditional approach of representing the PDL as a simple layer of solid material and to an absent PDL. The same study design was then applied to a high-resolution model of the human molar region, which is the first time that the fibrous structure of the PDL has been included in a model with realistic tooth and bone geometry. Finally, molar region models of five additional species (cat, cercocebus, pig, rabbit and sheep) were tested with and without a PDL.

The results from the research showed that omission of the PDL creates a more rigid model, reducing the strains observed in the mandibular corpus for all six species studied. This suggests that the results obtained are not specific to the human molar region, but may be true for the mammalian mandible in general. Compared to a solid PDL, the fibrous PDL altered the strains in the models, in particular increasing the strains observed in the tooth socket. This may be important for the management of orthodontic treatment, as strains in this region are thought to play an important role in bone remodelling during orthodontic tooth movement.

Acknowledgements

The completion of this project would not have been possible without the help of many people to whom I am deeply grateful. In particular, I would like to thank the following people.

My supervisors Prof. Michael Fagan and Dr. Flora Gröning for their continuous help, support and guidance throughout this project.

Dr. Peter Watson for providing much assistance during the project and Prof. Ulrich Witzel whose work laid the foundations for this project and who has provided additional advice throughout.

Dr. Neil Curtis and Dr. Catherine Dobson who provided additional support at various stages of the project, and Sue Taft for providing technical support and especially for scanning the mandibles used in this project.

The staff in the School of Engineering and the Graduate School at the University of Hull for their assistance.

My friends and colleagues in the Centre for Medical Engineering and Technology at the University of Hull.

The Biotechnology and Biological Sciences Research Council (BBSRC) (BB/I008462/1) and Marie Curie Actions Integration Grant (FP7-PEOPLE PERG7-GA-2010-268430) who provided funding for this research, and the University of Hull who provided additional funding for conferences and publications related to the work.

Finally, I would like to thank my family for their constant support and encouragement throughout everything I have done.

List of Contents

Abstract	
Acknowledgements	
List of Contents	i
List of Tables	vi
List of Figures	vii
List of Appendices	xv
Chapter 1: Introduction	1
1.1 Project Background	1
1.2 Project Aim	5
1.3 Project Methodology	5
1.4 Summary of Thesis Chapters	6
Chapter 2: Literature Review	8
2.1 Introduction	8
2.2 Bone	8
2.2.1 Introduction to Bone	8
2.2.2 Wolff's Law and the Mechanostat Theory	9
2.2.3 Bone Functional Adaptation	10
2.2.4 Finite Element Modelling of Bone Adaptation	13
2.3 Mandible	14
2.3.1 Introduction to the Mandible	14
2.3.2 Biomechanics of the Mandible	14
2.3.3 Functional Morphology of the Mandible	17
2.3.4 Material Properties of Mandibular Bone	18

2.4 Periodontal Ligament	21
2.4.1 Structure and Function of the Periodontal Ligament	21
2.4.2 Material Properties of the Periodontal Ligament	25
2.4.3 Finite Element Modelling with the Periodontal Ligament	29
2.5 Orthodontic Tooth Movement	35
Chapter 3: Finite Element Modelling of a Single Tooth with Fibrous Periodontal Ligament	39
3.1 Introduction	39
3.2 Materials and Methods	41
3.2.1 Model Creation	41
Material Properties	43
Loading and Boundary Conditions	44
3.2.2 Model Testing	46
No PDL Model	46
Boundary Conditions	46
Convergence	49
Validation	49
Sensitivity Study	49
3.2.3 Solid PDL versus Fibrous PDL	49
3.3 Results	51
3.3.1 Model Testing	51
No PDL Model	51
Boundary Conditions	52
Convergence	52
Validation	52
Sensitivity Study	53

3.3.2 Solid PDL versus Fibrous PDL	56
Occlusal Load	58
Orthodontic Load	58
3.4 Discussion	62
3.4.1 Model Testing	62
3.4.2 Solid PDL versus Fibrous PDL	63
Occlusal Load	63
Orthodontic Load	64
Chapter 4: Human Molar Region Finite Element Models	69
4.1 Introduction	69
4.2 Materials and Methods	72
4.2.1 Mesh Generation	72
Micro-computed Tomography Scanning	72
Thresholding and Manual Segmentation	72
Mesh Generation	75
4.2.2 Model Development	75
Initial Model Testing	76
Boundary Conditions	76
Initial Material Properties for the Convergence Study	77
Convergence Test	78
PDL Fibres	80
Optimisation	82
Final Models	84
4.2.3 Model Loading	85
Occlusal Load	86
Orthodontic Load	86

4.3 Results	88
4.3.1 Model Development – Convergence Test	88
4.3.2 Occlusal Load	88
Trabecular Tissue Modelling	88
PDL Modelling	93
4.3.3 Orthodontic Load	99
Distomesial Orthodontic Load	99
Buccolingual Orthodontic Load	102
4.4 Discussion	107
4.4.1 Model Development	107
4.4.2 Occlusal Load	107
4.4.3 Orthodontic Load	108
Chapter 5: Other Species Molar Region Finite Element Models	110
5.1 Introduction	110
5.2 Materials and Methods	111
5.2.1 Mesh Generation	112
Micro-computed Tomography Scanning	112
Thresholding and Manual Segmentation	112
Mesh Generation	114
5.2.2 Model Development	116
Initial Model Testing	116
Boundary Conditions	116
Material Properties	119
5.2.3 No PDL versus Solid PDL	119

5.3 Results	120
5.3.1 No PDL versus Solid PDL	120
5.4 Discussion	127
Chapter 6: Discussion	129
6.1 Introduction	129
6.2 Occlusal Loading	129
6.3 Orthodontic Loading	132
6.4 Should PDL Fibres be Included in Finite Element Models?	136
6.5 Strengths and Weaknesses of this Study	137
Chapter 7: Conclusions and Future Work	138
7.1 Conclusions	138
7.2 Future Work	139
Appendix I: List of Publications	142
References	143

List of Tables

Table 2.1 Material property values assigned to the periodontal ligament in finite element models from a selection of articles (Rees, 2001: P. 430: Table 5).

(Page 30)

Table 3.1 Mechanical properties assigned to each material in the fibrous PDL model.

(Page 44)

Table 3.2 Vertical tooth displacement results for original models and u-shaped mandible models.

(Page 52)

Table 3.3 Results from sensitivity analysis with fibrous PDL model (numbers in bold represent the original model with the material properties shown in Table 3.1).

(Page 56)

Table 4.1 Mechanical properties assigned to each material in the original Fibrous PDL Trabecular Structure model.

(Page 82)

Table 4.2 Mechanical properties assigned to each material in all six different models.

(Page 85)

Table 5.1 Final number of elements in each species model along with the number of insufficiently constrained elements which were removed.

(Page 117)

List of Figures

Figure 1.1 An illustration of the typical steps involved in creating and analysing a finite element model of a biological structure from a microCT scan (Gröning, 2013).

(Page 2)

Figure 1.2 Schematic representation of the tooth and supporting structures (Zhurov et al., 2007: P. 224: Fig. 1).

(Page 3)

Figure 2.1 Schematic representation of the feedback loop for bone functional adaptation (Ruff et al., 2006: P. 485: Fig. 1).

(Page 10)

Figure 2.2 Schematic representation of the regulatory process for bone remodelling (Huiskes, 2000: P. 149: Fig. 5).

(Page 11)

Figure 2.3 Graphic representation of fluid flow through the canalicular spaces caused by bending forces. Fluid is driven from regions of compression to regions of tension flowing across osteocytes. This provides nutrients for the osteocytes whilst also causing shear stresses on the cell membranes and creating a streaming potential (Turner & Pavalko, 1998: P. 347: Fig. 1).

(Page 12)

Figure 2.4 Approximate principal axes of stress shown as field lines in a loaded femoral head (left) and the trabecular structure in a femur (right) demonstrating the close alignment of trabecular structures with stress field lines (Chen & Ingber, 1999: P. 85: Fig. 3).

(Page 14)

Figure 2.5 Loading of the mandible during a unilateral molar bite. F_b is the bite force, F_{m_b} and F_{m_w} and F_{j_b} and F_{j_w} are the muscular and joint forces at the balancing and working sides. The distortion of the corpus can be described as a combination of sagittal bending, torsion and lateral transverse bending (Van Eijden, 2000: P. 130: Fig. 9).

(Page 16)

Figure 2.6 Alternative models of mandibular corpus as either open (left) or closed (right) cross-sections (Daegling *et al.*, 2008: P. 135: Fig. 7.3).

(Page 16)

Figure 2.7 Schematic representation of the fibrous structure of the PDL showing the generic location and orientation of the fibres: (a) transverse plane; (b) sagittal plane (Schroeder, 2000: P. 219: Fig. 2.14).

(Page 22)

Figure 2.8 Transmission electron micrograph showing a transversely sectioned collagen fibre bundle in the PDL (Berkovitz, 1990: P. 54: Fig. 4).

(Page 23)

Figure 2.9 Scanning electron micrograph of a transverse section of a PDL showing the wavy appearance of collagen fibres (Berkovitz, 1990: P. 54: Fig. 3).
(Page 24)

Figure 2.10 Stress-strain plot for the PDL from an experiment by Toms *et al.* (2002a: P. 176: Fig. 3) showing how the nonlinear behaviour may be simplified as bilinear.
(Page 27)

Figure 2.11 Schematic representation of bending of the alveolar bone caused by an orthodontic load (Meikle, 2006: P. 228: Fig. 7).
(Page 36)

Figure 2.12 Schematic representation of the stretched fibre hypothesis (Melsen, 2001): (a) an orthodontic load is applied; (b) PDL fibres are stretched on one side and compressed on the other; (c) bone formation occurs on the side where the fibres are stretched and resorption occurs on the side where they are compressed (Henneman *et al.*, 2008: P. 301: Fig. 2).
(Page 38)

Figure 3.1 Simplified two dimensional representation of a tooth-PDL-bone complex illustrating three hypotheses for strain-based bone remodelling during orthodontic tooth movement: (a) “pressure-tension hypothesis” showing tooth displacement leading to compression and tension in the surrounding bone; (b) “alveolar bending hypothesis” showing tooth movement causing bending of the alveolar bone; (c) “stretched fibre hypothesis” showing stretching and compression of PDL fibres leading to low and high strain areas in the surrounding bone. The red arrows indicate the direction of the applied orthodontic force.
(Page 40)

Figure 3.2 Single tooth FE model including dimensions in millimetres: (a) the whole three-dimensional single tooth model; (b) section through tooth, PDL and alveolar bone showing the location of the link elements which span the PDL layer connecting the tooth and alveolar bone; (c) section through the centre of the model showing the tooth, PDL and alveolar bone including an expanded view of the apex region.
(Page 42)

Figure 3.3 Tooth model showing loading and boundary conditions applied, where triangles represent constraints and red arrows represent applied forces: (a) vertical occlusal load; (b) buccolingual orthodontic load; (c) mesiodistal orthodontic load; (d) section through centre of tooth model showing a typical plane from which strain results were taken.
(Page 45)

Figure 3.4 Original single tooth model and U-shaped tooth model: (a) original single tooth model showing load and boundary conditions; (b) finite element mesh for U-shaped model showing the location of the original model within the U-shaped model along with the vertical occlusal load and boundary conditions applied; (c) area plot showing areas meshed with shell elements.
(Page 47)

Figure 3.5 Superior view of a replica human mandible used to approximate the dimensions for the U-shaped models.
(Page 48)

Figure 3.6 Contour plots showing the minimum principal microstrain in the trabecular bone region of the no PDL and solid PDL models due to the 500 N occlusal load.
(Page 51)

Figure 3.7 Solid PDL model: the minimum principal microstrain distribution in the trabecular bone region of the original single tooth model and the corresponding region of the U-shaped model for the solid PDL models due to the 500 N occlusal load. Directions are shown only on the original model plots but can be inferred for the U-shaped model plots. Directions are represented by M for mesial, D for distal, B for buccal and L for lingual.
(Page 54)

Figure 3.8 Fibrous PDL model: the minimum principal microstrain distribution in the trabecular bone region of the original single tooth model and the corresponding region of the U-shaped model for the fibrous PDL models due to the 500 N occlusal load. Directions are shown only on the original model plots but can be inferred for the U-shaped model plots. Directions are represented by M for mesial, D for distal, B for buccal and L for lingual.
(Page 55)

Figure 3.9 Contour plots showing nodal solutions for the principal microstrains on the outside surface of the alveolar bone for the solid PDL and fibrous PDL models due to the 500 N occlusal load: (a) maximum principal microstrain; (b) minimum principal microstrain. Directions are represented by M for mesial and D for distal.
(Page 57)

Figure 3.10 Maximum and minimum principal strains on the buccal and lingual sides of the tooth model from the 500 N occlusal load, along three regions within the model. The graphs relate strain to the vertical distance away from the top of the tooth socket.
(Page 59)

Figure 3.11 Maximum and minimum principal strains on the mesial and distal sides of the tooth model from the 1 N orthodontic load in the mesiodistal direction, along three regions within the model. The graphs relate strain to the vertical distance away from the top of the tooth socket.
(Page 60)

Figure 3.12 Maximum and minimum principal strains on the buccal and lingual sides of the tooth model from the 1 N orthodontic load in the buccolingual direction, along three regions within the model. The graphs relate strain to the vertical distance away from the top of the tooth socket.
(Page 61)

Figure 4.1 Schematic representation of a cross section through mandibular bone. Trabecular bone refers to the material forming the individual trabeculae. Trabecular filling refers to the material in the pores surrounding the trabeculae. Trabecular tissue refers to the combination of trabecular bone and trabecular filling. Cortical bone refers to the dense bone around the outer surface of the mandible.

(Page 70)

Figure 4.2 Surface model showing three teeth and surrounding PDL, including the two materials forming the PDL around the middle tooth, viewed from the lingual side. From left to right: second premolar, first molar and second molar.

(Page 73)

Figure 4.3 Surface models showing the buccal side and the cut mesial surface of the mandibular bone: (a) cortical bone and trabecular bone without trabecular filling; (b) cortical bone and trabecular bone with trabecular filling.

(Page 74)

Figure 4.4 Surface model showing the final human molar region model including teeth, bone and PDL (in pink), viewed from the buccal side.

(Page 75)

Figure 4.5 Finite element model, viewed from the buccal side, showing loading and boundary conditions applied for the occlusal load case, where light blue triangles represent constraints and red arrows represent applied forces.

(Page 77)

Figure 4.6 Nodes on the outer surface of the cortical bone selected for the convergence test and for choosing the Young's modulus value for the trabecular filling: (a) finite element model, viewed from the buccal side showing the approximate location of the plane from which nodes were selected; (b) nodes from the plane shown in (a), viewed from the mesial side, around the outer surface of the tooth and cortical bone indicating the location of the five nodes selected. The red arrows indicate the viewing direction in (b) compared to that in (a).

(Page 78)

Figure 4.7 Finite element models used for the convergence test, viewed from the buccal side, showing loading and boundary conditions applied, where light blue triangles represent constraints and red arrows represent applied forces: (a) 1.2 million element model; (b) 4.2 million element model.

(Page 79)

Figure 4.8 Details of how the link elements representing the PDL fibres were added: (a) buccal side view of one of the two materials making up the PDL around the middle tooth; (b) one ring of elements selected as indicated by the red arrow; (c) buccal side view of nodes selected from the outer surface on the top of the ring, *i.e.* adjacent to the alveolar bone, and the inner surface on the bottom of the ring, *i.e.* adjacent to the tooth, for creating oblique PDL fibres; (d) superior view of nodes showing nodes through which link elements were created.

(Page 80)

Figure 4.9 Buccal side view of 2,112 link elements, added to the fibrous PDL models, connecting the alveolar bone to the tooth root through the PDL.
(Page 81)

Figure 4.10 Schematic diagram summarising the steps involved in the optimisation process to match the tooth displacements, as described in the text.
(Page 83)

Figure 4.11 Finite element models showing loading and boundary conditions applied for the two orthodontic load cases, where light blue triangles represent constraints and red arrows represent applied forces: (a) two views of the distomesial orthodontic load; (b) two views of the buccolingual orthodontic load. Directions are represented by D for distal, M for mesial, B for buccal and L for lingual.
(Page 87)

Figure 4.12 Strain graphs showing maximum principal strain, minimum principal strain and Von Mises strain results from the convergence test models.
(Page 89)

Figure 4.13 Maximum principal strain difference plots for the strain differences, in microstrain, between the trabecular structure and bulk material models with each of the three PDL types.
(Page 90)

Figure 4.14 Minimum principal strain difference plots for the strain differences, in microstrain, from trabecular structure and bulk material models with each of the three PDL types.
(Page 91)

Figure 4.15 Vertical strain profiles for maximum and minimum principal strains on the buccal and lingual surfaces of the cortical bone from the 500 N occlusal load. Graphs compare results from trabecular structure and bulk material models for each of the three PDL representations. The red arrows indicate the direction of the applied load.
(Page 92)

Figure 4.16 Maximum principal strain difference plots for the strain differences, in microstrain, between models with bulk material trabecular tissue but different PDLs as indicated.
(Page 94)

Figure 4.17 Minimum principal strain difference plots for the strain differences, in microstrain, between models with bulk material trabecular tissue but different PDLs as indicated.
(Page 95)

Figure 4.18 Maximum principal strain difference plots for the strain differences, in microstrain, between models with trabecular structure trabecular tissue but different PDLs as indicated.
(Page 96)

Figure 4.19 Minimum principal strain difference plots for the strain differences, in microstrain, between models with trabecular structure trabecular tissue but different PDLs as indicated.

(Page 97)

Figure 4.20 Vertical strain profiles for maximum and minimum principal strains on the buccal and lingual surfaces of the cortical bone from the 500 N occlusal load. Graphs compare results from no PDL, solid PDL and fibrous PDL models for both trabecular tissue types. The red arrows indicate the direction of the applied load.

(Page 98)

Figure 4.21 Vertical strain profiles for maximum and minimum principal strains on the distal and mesial surfaces of the alveolar bone around the distal (D) tooth root from the 1 N distomesial orthodontic load. Graphs compare results from trabecular structure and bulk material models for each of the three PDL types. The red arrows indicate the direction of the applied load. The Image at the top indicates the viewing direction for the results where D is distal side and M is the mesial side of the model. [Note the different scales of the x-axes].

(Page 100)

Figure 4.22 Vertical strain profiles for maximum and minimum principal strains on the distal and mesial surfaces of the alveolar bone around the mesial (M) tooth root from the 1 N distomesial orthodontic load. Graphs compare results from trabecular structure and bulk material models for each of the three PDL types. The red arrows indicate the direction of the applied load. [Note the different scales of the x-axes].

(Page 101)

Figure 4.23 Vertical strain profiles for maximum and minimum principal strains on the distal and mesial surfaces of the alveolar bone around both the distal (D) and mesial (M) tooth roots from the 1 N distomesial orthodontic load. Graphs compare results from no PDL, solid PDL and fibrous PDL models each with trabecular structure trabecular tissue. The red arrows indicate the direction of the applied load.

(Page 102)

Figure 4.24 Vertical strain profiles for maximum and minimum principal strains on the buccal and lingual surfaces of the alveolar bone around the distal tooth root from the 1 N buccolingual orthodontic load. Graphs compare results from trabecular structure and bulk material models for each of the three PDL types. The red arrows indicate the direction of the applied load. The Image at the top indicates the viewing direction for the results where B is buccal side and L is the lingual side of the model. [Note the different scales of the x-axes].

(Page 104)

Figure 4.25 Vertical strain profiles for maximum and minimum principal strains on the buccal and lingual surfaces of the alveolar bone around the mesial tooth root from the 1 N buccolingual orthodontic load. Graphs compare results from trabecular structure and bulk material models for each of the three PDL types. The red arrows indicate the direction of the applied load. [Note the different scales of the x-axes].

(Page 105)

Figure 4.26 Vertical strain profiles for maximum and minimum principal strains on the buccal and lingual surfaces of the alveolar bone around both the distal and mesial tooth roots from the 1 N buccolingual orthodontic load. Graphs compare results from no PDL, solid PDL and fibrous PDL models each with trabecular structure trabecular tissue. The red arrows indicate the direction of the applied load.

(Page 106)

Figure 5.1 Surface models showing the five final models, all including teeth, bone, and PDL (in pink), viewed from the buccal side: (a) cat; (b) cercocebus; (c) pig; (d) rabbit; (e) sheep.

(Page 115)

Figure 5.2 Finite element models, viewed from the buccal side, for each of the five mammals, showing loading and boundary conditions applied, where light blue triangles represent constraints and red arrows represent applied forces: (a) cat; (b) cercocebus; (c) pig; (d) rabbit; (e) sheep.

(Page 118)

Figure 5.3 Maximum and minimum principal strain difference plots for the strain differences, in microstrain, between no PDL and solid PDL cat models.

(Page 121)

Figure 5.4 Vertical strain profiles for maximum and minimum principal strains on the buccal and lingual surfaces of the cortical bone around the middle tooth for the cat models. Graphs compare results from the no PDL and solid PDL models. The red arrow indicates the direction of the applied load.

(Page 121)

Figure 5.5 Maximum and minimum principal strain difference plots for the strain differences, in microstrain, between no PDL and solid PDL cercocebus models.

(Page 122)

Figure 5.6 Vertical strain profiles for maximum and minimum principal strains on the buccal and lingual surfaces of the cortical bone around the middle tooth for the cercocebus models. Graphs compare results from the no PDL and solid PDL models. The red arrow indicates the direction of the applied load.

(Page 122)

Figure 5.7 Maximum and minimum principal strain difference plots for the strain differences, in microstrain, between no PDL and solid PDL pig models.

(Page 123)

Figure 5.8 Vertical strain profiles for maximum and minimum principal strains on the buccal and lingual surfaces of the cortical bone around the middle tooth for the pig models. Graphs compare results from the no PDL and solid PDL models. The red arrow indicates the direction of the applied load.

(Page 123)

Figure 5.9 Maximum and minimum principal strain difference plots for the strain differences, in microstrain, between no PDL and solid PDL rabbit models.

(Page 125)

Figure 5.10 Vertical strain profiles for maximum and minimum principal strains on the buccal and lingual surfaces of the cortical bone around the middle tooth for the rabbit models. Graphs compare results from the no PDL and solid PDL models. The red arrow indicates the direction of the applied load.

(Page 125)

Figure 5.11 Maximum and minimum principal strain difference plots for the strain differences, in microstrain, between no PDL and solid PDL sheep models.

(Page 126)

Figure 5.12 Vertical strain profiles for maximum and minimum principal strains on the buccal and lingual surfaces of the cortical bone around the middle tooth for the sheep models. Graphs compare results from the no PDL and solid PDL models. The red arrow indicates the direction of the applied load.

(Page 126)

List of Appendices

Appendix I: List of Publications
(Page 142)

Chapter 1

Introduction

1.1 Project Background

Unwanted alveolar bone resorption causes problems during orthodontic treatment, affects the stability of dental implants, and leads to tooth loss in the elderly (Hollins, 2008; Clerehugh *et al.*, 2009). Many experimental studies have shown that bone mass and structure is adapted to its mechanical environment and that strain magnitudes (among other factors such as strain frequency) play a key role in this adaptation, *i.e.* bone formation has been linked to an increase in strain magnitudes, *e.g.* resulting from a new exercise regime, whereas bone resorption is often associated with a decrease in strain magnitudes as in the case of prolonged bed rest (*e.g.* Hert *et al.* 1969; Liskova & Hert, 1971; Lanyon *et al.*, 1982; Lanyon & Rubin, 1984; Burr *et al.*, 2002; Robling *et al.*, 2002; Warden *et al.*, 2005). Therefore, in order to improve the outcome of dental treatments, it is important to understand the stresses and strains occurring in the alveolar bone around the teeth.

Internal stresses and strains cannot currently be directly measured *in vivo* in humans, and so must be determined by other means (Daegling & Hylander, 2000; Van Driel *et al.*, 2000). One of the most widely used methods for theoretical analysis of biological structures is finite element analysis. It involves dividing a structure into a number of smaller pieces (elements) which combine to form a mesh which approximates the geometry of the real structure. Each of these elements can easily be analysed using simple equations for stress and strain and the results are combined together to give the solution throughout the mesh. In theory, as the number of elements increases the mesh more closely matches the real structure and the solution becomes more accurate (Mac Donald, 2007). Finite element analysis is a “full-field technique”, capable of showing stresses and strains throughout the whole structure, and thus is a useful tool for studying the relationship between the forces applied to a bone and its morphology in a non-destructive way.

Producing accurate, biologically representative, finite element models can be very challenging. The validity of such models is highly dependent on faithfully representing the geometry and material properties of the structure, as well as applying the correct loading and boundary conditions (Marinescu *et al.*, 2005). Biomechanical finite element models are often produced from micro-computed tomography (microCT) data and, although image processing can introduce some errors, this leads to models which are good geometric representations of the biological structures (Hohmann *et al.*, 2011). However, determining realistic material properties, loading and boundary conditions remains a major challenge for biomechanical modelling. The general process by which these models are usually created and analysed is shown in Figure 1.1.

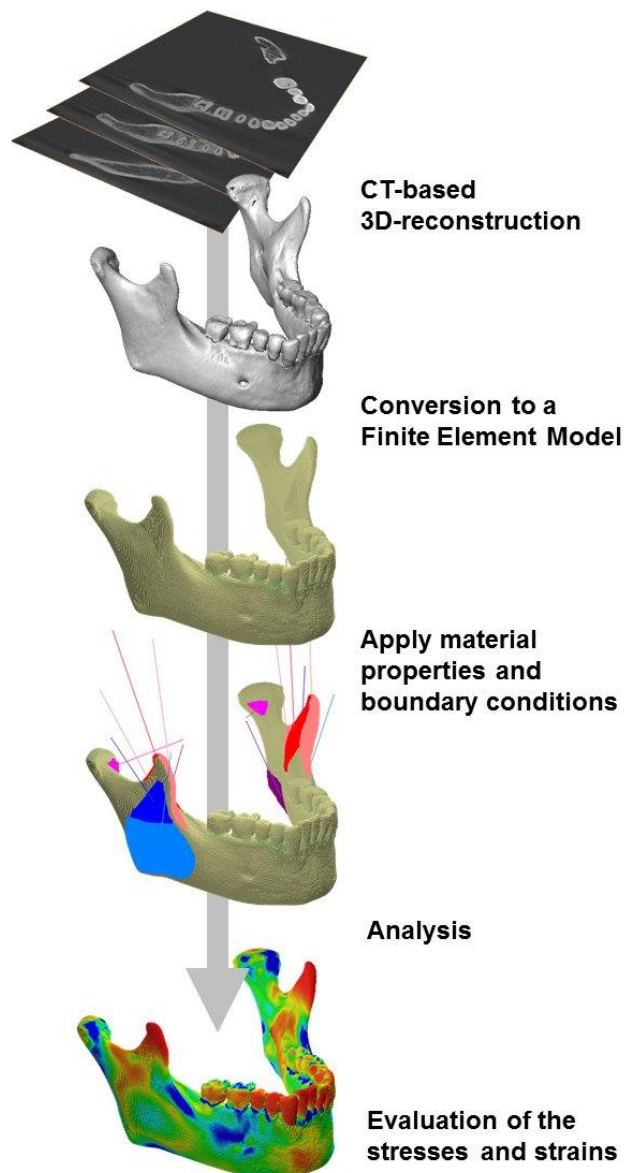


Figure 1.1 An illustration of the typical steps involved in creating and analysing a finite element model of a biological structure from a microCT scan (Gröning, 2013).

In any finite element model of the mandible, or a section of the mandible, there are a number of different materials which need to be modelled. A schematic representation of the tooth anatomy and supporting structures is shown in Figure 1.2. Depending on the size and level of complexity of the model, materials which are commonly represented in finite element models include enamel, dentine, periodontal ligament (PDL), cortical bone and trabecular bone.

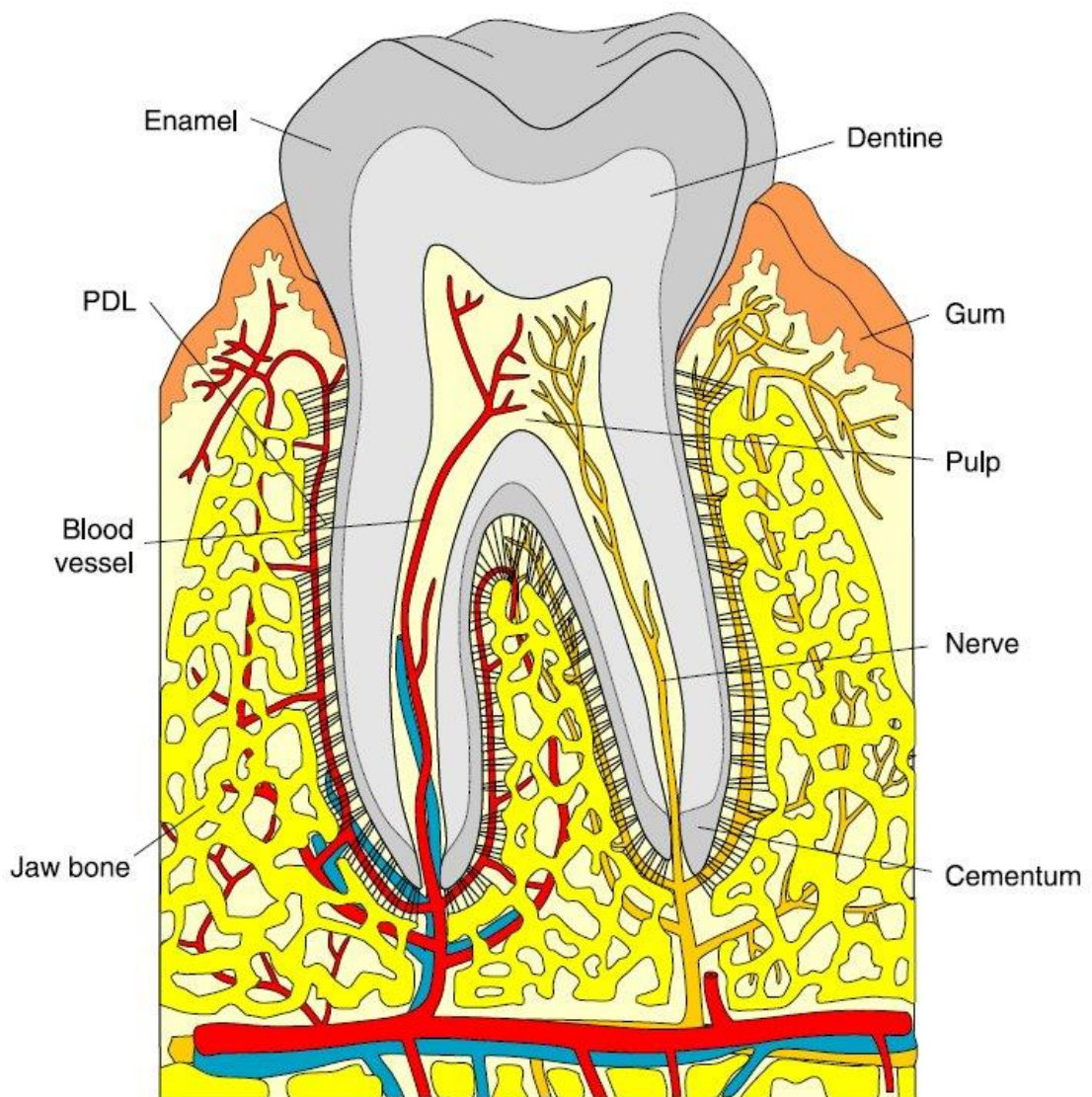


Figure 1.2 Schematic representation of the tooth and supporting structures (Zhurov et al., 2007: P. 224: Fig. 1).

Although there are many components involved, the PDL causes arguably the most difficulty in dental finite element models (Daegling & Hylander, 2000). The PDL is a soft fibrous connective tissue which joins the cementum of the tooth root to the alveolar bone thus anchoring the tooth in its socket (Rees & Jacobsen, 1997; Dorow *et al.*, 2003). The primary function of the PDL is to secure the tooth in its socket (Toms *et al.*, 2002b). Due to its location, the PDL plays an important role in the transmission of masticatory and orthodontic loads from the teeth to the surrounding bone (Qian *et al.*, 2001; Gröning *et al.*, 2012b). It is also important for tooth mobility since it has a low stiffness compared to the materials around it (Naveh *et al.*, 2012b).

The PDL contains both elastic components, mainly collagen fibres, and fluid components such as blood and lymph vessels and interstitial fluid (Dorow *et al.*, 2002). It is approximately $0.25\text{mm} \pm 50\%$ wide with the fibres making up around 50 to 75 % of the volume of the tissue (Rees & Jacobsen, 1997; Dorow *et al.*, 2003). The collagen fibres are grouped together in principal fibre bundles and form a meshwork similar to a stretched fishing net extending between the cementum and alveolar bone (Sloan, 1979; Berkovitz, 1990; McCulloch *et al.*, 2000). The complex arrangement of fibres ensures that regardless of the direction of force applied, some fibre bundles are always placed in tension (Berkovitz, 1990). The fibres are also thought to transmit vertical forces from the teeth as lateral forces to the tooth socket and in doing so, help to prevent high stresses occurring at the apex of the tooth root (Atmaram & Mohammed, 1981). The PDL has been shown to have nonlinear, viscoelastic material properties which vary at different locations and in different directions along the tooth root (Berkovitz, 1990; Dorow *et al.*, 2002; Cattaneo *et al.*, 2009). However, whilst attempts have been made to characterise the material properties of the whole PDL, little is known about the specific material properties or geometry of the individual PDL fibres (Qian *et al.*, 2001).

When simulating masticatory loads with a finite element model of the mandible, how the PDL is modelled can have a considerable influence on the results produced. Whether or not to include the PDL in such models, as well as what material properties to assign if it is included, is the subject of much debate throughout the literature (*e.g.* Gröning *et al.*, 2011a; Gröning & Fagan, 2012; Grosse *et al.*, 2012). When it is included, most models idealise the PDL as a layer of solid, homogeneous and isotropic material (Fill *et al.*, 2012). Although some authors have attempted to represent its material properties more accurately (*e.g.* Cattaneo *et al.*, 2005, 2008, 2009), only a few have attempted to include its fibrous structure (Atmaram & Mohammed, 1981; Witzel *et al.*, 1998; Provatidis, 2000; Katona & Qian, 2001; Qian *et al.*, 2001; Limbert *et al.*,

2003; Meyer *et al.*, 2010). So far, those models which include the PDL fibres have only investigated their effect under low loads, typical of orthodontic tooth movement, and in models with only a single tooth.

1.2 Project Aim

The primary aim of this project was to investigate the effect of including the PDL in mandibular finite element models, and in particular to investigate the effect of including the fibrous structure of the PDL in these models. Three different ways of representing the PDL were to be compared: fibrous PDL, solid PDL and no PDL. In order to do this, the initial aim of the project was to develop a time efficient semi-automatic method of modelling the PDL fibres with commercial finite element software.

The investigation focused on how different ways of modelling the PDL affects strains in the alveolar bone under occlusal loads and under orthodontic loads. The ultimate aim of this research is to increase our understanding of the stresses and strains of the bone under these loads (which are currently impossible to directly measure *in vivo* in humans) and how the bone adapts to these.

1.3 Project Methodology

This project involved three successive finite element studies, each building upon the findings of the previous study. First, a simplified geometry model was created of a single tooth with one root. This was used to develop a method of including the fibrous structure of the PDL in finite element models. To assess the effect of including the PDL fibres, results from this fibrous PDL model were then compared to results from the same model with a solid PDL, using both occlusal and orthodontic loads.

The second study again compared different ways of representing the PDL using real tooth geometry obtained from a microCT scan of a human mandible rather than the simplified geometry of the previous study. Models were created with no PDL, solid PDL and fibrous PDL, using a similar method for adding the PDL fibres to that developed previously. Additionally, different methods of representing the trabecular tissue were also investigated. To assess the effect of the different methods of representing the PDL and the trabecular tissue, results were again compared for the different types of models under the application of both occlusal and orthodontic loads.

The third and final study assessed the effects of including the PDL in molar region models of five additional species: cat, cercocebus, pig, rabbit and sheep. This study aimed to determine whether the findings from the previous study were specific to the human molar region, or whether they may be true for mammalian mandibles in general. In this study, PDL fibres were not considered, and results were compared for models with and without a PDL when an occlusal load was applied.

1.4 Summary of Thesis Chapters

The remainder of this thesis is divided into the following chapters:

- **Chapter 2** provides an overview of the relevant background literature. This includes first an introduction to bone and a review of the mechanical adaptation of bone. The anatomy, biomechanics and material properties of the mandible are then discussed along with an introduction to mandibular functional morphology. This is followed by a review of the structure, function and material properties of the PDL and how it has been represented in previous finite element models. Finally, orthodontic tooth movement is discussed with particular emphasis on possible biomechanical causes related to the mechanical adaptation of bone.
- **Chapter 3** describes the creation of an idealised single tooth 3D finite element model. This included developing a novel method of representing the fibrous structure of the PDL in finite element models, using link elements to represent the fibres. This study was designed to investigate the effect of including these fibres in finite element models when applying either occlusal or orthodontic loads. The results presented in this chapter have already been published in PLoS ONE (see Appendix 1).
- **Chapter 4** presents a finite element study using a human molar region based on a microCT scan of a real mandible. A similar method is used to that in the previous chapter for including the PDL fibres. This study investigates different methods of representing the PDL, as well as different methods of modelling the trabecular tissue, using both occlusal and orthodontic loads.

- **Chapter 5** describes the final study for this project, creating finite element models of the molar regions from the five other species. This study investigates the effect of including the PDL in these models by comparing results from models with and without a PDL when an occlusal load is applied.
- **Chapter 6** presents a discussion of the results from the three studies presented in the previous chapters. This discussion focuses on the effect of including the PDL in these models and of including its fibrous structure. Comments are made on the effects of the PDL under both occlusal and orthodontic loads, with consideration given to possible biomechanical causes for alveolar bone remodelling in orthodontic tooth movement. Strengths and weaknesses of the project are also discussed as well as whether or not PDL fibres should be included in future finite element models.
- **Chapter 7** summarises the final conclusions from the project and outlines some possibilities for future research which could be carried out to build upon the work presented in this thesis.

Chapter 2

Literature Review

2.1 Introduction

This chapter gives an overview of the literature related to this project. The aim of this project was to investigate the effect of including the periodontal ligament in finite element models and to better understand the stress and strains in the mandibular bone and how bone adapts to these. This review begins by looking at bone in general, and especially how bone is thought to adapt to its mechanical environment. The mandible is then discussed. This includes looking at the biomechanics of the mandible and how it is thought to be adapted to the strains placed upon it. Following this the periodontal ligament is discussed in more detail. First its structure and function are described followed by its material properties before looking at how previous authors have attempted to include it in finite element models. Finally, orthodontic tooth movement is examined and an overview is given on some current thoughts about the biomechanical causes of orthodontic tooth movement.

2.2 Bone

2.2.1 Introduction to Bone

The human skeleton has a number of important functions: for example, it acts as a reservoir for essential minerals, provides rigid levers for muscles to act against and provides protection for many of the body's vital organs (Turner & Pavalko, 1998). Skeletal tissues include bone, cartilage, enamel and dentin (Hall, 2005). However, it is bone that is the primary focus for this project. Bone is a composite material made primarily out of a collagen framework packed with crystals of calcium phosphate mineral and a number of other constituents including water (Currey, 2002).

2.2.2 Wolff's Law and the Mechanostat Theory

Since the nineteenth century, the trabecular structure of cancellous bone has widely been considered to be an optimised structure, adapted to suit its mechanical environment (Tsubota *et al.*, 2009). The concept of a relationship between the form and function of bones, produced and maintained by mechanical forces, is commonly known as Wolff's law (Huiskes, 2000). Wolff's law is named after Julius Wolff, who is often credited with discovering bone adaptation due to altered loads, or bone remodelling, after he wrote his highly influential paper on the law of bone transformation (Wolff, 1892, 1986; Lee & Taylor, 1999). A number of authors have been quite critical of Wolff's law, including Currey (2002) who calls the law "unhelpful" and Lee and Taylor (1999) who suggests that the process described by Wolff is not in keeping with what is currently understood as Wolff's law. Nevertheless, whilst some have questioned Wolff's law, the idea that bones are mechanically optimal structures, according to some kind of basic rule, is widely accepted and mechanical load transduction into bone response continues to be extensively investigated (Huiskes, 2000; Ruff *et al.*, 2006).

The bone adaptation process is error-driven: it is primarily controlled not by the many cycles of "normal" strain but rather by the much smaller number of cycles of "abnormal" strain (Lanyon, 1992). Therefore, bone is known to accommodate to routine daily loading signals although the exact mechanisms involved are not well understood (Turner & Pavalko, 1998). The signal sent by osteocytes to the basic multicellular units (BMUs), consisting of osteoclasts and osteoblasts, is based on some reference value for typical loading to regulate whether net bone formation or resorption occurs (Huiskes, 2000). In an attempt to understand the mechanical and biological factors involved in bone remodelling, Frost (1987) developed his mechanostat theory in which local strains regulate bone mass using the mechanostat in a similar way to local temperatures regulate a room heater using a thermostat. In the mechanostat theory, BMUs maintain the local bone mass, controlled by a mechanical feedback loop requiring a set point which represents typical daily loading. According to the mechanostat theory strains during typical loading should be around 800 to 1500 microstrain (Frost, 1987). If strains are above that range bone formation is triggered and if strain falls below that range bone resorption is triggered. In this way, bone mass is adjusted so that strains should then fall within the set range. A simple diagram illustrating this is shown in Figure 2.1. The mechanostat theory has many critics, for example Turner (1999), however, it has

contributed significantly to an increased awareness of mechanical factors in the regulation of bone adaptation (Huiskes, 2000).

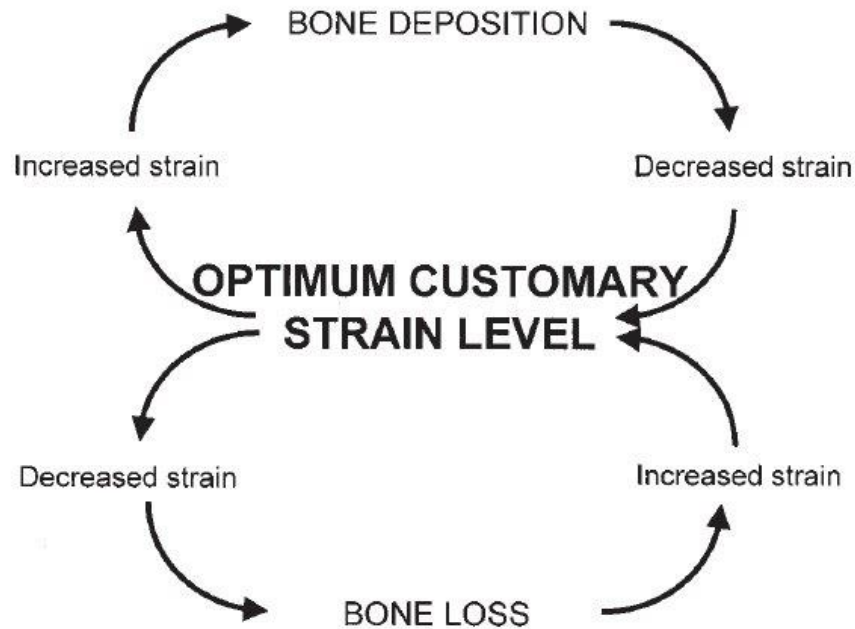


Figure 2.1 Schematic representation of the feedback loop for bone functional adaptation (Ruff et al., 2006: P. 485: Fig. 1).

2.2.3 Bone Functional Adaptation

Bone adaptation involves the processes of modelling and remodelling. Bone modelling involves altering the overall shape of the bone: bone is either added or taken away from the periosteal or endosteal surfaces (Currey, 2002). Remodelling affects all surfaces and involves a formation and resorption process where new bone replaces old bone whilst the total amount of bone is unchanged (Currey, 2002; Tsubota *et al.*, 2009). For bone adaptation to take place bone cells must detect mechanical signals and transform these signals into appropriate changes in the bone architecture (Turner & Pavalko, 1998). The load applied to the bone is distributed by the trabecular architecture and sensed by osteocytes. The osteocytes then send a biochemical signal to the bone surface which regulates net bone resorption or formation by BMUs. Osteoclasts are responsible for bone resorption and osteoblasts are responsible for bone formation (Huiskes, 2000). A schematic representation of this process is shown in Figure 2.2.

Proposed local feed-back control mechanism

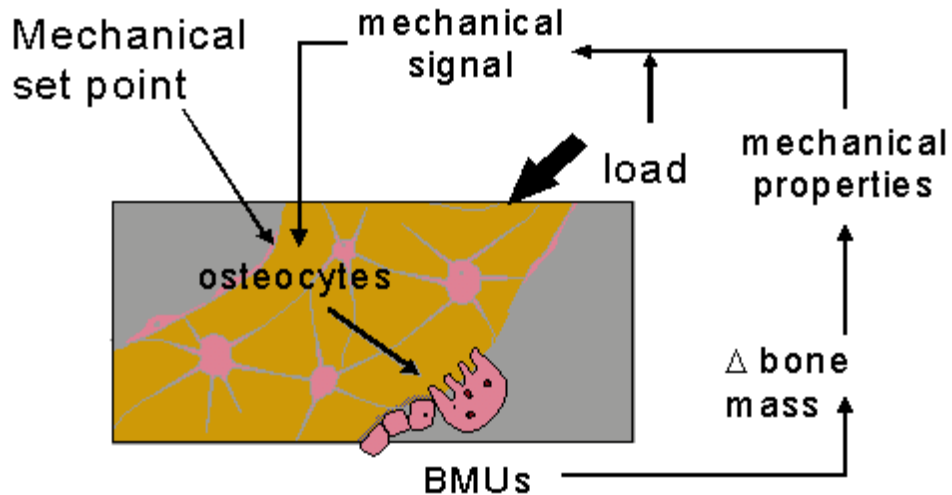


Figure 2.2 Schematic representation of the regulatory process for bone remodelling (Huiskes, 2000: P. 149: Fig. 5).

Whilst it is known that BMUs act as the effector units in bone remodelling the mechanisms by which bone adaptation works are not well understood (Turner & Pavalko, 1998; Huiskes, 2000). The conversion of a biophysical force into a cellular response is known as mechanotransduction and involves four phases: mechanocoupling, biochemical coupling, transmission of the signal and the effector cell response (Turner & Pavalko, 1998). Strain, rather than stress, is thought to be the direct stimulus on bone cells with principal tensile or compressive strains considered the most important for bone adaptation and shear strains seeming to have little effect (Qin *et al.*, 1996). It is also known that bone adaptation only occurs in the presence of dynamic loads, while static loads appear to have no effect (Turner & Pavalko, 1998; Huiskes, 2000). Similarly, increasing the duration of skeletal loading does not appear to produce a corresponding increase in bone mass (Rubin & Lanyon, 1984), whereas the rate frequency and magnitude of loading are all thought to be important (Turner, 1998). Osteocytes are assumed to act as the sensors for bone adaptation because of their location within the bone meaning that when bone is deformed the osteocytes within the bone are deformed the same amount (Turner & Pavalko, 1998). Although the osteocytes are deformed themselves by mechanical loads, researchers have found that the strains needed to activate bone cells *in vitro* can be up to a hundred times that required *in vivo*.

This has led to the belief that fluid flow through the canalicular spaces is the most important tissue-level effect (Turner *et al.*, 1994). Bending forces create pressure gradients in bone tissue causing extracellular fluid flow across the osteocytes. This fluid flow causes shear stresses on the cell membranes and also creates an electric field in the bone called a streaming potential (Chakkalakal, 1989; Duncan & Turner, 1995). It is thought that both the electrical and mechanical signals may play a role in mechanotransduction although cell culture experiments have suggested that it may be the fluid shear effects that are most important (Hung *et al.*, 1996; Reich *et al.*, 1990). A graphic representation of this process is shown in Figure 2.3.

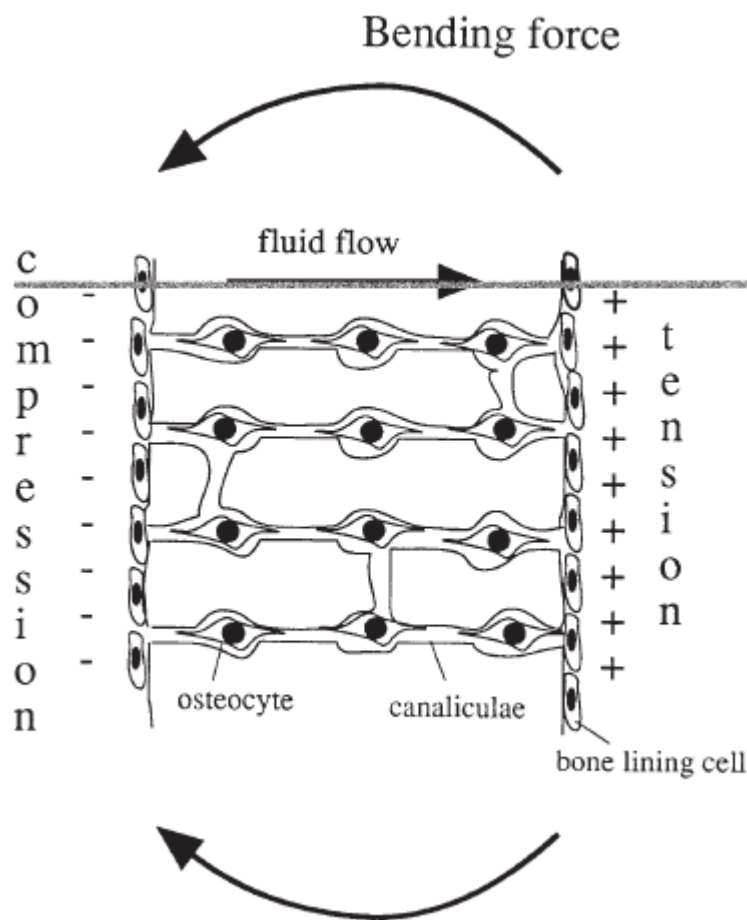


Figure 2.3 Graphic representation of fluid flow through the canalicular spaces caused by bending forces. Fluid is driven from regions of compression to regions of tension flowing across osteocytes. This provides nutrients for the osteocytes whilst also causing shear stresses on the cell membranes and creating a streaming potential (Turner & Pavalko, 1998: P. 347: Fig. 1).

Ultimately, whatever the mechanism involved, bone adaptation involves a mechanosensory apparatus and several mechanochemical pathways within the bone which lead to architectural changes that adjust and improve the bone structure to its

prevailing mechanical environment (Turner & Pavalko, 1998). Wolff sort to uncover the mathematical rules according to which bone is designed (Huiskes, 2000). Whilst no definitive mathematical rules have been established for bone adaptation, Turner and Pavalko (1998) summarised what is currently known into three fundamental rules which must be used to derive mathematical formulas from which structural bone changes can be predicted:

- 1) Bone adaptation is driven by dynamic, rather than static, loading
- 2) Extending the loading duration has a diminishing effect on further bone adaptation
- 3) Bone cells accommodate to a mechanical loading environment, making them less responsive to routine or customary loading signals

2.2.4 Finite Element Modelling of Bone Adaptation

Establishing mathematical rules governing bone adaptation allows computer simulations of the process to be done using, for example, finite element analysis (FEA). For example, Tsubota *et al.* (2009) demonstrate the ability of computer simulations to reproduce bones trabecular structure using a finite element (FE) model of a proximal human femur. In their FE model, Tsubota *et al.* (2009) assumed that nonuniformity of local stress drove the trabecular surface remodelling to seek a uniform stress state and this lead the simulation to closely reproduce the trabecular structure seen in the femur. Since the nineteenth century scientists have observed that the trabecular structure in the femur conforms closely to the stress trajectories applied to it under normal loading. This is shown in Figure 2.4. Whilst numerous computer algorithms have been shown to reproduce these trabecular patterns, usually in the femur, Huiskes (2000) argues that the correspondence between trabecular architecture and stress trajectories through the bone is circumstantial and not causal. Huiskes (2000) suggests that there are in fact no mathematical optimisation rules for bone architecture but rather there is simply a biological regulatory process which provides a structure which is sufficiently adapted to mechanical demands. In other words, the trabecular architecture is merely adequate rather than optimal. This is in agreement with Frost (1987), who noted that bone mass can be over adequate but never inadequate.

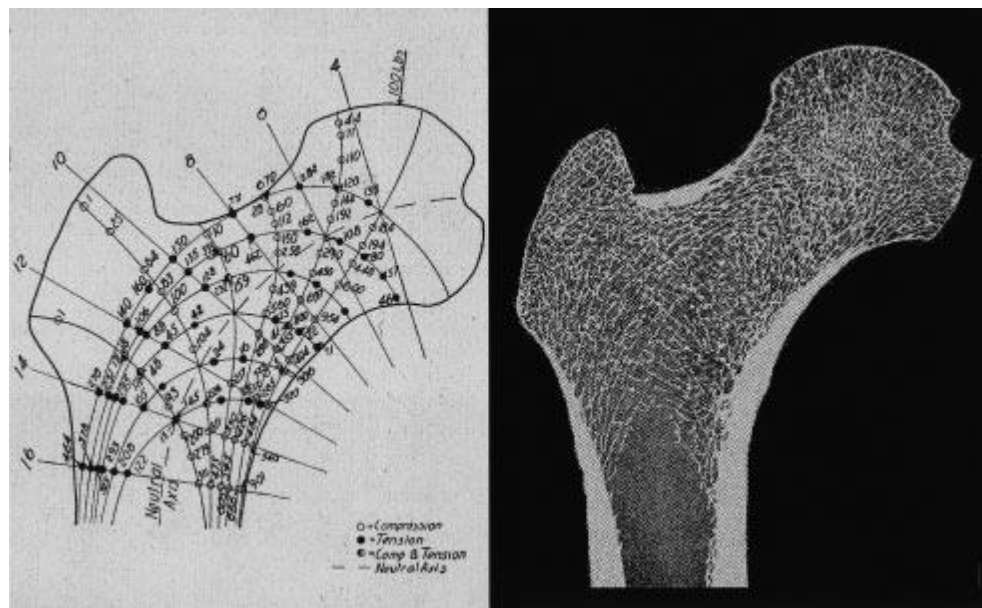


Figure 2.4 Approximate principal axes of stress shown as field lines in a loaded femoral head (left) and the trabecular structure in a femur (right) demonstrating the close alignment of trabecular structures with stress field lines (Chen & Ingber, 1999: P. 85: Fig. 3).

2.3 Mandible

2.3.1 Introduction to the Mandible

Bone adaptation theories and models have been extensively investigated, particularly in long bones (Middleton *et al.*, 1996a; Qian *et al.*, 2001). However, there is now increasing interest in investigating other areas such as the mandible. Much work has been done to investigate the bones and muscle of the mandible since it is relatively easily accessed for observations and experiments, both *in vitro* and *in vivo*, and is therefore well suited to investigation (Herring, 1993). Ashman and Van Buskirk (1987) compared the mandible to a bent long bone; however, in reality it is much more complicated than that.

2.3.2 Biomechanics of the Mandible

It is important to understand the biomechanics of the mandible since this may provide information about the factors that determine the structure of mandibular bone (Van Eijden, 2000). Loads in the mandible are somewhat different to those in long bones such as the femur which are primarily axial (Ashman & Van Buskirk, 1987). Also, unlike for straight bones, the neutral axis of the mandible does not run through its centre

of mass and therefore the bending stresses through its cross-section are nonlinearly distributed (Van Eijden, 2000). The biomechanics of the mandible are very complex due to both the number of structures and tissues involved and the kinds of forces generated (Benazzi *et al.*, 2012). Loads in the mandible are produced during mastication, biting, swallowing, speech and parafunctional habits (Middleton *et al.*, 1996a; McCulloch *et al.*, 2000). Forces are transmitted to the mandibular bone through the tooth via the periodontal ligament (PDL) as well as arising from the muscles of mastication and due to reaction forces at the temporomandibular joint (Ashman & Van Buskirk, 1987; Daegling *et al.*, 2008). These loads cause a combination of sagittal bending, transverse bending and corpus rotation causing a superposition of shearing, bending and torsional stresses and strains throughout the mandible (Van Eijden, 2000; Daegling *et al.*, 2008). This complex loading situation is shown in Figure 2.5. It should be noted that this situation is for the mandible only and not the maxilla. Beyond the tooth socket, the effects of *in vivo* loading differ between the mandible and maxilla because of the noticeable form differences between the two, such as the hard palate which greatly reduces bending and twisting of the maxilla (Daegling & Hylander, 1997).

Cross-sections of mandibular corpus are approximately oval with the vertical dimension being larger than the transverse dimension (Van Eijden, 2000). This has led to much debate throughout the literature about whether this cross section behaves as an open or closed section. Whether the mandible behaves as an open or closed section is of interest because the mechanical behaviours of open and closed sections are quite different. For example, if a hollow cylindrical rod is transformed into an open section by a longitudinal slit it will have much less torsional strength and rigidity than it would have had as a closed section (Daegling *et al.*, 2008). For the mandible to behave as an open section this would mean that tooth roots, the PDL and the tooth sockets all have no mechanical role in resisting mandibular loads (Daegling *et al.*, 2008). An idealised representation of what the mandibular cross-section would look like as an open or closed section is shown in Figure 2.6. Torsional rigidity of the mandibular corpus has been shown to be influenced by the presence of teeth and of the PDL (Daegling *et al.*, 1992). Therefore, Daegling and Hylander (1998) concluded that under torsional loads the mandible behaves as a closed section. Conversely, Marinescu *et al.* (2005) found that the roots of unloaded teeth do not have much effect on mandibular stiffness in bending. Therefore, in bending the mandible may best be modelled as an open section (Daegling *et al.*, 2008). Ultimately, it is probably best to say that the mandibular corpus

behaves in a manner that is somewhat removed from either open or closed section ideals (Daegling & Hylander, 2000).

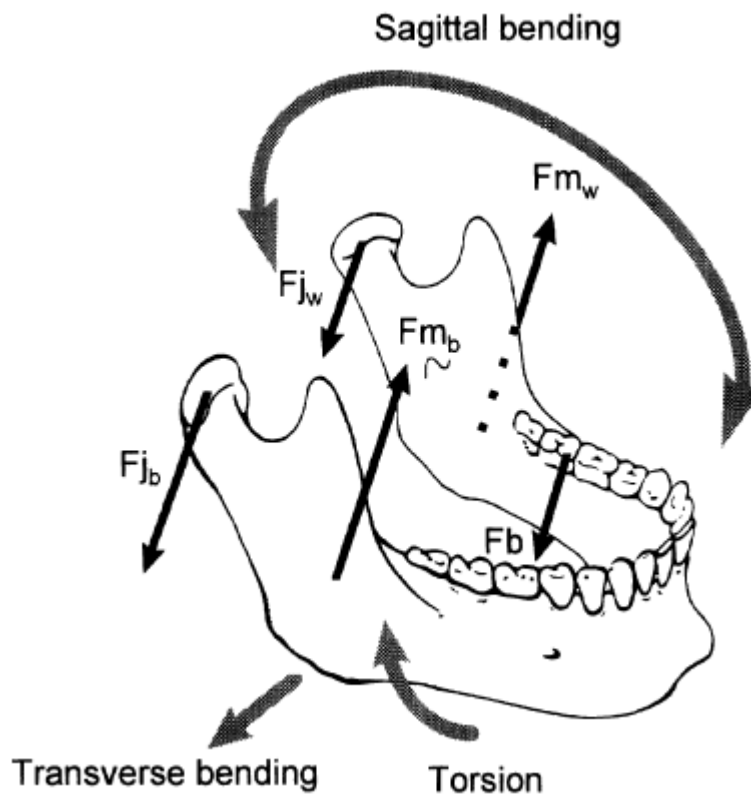


Figure 2.5 Loading of the mandible during a unilateral molar bite. F_b is the bite force, F_{m_b} and F_{m_w} and F_{j_b} and F_{j_w} are the muscular and joint forces at the balancing and working sides. The distortion of the corpus can be described as a combination of sagittal bending, torsion and lateral transverse bending (Van Eijden, 2000: P. 130: Fig. 9).

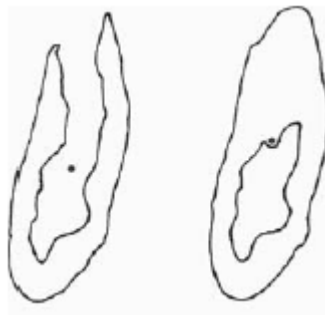


Figure 2.6 Alternative models of mandibular corpus as either open (left) or closed (right) cross-sections (Daegling *et al.*, 2008: P. 135: Fig. 7.3).

2.3.3 Functional Morphology of the Mandible

Unfortunately, there is only limited information available about deformations, stress and strains in the human mandible (Van Eijden, 2000). However, Daegling *et al.* (2008) state that the *in vivo* strain environment of the mandible is well understood, but a precise stress analysis has remained elusive. This has fuelled much discussion as to whether masticatory strains and mandibular morphology are functionally linked as well as whether mandibular morphology can be related to dietary specialisation (Daegling & Hylander, 1997, 2000). Functional morphology may be defined as combining information on anatomy, mechanics and behaviour in order to understand selective influences on the animals (Herring, 1993). Despite much uncertainty, the majority of those working in the field of mandibular functional morphology have assumed that mandibular morphology and masticatory loads are functionally linked (Daegling & Hylander, 2000). However, the effect of masticatory force on the mandible is not sufficiently understood (Borák *et al.*, 2011).

Some experimental studies and theoretical models of human mandibles have found that the largest stresses in the mandible occur in and around the alveolar bone of the tooth socket due to the local effects of biting forces (Daegling & Hylander, 1997). These findings have led to serious questions about the functional morphology of the mandible: if the highest stresses in mastication can be resisted by relatively thin and porous alveolar bone, why should much thicker compact bone be needed to reinforce the basal corpus where stresses are presumably much lower (Daegling & Hylander, 1997)? Daegling and Hylander (1997) argue that these findings may be misleading. Occlusal loads do not occur in isolation *in vivo*. As well as the occlusal forces associated with mastication there are also the muscular forces and condylar reaction forces which cause a bending and twisting of the corpus. These additional forces will produce stresses along the basal corpus as well as the alveolar process and so occlusal forces will have a significant impact on both alveolar and basal strains (Daegling & Hylander, 1997). However, due to the inherent limitations of both theoretical and experimental techniques, strain gradients in the alveolar bone remain relatively unknown (Daegling & Hylander, 1997).

There are a number of other observations concerning the mandible which add to the confusion about the relationship between its form and function. For example, the lingual side is characterised by thinner cortical bone compared to the buccal side (Benazzi *et al.*, 2012). There have been some proposals as to why this may occur,

however, no definitive reason has been accepted for this asymmetry and there is still much uncertainty about its functional significance. Another observation is that despite the high stresses predicted by many experiments, primates are not known to get mandibular stress fractures (Daegling & Hylander, 1997). One simple explanation for this is that the formation rate of the bone exceeds its fatigue limit (Frost, 1997).

Van Eijden (2000) states that the amount of bone tissue at a particular location of the mandible cannot simply be considered to be proportional to the magnitude of the mechanical loading at that location. It is not known to what extent and by what mechanism loading conditions affects modelling and remodelling of the mandible, but it is important to remember that mechanical loading is not the only factor governing bone mass and geometry (Daegling & Hylander, 1997; Van Eijden, 2000). Therefore, Daegling and Hylander (2000) acknowledge the possibility that mandibular morphology is merely inherited rather than functionally significant. However, after reviewing available experimental and theoretical evidence, Daegling and Hylander (1997) conclude that the assumption that masticatory strains and mandibular morphology are functionally linked is both empirically supported and theoretically justified.

2.3.4 Material Properties of Mandibular Bone

Due to the continuing debate surrounding mandibular morphology, investigations into the stress and strain distribution during biting and chewing is now a major topic throughout the literature (Benazzi et al., 2012). There have been a wide variety of attempts to model the mandibular stress environment, however, all have had to deal with the problem that stress is not directly measureable in the mandible but must be inferred by other means (Daegling & Hylander, 2000). In order to do this it is necessary to know the material properties of the mandible. The majority of investigations on the material properties of bone have focused on long bones, especially the femur (Ashman & Van Buskirk, 1987). Characterising the material properties of the mandible is not an easy task. The mandible contains different types of bone including cortical bone, trabecular bone and alveolar bone each with different material properties.

Ashman and Van Buskirk (1987) used a continuous-wave ultrasound technique to measure the orthotropic elastic constants of ten small cortical bone specimens taken from various locations within a single fresh-frozen human mandible. The locations from which the specimens were taken ranged from the chin to the ramus and included specimens from the buccal, lingual and inferior aspects of the mandibular corpus.

Ashman and Van Buskirk (1987) observed no systematic variation in the elastic properties from specimen to specimen and thus concluded that the mandible had homogeneous material properties. However, their results indicated that the material properties were not the same in all directions and so they conclude that whilst the mandible was homogenous, it was also anisotropic (Ashman & Van Buskirk, 1987). By comparing results they obtained for the mandible with previous data on the material properties of human and canine femurs, Ashman and Van Buskirk (1987) noted that the results were reasonably similar. This led to the speculation that the mandible behaves like a slightly less stiff long bone bent into the shape of a horseshoe.

A similar, though much larger, investigation into the material properties of mandibular cortical bone was performed by Schwartz-Dabney and Dechow (2003). Schwartz-Dabney and Dechow (2003) calculated the elastic properties of mandibular cortical bone from ten fresh adult dentate mandibles using measured ultrasonic velocities. They recorded measurements from a total of six hundred bone specimens collected from throughout the entire surface of the mandible. Contrary to the results obtained by Ashman and Van Buskirk (1987), Schwartz-Dabney and Dechow (2003) found regional variation between the symphysis, corpus and ramus both within and between mandibles. In fact, they stated that their results indicate a greater degree of regional material property variation within human mandibular cortical bone than has been reported in other bones (Schwartz-Dabney and Dechow, 2003). This suggests that human mandibular cortical bone may be both heterogeneous and anisotropic. However, the mandible is noticeably stiffer in the longitudinal direction than in transverse directions (Van Eijden, 2000). Therefore, to simplify the situation, Van Eijden (2000) suggests that the mandible could be considered transversely isotropic, having a high modulus in the longitudinal direction and a lower modulus in all transverse directions.

The material properties of trabecular bone are not the same as cortical bone due to the differences in their architecture: both the strength and stiffness of trabecular bone are generally reported to be lower than that of cortical bone (Van Eijden, 2000). It should be noted that, due to its porosity, the cortical bone of the alveolar process has often been found to be less stiff than cortical bone elsewhere in the mandible, yet still stiffer than the trabecular bone (Daegling *et al.*, 2008). However, Schwartz-Dabney and Dechow (2003) did not find consistent evidence that the alveolar bone is less stiff than the inferiorly situated basal cortical bone and so this is still the subject of some debate. The elastic modulus of cortical bone varies between 10 to 20 GPa depending on the bone architecture and type of loading (Van Eijden, 2000). In contrast, the elastic

modulus of trabecular bone has been found to range from 0.76 to 20 GPa depending on the density and orientation of the trabeculae (Van Eijden, 2000). However, much like for cortical bone, the material properties of trabecular bone have primarily been investigated in long bones and vertebral bodies (Misch *et al.*, 1999). Furthermore, far more data is available on the material properties of mandibular cortical bone than mandibular trabecular bone (Van Eijden, 2000).

Misch *et al.* (1999) investigated the mechanical properties of trabecular bone in the human mandible. They took measurements of trabecular bone tissue from the corpora of nine disarticulated, fresh-frozen human mandibles. In total, 76 cylindrical trabecular bone specimens were prepared and tested in vertical compression. Their results indicated regional variation in mechanical properties within the mandible. Contrary to the findings of Ashman and Van Buskirk (1987) with cortical bone, Misch *et al.* (1999) found the strength of human mandibular trabecular bone to be significantly lower than that previously reported for the proximal femoral trabecular bone. They also found that the anterior portion of the mandibular corpus had a greater trabecular bone density, which also correlated to it having a greater compressive strength and elastic modulus, than other regions.

The findings of Misch *et al.* (1999) are significant when considering the functional morphology of the mandible. Bite forces in the posterior region of the mandible may be two to three times higher than those in the anterior region (Misch *et al.*, 1999). Since bite forces are higher in the posterior portion yet the stiffness and compressive strength were both higher in the anterior region, Misch *et al.* (1999) concluded that occlusal loads may not be the primary mediator of the internal architecture of the mandibular trabecular bone. This conclusion agrees with the earlier findings of Ralph and Thomas (1988). Ralph and Thomas (1988) examined the percentage porosity of dentate human mandibles. In a dentate mandible the trabecular bone is surrounded by a thick cortical shell on one side and tooth sockets on the other (Misch *et al.*, 1999). Ralph and Thomas (1988) found that the cortical plates of the mandible appeared to provide the majority of the bony support for teeth rather than the trabecular bone which they found to be randomly arranged throughout the mandible.

Similarly, other finite element (FE) models of the human mandible have also shown that cortical bone plays an important role in the dissipation of occlusal loads in the mandible (Misch *et al.*, 1999). However, as previously discussed, occlusal loads do not occur in isolation without muscular and reaction forces (Daegling *et al.*, 2008). Torsion is the most significant loading occurring during mastication and biting and

since muscle attachments are located posteriorly on the mandible, the anterior portion of the mandible experiences a large moment load, even in the absence of occlusal loads due to buccolingual flexure (Misch *et al.*, 1999; Daegling *et al.*, 2008). Therefore, the findings of Misch *et al.* (1999) and Ralph and Thomas (1988) do not refute the claim that mandibular morphology and masticatory loads are functionally linked (Daegling & Hylander, 2000). It is also worth noting that in a typical human mandible, molars have two roots whereas incisors, canines and premolars only have one (Hollins, 2008). Occlusal loads will therefore be dissipated differently in the anterior portion of the mandible than in the posterior portion and so it is difficult to draw any meaningful conclusions solely based on the magnitude of the loading in these regions.

2.4 Periodontal Ligament

2.4.1 Structure and Function of the Periodontal Ligament

The material properties and biomechanics of the mandible provide many challenges for computer simulations. However, it is the periodontium which causes arguably the most difficulties. The periodontium is the collective name for the structures supporting the teeth and maintaining them in the mandible and maxilla. Four principal components make up the periodontium: gingivae, periodontal ligament (PDL), cementum and alveolar bone (Hohmann *et al.*, 2011). The periodontium is also surrounded by dental tissues such as enamel, dentin and pulp as well as other supporting tissue such as the trabecular and cortical bone of the mandible (Benazzi *et al.*, 2012).

Daegling and Hylander (2000) describe the PDL as an enigma that impedes every model of mandibular behaviour. The PDL is a thin, soft, densely packed, highly vascular, fibrous connective tissue which joins the cementum of the tooth root to the alveolar bone providing an anchorage for the tooth in its socket (Sloan, 1979; Rees & Jacobsen, 1997; Dorow *et al.*, 2003; Komatsu *et al.*, 2007; Hohmann *et al.*, 2011). The PDL is unique since it is the only ligament in the body to span two distinct hard surfaces (Middleton *et al.*, 1996a; McCulloch *et al.*, 2000). The PDL is composed of both elastic components, mainly collagen, and fluid components, including blood and lymph vessels and interstitial fluid (Dorow *et al.*, 2002). The oblique orientation of the principal fibres in the PDL means the PDL functions as a suspensory ligament with the tooth root forming a generic Y-shaped suspension system (Atmaram & Mohammed, 1981; Katona & Qian, 2001). The collagen fibres, which anchor into the cementum and alveolar bone,

are typically classified into five groups based on their location: crestal fibres, horizontal fibres, oblique fibres, apical fibres and interradicular fibres (Berkovitz, 1990). An idealised representation of the principal fibres of the PDL, for a single rooted tooth, along with other components of the periodontium such as the gingival fibres, tooth and alveolar bone is shown in Figure 2.7. The primary functions of the PDL are to stabilise the tooth in the bone as well as providing proprioceptive and reparative functions (Toms *et al.*, 2002b). As well as holding the tooth inside the jaw, the PDL also plays a crucial role in load transfer, transmitting both functional masticatory forces and orthodontic forces from the tooth to the surrounding bone (Qian *et al.*, 2001; Gröning *et al.*, 2012b). Since it has a low stiffness compared to the materials around it, the PDL also plays an important role in tooth mobility (Hohmann *et al.*, 2011; Naveh *et al.*, 2012b).

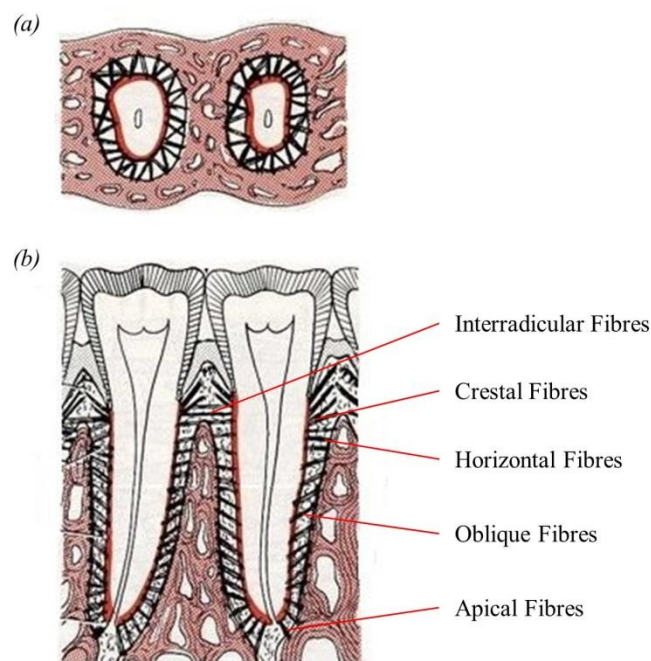


Figure 2.7 Schematic representation of the fibrous structure of the PDL showing the generic location and orientation of the fibres: (a) transverse plane; (b) sagittal plane (Schroeder, 2000: P. 219: Fig. 2.14).

The PDL is approximately $0.25 \text{ mm} \pm 50 \%$ wide and is composed of collagenous fibres, running in various directions between the root and bone, embedded in a gelatinous ground substance containing cells and neurovascular tissue (Rees & Jacobsen, 1997; Toms *et al.*, 2002b; Komatsu *et al.*, 2007). The fibres of the PDL make up approximately 50 to 75 % of the volume of the tissue (Dorow *et al.*, 2003). The high density and spatial configuration of the fibres contribute to them having a substantial influence on the mechanical properties of the PDL (Dorow *et al.*, 2003). Biochemically,

the major type of collagen found in the PDL is type I collagen although around twenty per cent is type III (Berkovitz, 1990). In fact, it has been shown that there are at least fourteen different types of collagen in the PDL (Provatidis, 2000). It is generally accepted that the collagen fibres are grouped together to form principal fibre bundles with different orientations in different locations within the ligament (Sloan, 1979; Berkovitz, 1990). An example of a fibre bundle is shown in Figure 2.8. These fibre bundles follow a wavy course appearing to have a crimped or undulating structure along their length as shown in Figure 2.9. Fibre bundles branch frequently and criss-cross with other fibres allowing the fibres to resist forces tending to rotate the tooth in a similar manner to the spokes of a wheel (Sloan, 1979). This forms a meshwork similar to a stretched fishing net extending between the cementum and alveolar bone (Sloan, 1979; McCulloch *et al.*, 2000). The ends of the fibres are secured by inserting into the bone or cementum and calcifying to form Sharpey's fibres (McCulloch *et al.*, 2000). The complex arrangement of the collagen fibres is thought to ensure that irrespective of the direction of an applied force some collagen bundles are always placed in tension (Berkovitz, 1990).

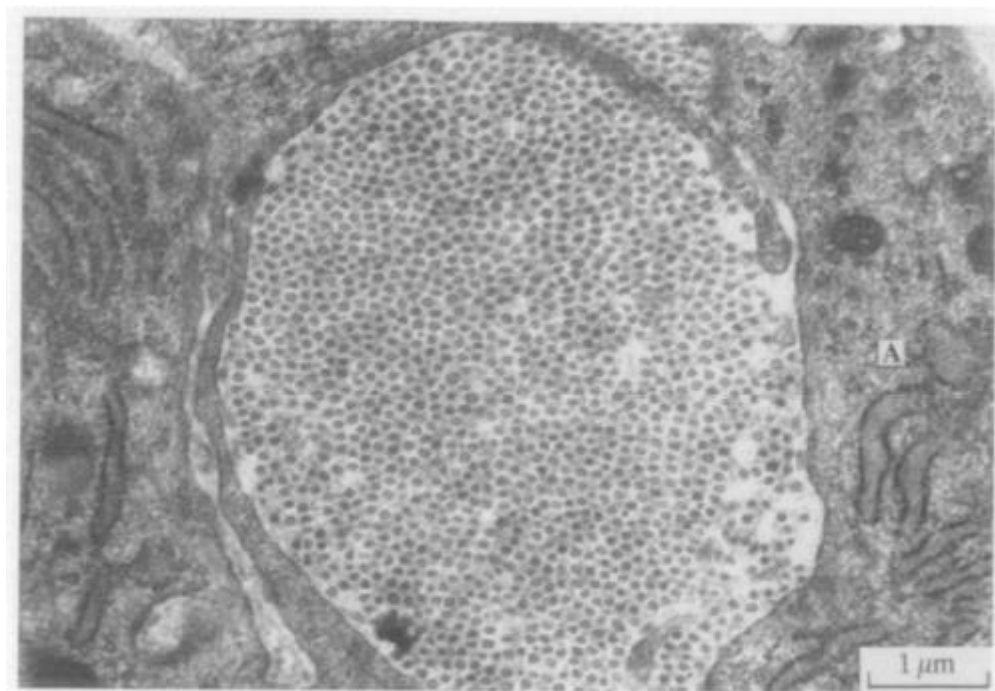


Figure 2.8 Transmission electron micrograph showing a transversely sectioned collagen fibre bundle in the PDL (Berkovitz, 1990: P. 54: Fig. 4).

The PDL contains a number of other important components as well as the collagen fibres. Firstly, it also contains oxytalan fibres (Berkovitz, 1990). These are pre-elastin type fibres although it is not clear why they do not mature to elastin in the PDL. They tend to lie parallel to the surface of the tooth root extending out only as far as the peripheral blood vessels and have not been observed to pass from the tooth to the bone (Berkovitz, 1990). The exact function of these fibres also remains unclear (Berkovitz, 1990). The remaining PDL volume is composed of blood vessels, cells and ground substance, about 70 % of which is bound water (Dorow *et al.*, 2003). The most predominant type of cells in the PDL are fibroblasts, however, it also contains endothelial cells, epithelial cells, sensory cells, osteogenic cells, osteoclastic cells and cementoblasts (McCulloch *et al.*, 2000). Compared to other ligaments and tendons the PDL is highly vascular (McCulloch *et al.*, 2000). The blood vessels of the PDL are connected to the systemic circulation and as well as providing nutrients they are thought to play a role in the mechanisms of tooth eruption and support (Berkovitz, 1990; Dorow *et al.*, 2003).



Figure 2.9 Scanning electron micrograph of a transverse section of a PDL showing the wavy appearance of collagen fibres (Berkovitz, 1990: P. 54: Fig. 3).

2.4.2 Material Properties of the Periodontal Ligament

Understanding the material properties of the PDL is essential in order to obtain a greater understanding of orthodontic tooth movement (Dorow *et al.*, 2003). As well as orthodontists, other specialists such as those interested in the mechanisms of tooth support or eruption and anyone interested in the functional morphology of the mandible also require an understanding of the material properties of the PDL (Berkovitz, 1990). However, conducting mechanical tests on the PDL is very challenging since isolating and preserving an appropriate sample is difficult (Hohmann *et al.*, 2011). It is also important to note that the majority of investigations on PDL material properties have been done with animal, rather than human, tissue (Berkovitz, 1990). Animal tissues are often a poor morphological representation of the corresponding human tissues (Jones *et al.*, 2001). However, many authors have assumed that there is no qualitative difference between human and animal PDL and other authors, such as Poppe *et al.* (2002), have reported very similar material properties.

The PDL has been shown to have nonlinear, viscoelastic material properties (Dorow *et al.*, 2002; Cattaneo *et al.*, 2009). Both the structure and properties of the PDL are also known to vary at different locations along the tooth root as well as depending on the state of eruption of the tooth (Berkovitz, 1990; Dorow *et al.*, 2002). Many authors have observed a correlation between anatomical location and mechanical behaviour of the PDL and this is generally attributed to the varying orientation and stiffness of the PDL fibres along the tooth root (Berkovitz, 1990; Qian *et al.*, 2001; Toms *et al.*, 2002b). The PDL, along with other ligaments and tendons, is known to remodel and alter the orientation of the fibres to optimise its load bearing capacity. This allows it to adapt to changes in applied loading on a much faster time scale than the adaptations of bone and cartilage (Chen & Ingber, 1999). However, little is known about the specific geometries and mechanical properties of the individual PDL fibres although it is thought that they too behave nonlinearly (Qian *et al.*, 2001).

Three systems in the PDL play a role in the transmission and damping of forces: the vascular system, the solid component, composed of collagen and other proteins, and the interstitial fluid (Parfitt, 1960; Van Driel *et al.*, 2000). A relatively large vascular content is necessary for the high perfusion rates required for the tissue (McCulloch *et al.*, 2000). It has also been suggested that because of the vast amount of blood vessels blood flow through the PDL gives the tissue the characteristics of a hydraulic damper (Van Driel *et al.*, 2000). Flow of interstitial fluid within the PDL space also helps

develop a hydrodynamic damping system which plays a major role in controlling the distribution of bite forces (Daegling & Hylander, 1997; Rees & Jacobsen, 1997; Poppe *et al.*, 2002). Therefore, tooth movement is dampened as blood is squeezed out of the blood vessels and interstitial fluid is forced into the adjacent bone marrow spaces in the alveolar bone (Dorow *et al.*, 2003). These fluid systems provide the main mechanism for the transmission of compressive loads on the PDL (Provatidis, 2000). Conversely, the PDL fibres are used to transmit mostly tensile loads to protect the tooth from intrusive, extrusive and rotational movements (Provatidis, 2000; Dorow *et al.*, 2003). Of course these three systems do not occur independently from each other: for example, an occlusal load will cause the fibre bundles to straighten out and stretch which may in turn compress adjacent blood vessels generating the viscoelastic properties (Sloan, 1979). It has been suggested that for low forces, below one newton, the fluid systems are most important in resisting the applied loads, whereas resistance to larger forces, such as those occurring during mastication, relies more on the fibrous components (Wills *et al.*, 1976). Ultimately, the mechanical behaviour of the PDL, as with other connective tissues, involves a sharing of stress between the different components which work together (Komatsu *et al.*, 2007).

Since obtaining an isolated sample of PDL is difficult many authors perform experiments measuring tooth movement *in situ* in order to determine the material properties of the PDL (Hohmann *et al.*, 2011). The majority of experimental data available on the stress-strain profile for the human PDL were obtained using only relatively small tooth movements (Borák *et al.*, 2011). Since the stiffness of the PDL is much lower than the surrounding tooth or bone tissue, many authors assume initial tooth movement under physiological loads is due almost exclusively to deformation of the PDL (Dorow *et al.*, 2002, 2003). However, any interactions with the surrounding tissue may interfere with data intended to represent the response of an individual tissue (Middleton *et al.*, 1996a). Furthermore, Dorow *et al.* (2002) highlight the fact that there is no defined uniaxial deformation state during tooth displacement. Instead, the tooth undergoes an uncontrolled tipping movement in the tooth socket (Dorow *et al.*, 2002).

The material properties of the PDL are often inferred from FE models. This is done by assigning different values to the PDL and comparing load-deflection results calculated by the model to results observed experimentally to see what values for the model best replicate the experimental results (Hohmann *et al.*, 2011). However, whilst this is common, Dorow *et al.* (2002) state that load-deflection behaviour of a point on the tooth crown cannot be used for quantitative determination of the material behaviour

of the PDL due to the uncontrolled tipping. Nevertheless, despite these problems many authors, for example Rees and Jacobsen (1997) and Ichim *et al.* (2007), have still attempted to quantify the material properties of the PDL using this approach.

Initial tooth movement is the reversible displacement of a tooth within its alveolar socket due to the application of a force system without remodelling of the surrounding bony structures (Poppe *et al.*, 2002). This movement is known to be nonlinear (Parfitt, 1960). Although it is nonlinear it can be characterised as a two-phase movement allowing simplification as bilinear rather than nonlinear (Poppe *et al.*, 2002; Borák *et al.*, 2011). Stress-strain plots for the PDL by Dorow *et al.* (2002, 2003) and Toms *et al.* (2002a) all show this bilinear property as an initial low stiffness region followed by a region of higher stiffness. An example graph is shown in Figure 2.10. This two-phase movement is widely accepted although there is some disagreement as to why it occurs.

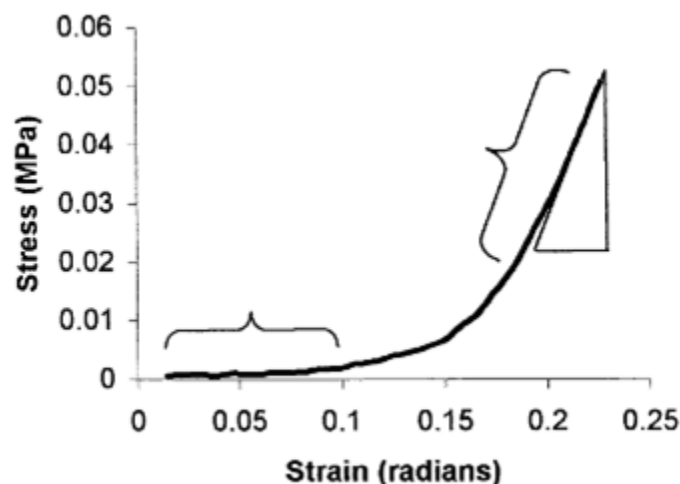


Figure 2.10 Stress-strain plot for the PDL from an experiment by Toms *et al.* (2002a: P. 176: Fig. 3) showing how the nonlinear behaviour may be simplified as bilinear.

The most common explanation for the two-phase tooth response to loading relates to the undulating appearance of PDL fibres in their unloaded state as shown in Figure 2.9. The first phase of the movement is attributed to the uncramping or uncurling of these fibres. During this phase the majority of the load resistance is assumed to come from the fluid component. The second phase is then attributed to the stretching of the fibres at which time they begin to assume most of the load (Sloan 1979; Poppe *et al.*, 2002; Toms *et al.*, 2002a; Dorow *et al.*, 2003). Conversely, Van Driel *et al.* (2000) rejects this explanation although similarly suggests the first phase is attributed to the

fluid systems within the PDL. Van Driel *et al.* (2000) argues that directly after loading, the fluid pressures in the PDL will rise on the side to which the force is directed thus preventing the uncurling of the PDL fibres. The criticisms by Van Driel *et al.* (2000) are supported by observations from other authors. For example, there is little information to determine whether or not the PDL fibres are actually straightened sufficiently during loading (Berkovitz, 1990). In fact, Berkovitz (1990) questions whether the PDL fibres really do have a wavy appearance suggesting that perhaps this is just an artefact associated with the preparation of the material before it is scanned.

The biological significance of the crimping seen in collagen is most commonly studied in tendons, commonly rat-tail tendon, which show a nonlinear stress-strain profile when loaded (Sloan, 1979; Berkovitz, 1990). Active contraction of living cells within the interstitial fluid pull the collagen into the undulating buckled structure. It is assumed that this is to keep the ligament under tension at all times (Chen & Ingber, 1999). In tendons, the crimps have a regular structure with a quantifiable periodicity and angular deflection (Berkovitz, 1990). The same is not true for the crimping seen in the PDL calling into question whether the crimping in the PDL fibres is homologous with the crimping seen in tendons (Berkovitz, 1990).

An alternative explanation for the two-phase movement is given by Borák *et al.* (2011) who suggest that the first phase corresponds to an elastic range of the PDL while the second phase corresponds to deformation of the alveolar bone with a stretch of the PDL on the tensile side. Previously, due to the difference in stiffness between the PDL and the surrounding tissues, tooth and bone deformations have been assumed to only be significant when under high, non-functional, loads (Dorow *et al.*, 2003). However, Naveh *et al.* (2012a) used microCT to view a tooth under load and observed that the alveolar bone was involved in resisting tooth movement even under low loads of a few tens of newtons. From this they concluded that the first phase of tooth movement is due mainly, but not only, to the PDL and the second phase of tooth movement is due mainly, but not only, to the alveolar bone.

The time-dependent mechanical behaviour of the PDL was investigated by Van Driel *et al.* (2000) by performing *in vivo* experiments on beagle dogs. When a load was applied they observed an instantaneous displacement followed by a creep displacement. They concluded that the creep displacement was due to the flow of interstitial fluid leading to a decrease in pressure within the PDL. From this they inferred that over time, the load resistance is transferred from the fluid component to the solid component which will be completely carrying the load once the tooth reaches equilibrium. They

conclude that those using a short term tooth response to evaluate the material properties of the PDL will overestimate its stiffness due to the initial fluid pressurisation (Van Driel *et al.*, 2000). However, not all time-dependent properties are thought to be due to the fluid systems: Komatsu *et al.* (2007) suggested that stretched fibres may progressively align along the direction of the initial strain application causing stress-relaxation of the PDL.

2.4.3 Finite Element Modelling with the Periodontal Ligament

As well as anchoring the tooth in the tooth socket, it has also been suggested that the PDL plays a role in bone remodelling, especially in the case of orthodontic tooth movement (Schwartz, 1932; Krishnan & Davidovitch, 2006). The suggestion that mandibular remodelling may be controlled by the PDL has led to an increased interest in studying the stress and strain distribution throughout the mandible and crania during mastication (Benazzi *et al.*, 2012). The first dental FE study was carried out over forty years ago by Farah *et al.*, (1973). A study by Koriath *et al.* (1992) was the first whole mandible model to try to include the dental structures and the PDL along with both the cortical and cancellous bone. If and how the PDL is included in FE models has been the subject of much debate throughout the literature ever since. Including the PDL in FE models significantly increases the time required both to produce and solve the model (Gröning *et al.*, 2011a). This may make some researchers reluctant to include it in their models. However, another reason many researchers choose not to include the PDL is due to the lack of reliable, quantitative, material property data for it (Rees, 2001; Toms & Eberhardt, 2003).

The PDL is a multi-phasic material and so its mechanical properties result from the compound effect of the material properties of all the individual structures within it (Poppe *et al.*, 2002; Cattaneo *et al.*, 2009). It is known to be a nonlinearly elastic material yet most FE models idealise it as a layer of solid homogeneous and isotropic material (Fill *et al.*, 2011, 2012). Another common idealisation for the PDL in FE models is to assume that it has a constant thickness. This assumption would appear less controversial in the literature and a recent study by Hohmann *et al.* (2011) reported that the stress field is insensitive to the thickness distribution throughout the PDL. However, this result disagrees with the findings of an earlier report by Toms and Eberhardt (2003) who found that stresses using a uniform thickness PDL were substantially different from stress predicted using a non-uniform thickness PDL.

Due to the obvious complexities concerning its material properties, there is much disagreement in the literature about the material properties to assign to the PDL in FE models. To highlight the scale of this disagreement, PDL material property values from a selection of articles are shown in Table 2.1. The range of Young's modulus value assigned to the PDL spans more than five orders of magnitude (Rees, 2001). Conversely, the value chosen for Poisson's ratio is relatively consistent. Poisson's ratio tends to be given a value close to 0.5 since the PDL is usually considered to be nearly incompressible despite there not being much experimental evidence to support this (Pietrzak *et al.*, 2002). This assumption is probably due to the fluid content of the PDL, however, the volume of fluid in the PDL is not constant. The blood vessels in the PDL are connected to the systemic circulation and so can alter the volume of fluid in the PDL by emptying or filling. Similarly, the interstitial fluid can also be interchanged with fluid reservoirs in the adjacent bone marrow (Dorow *et al.*, 2003).

Table 2.1 Material property values assigned to the periodontal ligament in finite element models from a selection of articles (Rees, 2001: P. 430: Table 5).

Article	Elastic Modulus (MPa)	Poisson's Ratio
Goel <i>et al.</i> , 1992	1750	0.49
Thresher & Saito, 1973	1379.0	0.45
Cook <i>et al.</i> , 1982	68.9	0.49
Ko <i>et al.</i> , 1992	68.9	0.49
Benazzi <i>et al.</i> , 2012	68.9	0.45
Wilson, 1991	50.0	0.45
Middleton <i>et al.</i> , 1996b	50	0.49
Rees, 2001	50	0.49
Wright, 1975	49	0.45
Ichim <i>et al.</i> , 2007	12	0.45
Takahashi <i>et al.</i> , 1980	9.8	0.45
Farah <i>et al.</i> , 1989	6.9	0.45
Chen & Chen, 1998	3	0.45
Reina <i>et al.</i> , 2007	3	0.45
Tanne & Sakuda, 1983	0.7	0.49
Yettram <i>et al.</i> , 1976	0.18	0.49
Hohmann <i>et al.</i> , 2011	0.1	0.45

For researchers producing dental FE models there are many more uncertainties to contend with other than just the PDL. For example, there are also no universally accepted material properties for either the tooth or bone (Qian *et al.*, 2001). Furthermore, some researchers choose to model the tooth as one material whereas some

attempt to include the different components, and the same can be said for the bone. Although it is difficult in practice, it is theoretically possible to fully account for all material properties within the FE model (Daegling & Hylander, 2000). Daegling and Hylander (2000) argue that a more difficult problem for researchers to overcome is applying the correct boundary conditions to the model. Marinescu *et al.* (2005) examine the effect of altering the boundary conditions on a mandibular FE model. They concluded that increasing the number of nodes constrained increases the apparent stiffness of the model and even a small change in the orientation of applied loads can have a large influence on the strains produced. Despite all the difficulties, there are many examples throughout the literature of FE models successfully validated against experimental data, even without necessarily accurately modelling all of the complex morphology and behaviour in the region surrounding the tooth. Due to all of the unknown issues involved with such models, Gröning *et al.* (2012b) strongly recommend that researchers conduct sensitivity analyses to assess the reliability of their FEA results and subsequent biological interpretations.

Although specific characteristics of the collagen fibres in the PDL are unclear, or difficult to describe, they are known to have nonlinear material properties (Qian *et al.*, 2001). The function of these fibres is generally understood to be both anchoring the tooth in its socket and to convert vertical loads on the tooth to horizontal loads in the alveolar bone (Atmaram & Mohammed, 1981). This would suggest that modelling the PDL as a layer of solid material would not accurately represent the stress distribution in the alveolar bone. Despite this, only a few authors have attempted to represent the collagen fibres in FE models: Atmaram and Mohammed (1981), Witzel *et al.*, (1998), Provatidis (2000), Katona & Qian (2001), Qian *et al.* (2001), Limbert *et al.* (2003) and Meyer *et al.* (2010).

Atmaram and Mohammed (1981) created a two-dimensional model of a molar tooth. To represent the fibres of the PDL they used beam elements, selecting the locations and orientations of these elements based on a histological section of a tooth. However, these beam elements were designed to support both tensile and compressive stress, though not bending stresses, whereas the collagen fibres in the PDL would likely support only tensile stresses, hence transferring vertical load through the tooth as horizontal tension in the alveolar bone. Also, the PDL is a composite material whereas in this article only the fibres are represented and not the material surrounding them which would also play a role in resisting any applied load. Naturally occurring composite materials, such as any human connective tissue, are thought to have a

structure which is optimised by sharing the stress applied to it between the different components (Komatsu *et al.*, 2007). Therefore it is possible that modelling just fibres alone may not be any more representative than the traditional approach of modelling the PDL as a layer of solid material.

Qian *et al.* (2001) attempted to model the principal fibres of the PDL as well as the surrounding material. Their model is a simplified three-dimensional reconstruction of a canine dog tooth. The fibrous PDL is modelled using reinforced elements which contain reinforcing fibres within linear, homogeneous elements. This more realistically represents the natural structure of the PDL than the model by Atmaram and Mohammed (1981). The reinforcing fibres in the model were assumed to be linearly elastic, unlike the fibres in the PDL which behave nonlinearly. As well as creating novel fibrous PDL FE models both Atmaram and Mohammed (1981) and Qian *et al.* (2001) also created corresponding continuous PDL models to compare their approach to the more traditional approach for modelling the PDL. Both concluded that their models produced more realistic results than the traditional approach although neither validated their models against any experimental data. Katona and Qian (2001) use FEA to examine the mechanism responsible for tooth eruption, using a model with a fibrous PDL very similar to that by Qian *et al.* (2001).

Provatidis (2000) produced five FE models varying how the PDL was modelled. Like Atmaram and Mohammed (1981) and Qian *et al.* (2001) they produced one model with a solid linear elastic, isotropic PDL since this is the most common way in which it is modelled. They also produced three models with only fibres to represent the PDL, similar to Atmaram and Mohammed (1981), and one model with both fibres and solid PDL, similar to Qian *et al.* (2001). The fibres were modelled as ideal springs. In the fibre only models these springs were set to function only in tension or compression whereas in the combined model they were set to transmit only tensile loads. However, to simplify the model, they only meshed the PDL, ignoring both the tooth and alveolar bone. They justified this assumption by arguing that, since stiffness of the PDL is so much lower than the surrounding tooth and bone, the tooth will behave as a rigid body when subjected to a low, non-occlusal load. They state that they have validated this assumption by comparing the results from a model of just the PDL to the results of a model including the tooth, bone and PDL. They used these models to determine the centre of rotation for the tooth with a horizontally applied one newton load. To assess which representation of the PDL was best they compared their results to those predicted by the theoretical Burstone's formula. Their results were inconclusive about which was

necessarily best. They found that the results from the combined model were highly dependent on both the volume concentration of fibres and the elastic modulus of the fibres.

Limbert *et al.* (2003) included the fibrous structure of the PDL in their FE model by creating a compressible transversely isotropic hyperelastic constitutive law to defining the material properties of the PDL. Vectors were defined to apply this law directionally in each element to simulate the orientation of the PDL fibres. They then compared the stress and strains observed from an isotropic model to their new model and found the distributions to be very different with much higher strains seen in the fibrous model.

Meyer *et al.* (2010) used tension-only link elements to represent the fibres of the PDL in their model. This was similar to the method used in the earlier work by Witzel *et al.* (1998) who also used link elements to represent the PDL fibres. However, Meyer *et al.* (2010) did not compare their fibrous PDL with other PDL representations. The purpose of their study was to examine the location of the centre of resistance for tooth movement in different directions rather than comparing different types of PDL.

Despite there being very few examples of studies which model the fibrous structure of the PDL, there are many studies which assign either bilinear or nonlinear material properties to the PDL. These studies try to replicate the properties of the PDL without replicating the structure of the tissue, which is similar to assigning material properties to the bone without modelling its trabecular structure. Toms and Eberhardt (2003) constructed a two-dimensional plane strain FE model of a mandibular premolar based on images taken from a human specimen. They created two models assigning linear elastic properties to one and nonlinear elastic properties to the other. The nonlinear elastic properties were based on previous experimental data (Toms *et al.*, 2002a) and the load-displacement results produced by the FE model closely agreed with this data. For the linear elastic model the PDL was divided into five different regions from top to bottom. These different regions were assigned different linear elastic material properties. From the results obtained Toms and Eberhardt (2003) concluded that the predicted stresses were different for the linear and nonlinear models particularly in the apex and cervical regions.

Similarly to Toms and Eberhardt (2003), Koriath and Hannam (1994) assigned different linear elastic material properties to different regions of the PDL, although they only divided the PDL into three regions rather than five. While both these articles used a similar approach, assigning different material properties to different locations of the

PDL, the stiffness distribution was different. In the model by Toms and Eberhardt (2003) the apex portion of the PDL was assigned the highest stiffness value whereas the apex was assigned the lowest stiffness value by Korioth and Hannam (1994).

Due to the amount of disagreement that exists in the literature about how to model the PDL many articles have sought to investigate what effect varying the mechanical properties of the PDL has on results obtained. A study by Wood *et al.* (2011) investigated the sensitivity of FEA results to variations in the behaviour of the PDL using a model of a primate cranium. They assigned linear elastic, hyperelastic and viscoelastic properties to the PDL as well as ignoring the PDL by treating it as cortical bone. They found that the effects of the PDL were local to the tooth socket and thus the PDL can be ignored if stresses and strains within the alveolar region are not required. They also concluded that if the PDL is required, modelling it with linear elastic material properties should be sufficient. Conversely, in a similar experiment only using a mandible rather than a crania, Gröning *et al.* (2011a) found that strain in the mandibular corpus is significantly increased when PDL is included leading them to conclude that the PDL should be included in all FE models of the masticatory apparatus regardless of whether or not the area of interest is far away from the alveolar region.

The results obtained by Gröning *et al.* (2011a) agreed with the earlier findings of Marinescu *et al.* (2005). Marinescu *et al.* (2005) conducted a validation study and sensitivity analysis using two FE models of a macaque mandible: a dentate model without any PDL and an edentulous model. To validate their FEA results they compared them to results obtained from an *in vitro* experiment. The sensitivity study involved examining the effects of altering the boundary conditions. However, in all cases the edentulous model was a closer match to the experimental data than the dentate model which always appeared too stiff. These results suggest that ignoring the PDL will artificially stiffen the model. Importantly, Marinescu *et al.* (2005) were taking strain readings from a point attached below the alveolar process on the opposite side of the mandible to the loaded tooth. This suggests that the effects of ignoring the PDL are not localised around the alveolar bone. However, these three studies are not directly comparable since Marinescu *et al.* (2005) and Gröning *et al.* (2011b) were both examining a mandible, whereas Wood *et al.* (2011) were examining a cranium.

Since it is difficult to determine the material properties of the PDL directly they are often inferred from FE models. This is done by assigning different values to the PDL and comparing results calculated by the model to results observed experimentally to see what values for the model best replicate the experimental results (Hohmann *et al.*,

2011). Rees and Jacobsen (1997) used FEA to replicate two independent experimental studies on the PDL: one by Picton (1963) and one by Tanne and Sakuda (1983). They found that for their FE model, assigning a Young's modulus value of 50 MPa, with a Poisson's ratio of 0.49, produced results which correlated well with the two experimental studies. These values are in agreement with an earlier study by Middleton *et al.*, (1996b). However, Rees and Jacobsen (1997) noted that from their results, Young's modulus values within the range of 20 to 150 MPa could be considered within the range of results obtained by the two experimental studies. Since the PDL is a viscoelastic material the observed stress is influenced by the rate of loading (Van Driel *et al.*, 2000). So, whilst these two independent studies may show similar results, many other experiments have found vastly different Young's modulus values for the PDL.

2.5 Orthodontic Tooth Movement

One important clinical consequence of mechanical adaptation of bone is orthodontic tooth movement, which occurs due to site-specific resorption and formation of alveolar bone (Cattaneo *et al.*, 2009). The crown loading conditions required to move teeth during orthodontic treatment are reasonably well understood (Middleton *et al.*, 1996a), typically with low continuous forces of around one newton applied for weeks at a time (Toms *et al.*, 2002b). Load transfer from the teeth to the surrounding bone is influenced by the PDL. Whilst bone remodelling has been widely investigated in long bones, the presence of the PDL makes direct application of these theories to alveolar bone remodelling more difficult.

Functional masticatory forces are typically hundreds of newtons applied for less than one second whereas orthodontic forces are typically low continuous forces around one newton applied for weeks (Toms *et al.*, 2002b). Light continuous forces will be perceived as intermittent by the periodontium which is important since bone remodelling only occurs in the presence of dynamic loads (Turner & Pavalko, 1998; Cattaneo *et al.*, 2009). Light continuous forces are required since they only partially obstruct the PDL vasculature, whereas heavy forces would choke the vessels preventing oxygen and nutrients being supplied to the surrounding tissues, leading to necrosis and hyalinisation of the PDL, and causing undermining bone resorption (Toms *et al.*, 2002a).

A number of different hypotheses have been suggested regarding the biomechanical nature of orthodontic tooth movement. One of the oldest hypotheses is

known as the “pressure-tension hypothesis” (Schwartz, 1932). This suggests that tooth movement in the direction of applied load compresses the PDL on the side to which the tooth is moved and stretches it on the opposite side. This leads to symmetric zones of compression and tension occurring in the periodontium, with the compression leading to bone resorption and tension causing bone formation (Cattaneo *et al.*, 2005, 2009). However, this hypothesis is not in agreement with how bone adaptation is generally understood (Melsen, 2001). To test this pressure-tension hypothesis Cattaneo *et al.* (2005) developed an FE model to examine the stress distribution in the periodontium after the application of an orthodontic load. They concluded that orthodontic tooth movement could not be explained simply by compression and tension in the direction of the applied load.

A second hypothesis regarding orthodontic tooth movement is the “alveolar bending hypothesis” first reported by Baumrind (1969). This suggests that as well as deforming the PDL, tooth movement also causes deformation of the alveolar bone. In this hypothesis, the walls of the tooth socket behave like cantilever beams, that is, they are essentially fixed at one end (towards the apex) and free at the other (towards the tooth crown). When an orthodontic load is applied, this displaces the free end and, since the other end is fixed, a slight bending of the tooth socket walls occurs. The bone on the side to which the tooth is pushed is bent away from the tooth and the bone on the other side is pulled towards the tooth. A simplified representation of this is shown in Figure 2.11

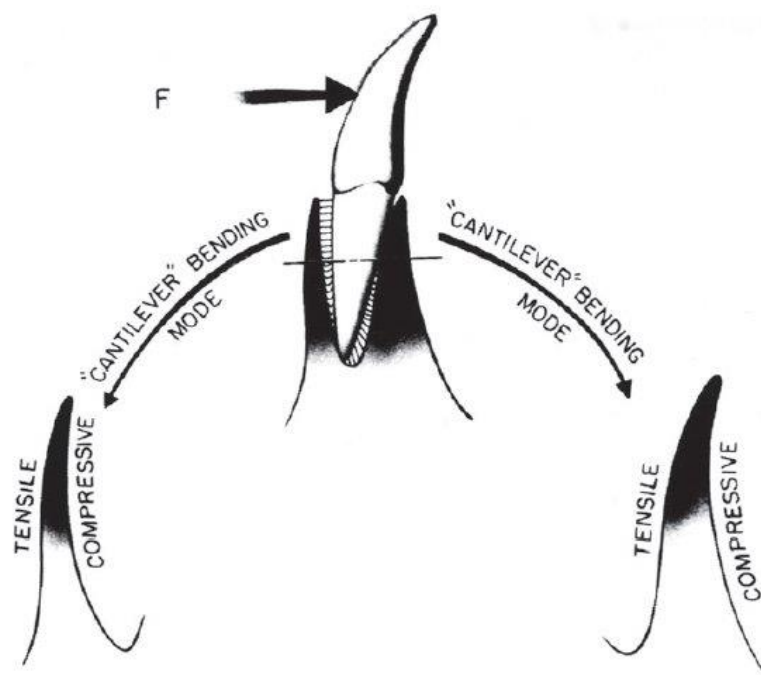


Figure 2.11 Schematic representation of bending of the alveolar bone caused by an orthodontic load (Meikle, 2006: P. 228: Fig. 7).

The alveolar bending hypothesis explains bone remodelling building on an idea initially proposed by Frost (1964), and further developed by Currey (1968). According to Currey (1968) strain gradients are responsible for determining the nature of bone adaptation where bone is added to a surface if, under the application of a load, the strains in the bone become more tensile with depth from the surface. Conversely, bone is removed if strains become less tensile with depth. Applying this idea to the alveolar bending hypothesis, bone would be added to the compressive surfaces of the alveolar bone and removed from the tensile surfaces causing the position of the tooth to move in the direction of the applied load.

More recently, a third hypothesis has been suggested by Melsen (2001) which is intended to match orthodontic tooth movement with orthopaedic bone remodelling in accordance with Frost's mechanostat theory (Frost, 1987), in which low strain leads to bone resorption and high strain leads to bone formation. The hypothesis suggested by Melsen (2001) is the "stretched fibre hypothesis". Typically teeth move in the direction of the applied force. The pressure-tension hypothesis assumes that displacement of the tooth in its socket compresses the alveolar bone in that direction and this bone is then resorbed and new bone is formed on the opposite side. However, Melsen (2001) suggests that this might not be the case due to the elastic fibres in the PDL. These PDL fibres will be compressed on the side to which the tooth is pushed, and stretched on the opposite side. Thus the PDL fibres will only exert force on the surrounding bone where they are in tension, not where they are in compression. Therefore, the PDL will provide little resistance to tooth movement in the direction of the applied force and so will transfer negligible load to the alveolar bone on that side. Conversely, the fibres will be stretched on the opposite side and thus the applied load will be essentially transferred there. The mechanostat theory can then be used to explain orthodontic tooth movement: under-loading of the alveolar wall causes bone resorption, while the load exerted by the stretched PDL fibres on the opposite side causes bone formation. A schematic representation of the stretched fibre hypothesis is shown in Figure 2.12. If this hypothesis is correct, then it would be important to include the fibres of the PDL in FE models, especially when investigating orthodontic tooth movement. Cattaneo *et al.* (2005, 2009) created finite element models to test these hypotheses and concluded that this third one most closely matched their results, however these models did not contain PDL fibres.

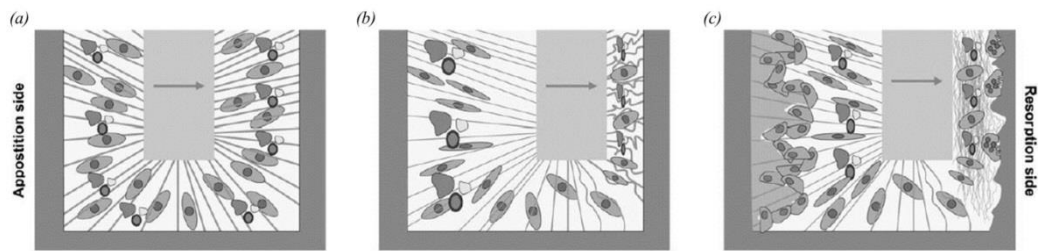


Figure 2.12 Schematic representation of the stretched fibre hypothesis (Melsen, 2001): (a) an orthodontic load is applied; (b) PDL fibres are stretched on one side and compressed on the other; (c) bone formation occurs on the side where the fibres are stretched and resorption occurs on the side where they are compressed (Henneman *et al.*, 2008: P. 301: Fig. 2).

Whether orthodontic tooth movement is triggered by strains in the alveolar bone, or whether it is actually triggered by strains in the PDL remains unclear (Cattaneo *et al.*, 2005). A number of previous FE models have shown strains in the alveolar bone to be much lower than those predicted by Frost's mechanostat (*e.g.* Middleton *et al.*, 1996; Bourauel *et al.*, 1999, 2000; Jones *et al.*, 2001). Due to this, many authors believe orthodontic tooth movement is actually triggered by strains in the PDL (*e.g.* Chen *et al.*, 2014). It is suggested that tooth displacement within the periodontium upsets the homeostatic environment of the PDL which is what triggers orthodontic tooth movement (Krishnan & Davidovitch, 2006). However, a synchrotron study by Dalstra *et al.* (2015) showed that the surface of the alveolar bone is not smooth and so they suggested that perhaps FE models have underestimated the strains in the tooth sockets by not accounting for local stress and strain concentrations due to the structure of the alveolar bone. So, in order to better understand the strains caused by orthodontic tooth movement more detailed finite element models are required.

Chapter 3

Finite Element Modelling of a Single Tooth with Fibrous Periodontal Ligament

3.1 Introduction

When simulating masticatory and orthodontic loads with a finite element model of the mandible or cranium, the way in which the periodontal ligament (PDL) is modelled can have a significant influence on the results produced. Whether or not to include the PDL, as well as what material properties to assign, is the subject of much debate throughout the literature (*e.g.* Wood *et al.*, 2011; Gröning *et al.*, 2011a, 2012b; Gröning & Fagan, 2012; Grosse *et al.*, 2012). However, accurately modelling the PDL may be the key to understanding functional bone adaptation in the mandible (Daegling and Hylander, 2000).

An important clinical consequence of bone adaptation in the mandible is orthodontic tooth movement which occurs due to site-specific resorption and formation of alveolar bone. There is still much debate as to the exact mechanisms responsible for triggering orthodontic tooth movement (see Section 2.5). Three hypotheses relating to the strains in the alveolar bone are the “pressure-tension hypothesis” (Schwartz, 1932), the “alveolar bending hypothesis” (Baumrind, 1969) and the “stretched fibre hypothesis” (Melsen, 2001). These hypotheses are illustrated in Figure 3.1.

Although the PDL is known to have a fibrous structure and nonlinear material properties (Berkovitz, 1990; Dorow *et al.*, 2002, 2003), when it is included in finite element models it is usually represented as a layer of solid material with isotropic material properties (Fill *et al.*, 2012). Some researchers have attempted to include more accurate material properties for the PDL in finite element models (*e.g.* Cattaneo *et al.*, 2005, 2008, 2009), however, only a few have attempted to include its fibrous structure (Atmaram & Mohammed, 1981; Witzel *et al.*, 1998; Provatidis, 2000; Katona & Qian, 2001; Qian *et al.*, 2001; Limbert *et al.*, 2003; Meyer *et al.*, 2010). Some of these studies (Provatidis, 2000; Qian *et al.*, 2001; Meyer *et al.*, 2010) have investigated orthodontic tooth movement, but did not focus on the mechanical stimuli for alveolar bone remodelling. Other studies have examined orthodontic bone remodelling (*e.g.* Cattaneo

et al., 2005, 2009) but did not include the fibrous structure of the PDL. So far there have been no finite element models used to examine these hypotheses which include a fibrous PDL. Therefore, this study involved developing a method of representing the fibrous structure of the PDL in finite element models which could then be used to assess the merits of the three hypotheses shown in Figure 3.1

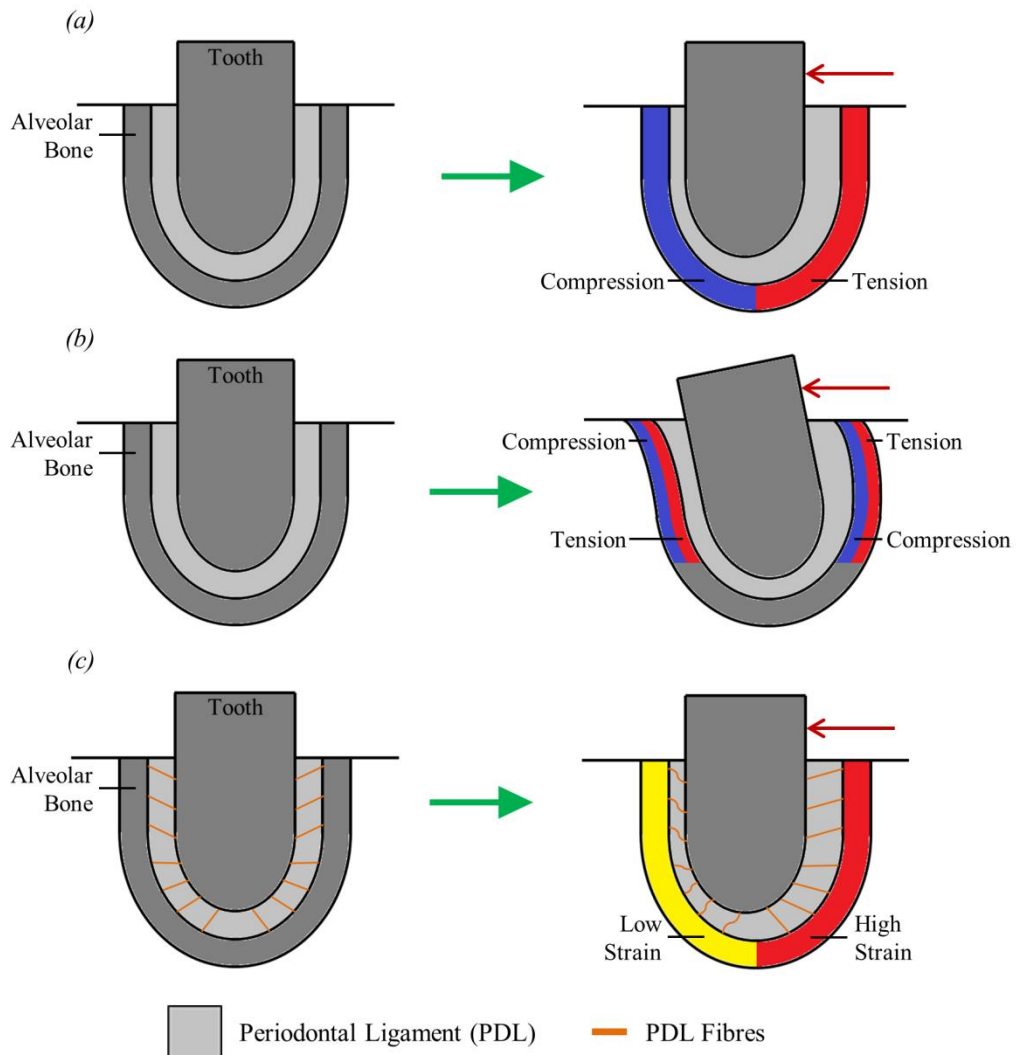


Figure 3.1 Simplified two dimensional representation of a tooth-PDL-bone complex illustrating three hypotheses for strain-based bone remodelling during orthodontic tooth movement: (a) “pressure-tension hypothesis” showing tooth displacement leading to compression and tension in the surrounding bone; (b) “alveolar bending hypothesis” showing tooth movement causing bending of the alveolar bone; (c) “stretched fibre hypothesis” showing stretching and compression of PDL fibres leading to low and high strain areas in the surrounding bone. The red arrows indicate the direction of the applied orthodontic force.

The overall aim of this study is to investigate the significance of including the fibres of the PDL in FE models when applying functional occlusal load and orthodontic loads. An idealised three-dimensional single tooth FE model was developed to test the effect of including the PDL fibres. Using the same basic model, three different representations of the PDL were tested: no PDL, solid PDL, and fibrous PDL. The models were validated against previously reported experimental studies, and a sensitivity analysis was conducted to examine the effect of altering the material properties. A number of different loads were then applied to each of the three models, and the strains produced in the surrounding bone were compared. The results from this single tooth model give an indication as to whether or not the increased time and effort to include PDL fibres would be justified in whole mandible models.

3.2 Materials and Methods

3.2.1 Model Creation

An idealised single tooth FE model was created using ANSYS software (version 13.0, ANSYS Inc., Canonsburg, PA, USA). The size and shape of the model, shown in Figure 3.2, were chosen to be comparable to a human tooth and are in keeping with similar models (*e.g.* Katona & Qian, 2001). The tooth root is surrounded by a uniform layer to represent the PDL, which is in turn surrounded by another uniform layer to represent the alveolar bone, both 0.2mm thick (Katona & Qian, 2001; Borák *et al.*, 2011). The tooth, PDL and alveolar bone components were then surrounded by a block to represent the mandibular bone.

The tooth and alveolar bone volumes were meshed with 10-noded high-order tetrahedral structural solid elements (SOLID187) (Kohnke, 2009). The mandibular bone block was modelled as trabecular bone surrounded by a 2.5mm thick layer of cortical bone, as shown in Figure 3.2. The trabecular bone was meshed with the same elements as the tooth and alveolar bone (SOLID187) (Kohnke, 2009) whereas the surrounding cortical bone was meshed using 6-noded triangular structural shell elements (SHELL281) (Kohnke, 2009). Since the bone in this model was idealised as a solid block, the regions required to be cortical bone were all thin flat shapes and were thus ideally suited to being modelled with shell elements.

Two different models were created, varying only in how the PDL was modelled: a solid PDL model and a fibrous PDL model. In the solid PDL model, the PDL volume

was again meshed with the same 10-noded elements (SOLID187) (Kohnke, 2009). Within the fibrous PDL model, to represent the fibre-reinforced matrix structure, the volume of the PDL was first meshed the same as for the solid PDL model. The PDL fibres were then added to the model using tension-only three-dimensional spar elements (LINK10) (Kohnke, 2009). These link elements connected nodes on the junction between the alveolar bone and PDL with nodes on the junction between the tooth root and PDL. In reality, these fibres show a complex arrangement throughout the PDL, however, in this model the fibres were given the simplified structure shown in Figure 3.2. The orientations of the fibres in this model were chosen based on published histological descriptions but are probably more vertical than would be the case in real PDL (Meyer *et al.*, 2010). In total, both models contained 101,326 higher order tetrahedral elements and 1,528 shell elements. The fibrous PDL model also had an additional 448 link elements.

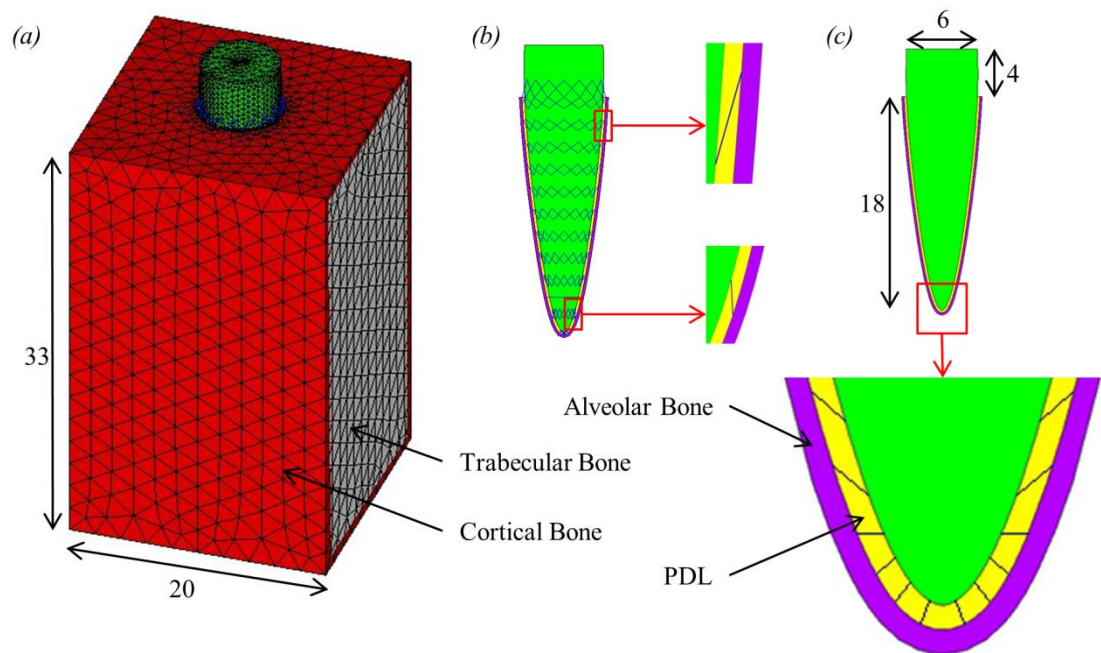


Figure 3.2 Single tooth FE model including dimensions in millimetres: (a) the whole three-dimensional single tooth model; (b) section through tooth, PDL and alveolar bone showing the location of the link elements which span the PDL layer connecting the tooth and alveolar bone; (c) section through the centre of the model showing the tooth, PDL and alveolar bone including an expanded view of the apex region.

Material Properties

The material properties assigned to the fibrous PDL model were obtained from previous studies (Table 3.1). The tooth was not separated into different components and was modelled entirely as dentin. This simplification has been used in previous studies (*e.g.* Poppe *et al.*, 2002; Cattaneo *et al.*, 2008) and is justifiable since it is strain in the bone (rather than the tooth) which is of interest here. The tooth, PDL and bone were all assumed to be homogeneous, isotropic and linear elastic materials. Although bone is known to have anisotropic material properties it is commonly simplified to isotropic in FE models and validation studies have determined that meaningful results can still be obtained from isotropic models (*e.g.* Gröning *et al.*, 2009; Gröning *et al.*, 2012a; Gröning *et al.*, 2012b). Similarly, the PDL is known to have nonlinear material properties yet most previous models which include the PDL, model it as a linear elastic material (Fill *et al.*, 2012).

For the PDL fibres, as well as defining the mechanical properties, it was necessary to specify the cross-sectional area and initial strain of the link elements. Approximately 50 to 75 % of the PDL tissue volume is made up of the PDL fibres (Dorow *et al.*, 2003). Therefore, the cross-sectional area of the link elements was calculated so that the combined volume of the link elements would be between 50 and 75 % of the PDL volume in the model. From this the cross-sectional area was chosen to be 0.06mm^2 . This value makes the link elements in the model one to two orders of magnitude thicker than the collagen fibres found in a real PDL (Berkovitz, 1990; Meyer *et al.*, 2010). This is due to the fact that the number of modelled PDL fibres is well below the number of fibres in the real PDL. No reliable data was available to suggest a suitable value for any initial strain of the link elements and so it was defined as zero.

The solid PDL model was constructed with the same method as the fibrous PDL model, except it did not include the link elements representing the PDL fibres. In order to make a fair comparison between the two models, it was necessary to adjust Young's modulus value given to the PDL component of the solid PDL model, while all other material properties remained the same. This value was adjusted so that the overall effective elastic modulus of the PDL layer in the two models was the same. From this it follows that any differences observed in the stress and strain values between the solid PDL and fibrous PDL models could be attributed to the structural difference, *i.e.* the presence or absence of PDL fibres, between the two models (rather than to the difference in the elastic modulus of the PDL) (Atmaram & Mohammed, 1981).

Table 3.1 Mechanical properties assigned to each material in the fibrous PDL model.

Component	Young's Modulus (MPa)	Poisson's Ratio
Trabecular bone ^a	56	0.30
Cortical bone ^b	17 000	0.30
Tooth ^b	17 000	0.30
PDL matrix ^c	1	0.45
PDL fibres ^d	1 000	0.35

^a Misch *et al.* (1999).

^b Gröning *et al.* (2011a).

^c Jones *et al.* (2001), Qian *et al.* (2001).

^d Gautieri *et al.* (2012), Katona and Qian (2001), Meyer *et al.* (2010), Rees and Jacobsen (1997).

As a criterion for adjusting Young's modulus we used tooth displacement, *i.e.* the two models were assumed to have the same overall effective elastic modulus when they showed the same tooth displacement under identical loading conditions. Tooth displacement was defined as the change in distance between the most apical node on the tooth root and the corresponding node on the alveolar bone (Katona & Qian, 2001). Thus, under a load of 500 N, the tooth displacement for the fibrous tooth model was 0.0703mm. This value would seem reasonable when compared to the vertical intrusion of 0.12mm cited by Borák *et al.* (2011) from an experiment by Kato (1982). To get the same displacement for the solid PDL model, it was found necessary to use a Young's modulus value of 12.2 MPa for the PDL layer (determined through the ANSYS optimisation facility).

Loading and Boundary Conditions

In single tooth FE models, one common way to apply the boundary conditions is simply to fix all nodes on the two opposing sides of the model to which the rest of the mandible would be connected (*e.g.* Qian *et al.* (2001)). However, a number of studies have reported that over-constraining a model can lead to inaccurate results (*e.g.* Marinescu *et al.* 2005). Therefore, this method was not used here. Instead, the boundary conditions illustrated in Figure 3.3 were applied. Briefly, all of the nodes around the edge of these two sides were constrained in the x-direction (mesiodistal, Figure 3.3) to represent the increased stiffness in this location due to the presence of cortical bone. The nodes on the

rear corners on the base of the model were also constrained in the y-direction (coronoapical) and the nodes on the front corners of the base were constrained in all degrees of freedom. This prevented rigid body translation of the model, while still allowing some deformation in the z-direction (buccolingual).

Three different types of load were applied separately to the model: a 500 N occlusal load and two different 1 N orthodontic loads. The occlusal load was applied as a single vector, point load, acting on the node at the centre of the tooth crown, parallel to the long axis of the tooth. Although occlusal loads may be more complex than this, the loading patterns and strain distribution in the tooth itself were not of interest in this study, therefore this simplification was considered acceptable in this current analysis. A load of 500 N was chosen to represent a maximal human bite force (Daegling & Hylander, 1997; O'Connor *et al.*, 2005; De Abreu *et al.*, 2014). To simulate an orthodontic load, a point force was applied to the node half way between the top of the bone and the top of the tooth on the far side of the tooth, as shown in Figure 3.3. The load applied was chosen to be 1 N to represent a typical load used during orthodontic treatment (Van Driel *et al.*, 2000). Two different orthodontic loads were simulated by varying the direction of the force applied to the node: a mesiodistal load and a buccolingual load.

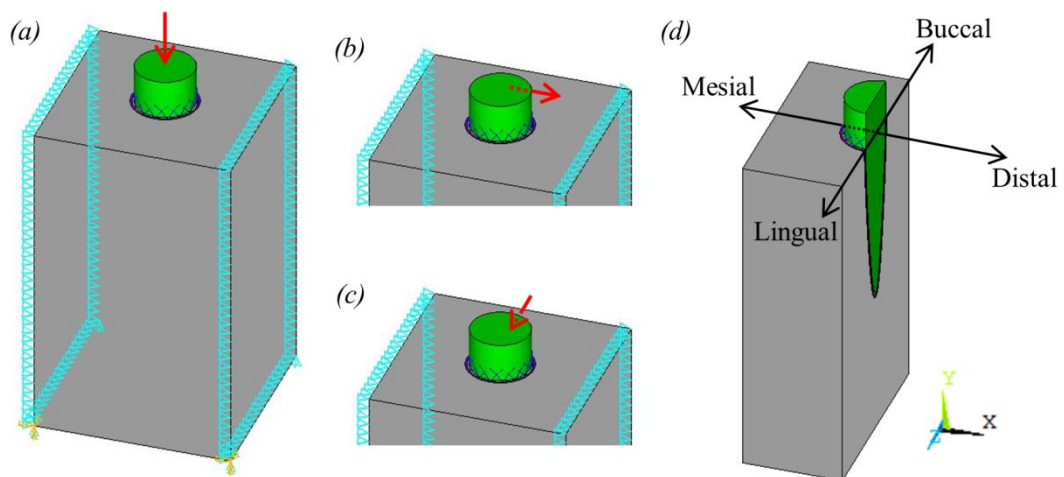


Figure 3.3 Tooth model showing loading and boundary conditions applied, where triangles represent constraints and red arrows represent applied forces: (a) vertical occlusal load; (b) buccolingual orthodontic load; (c) mesiodistal orthodontic load; (d) section through centre of tooth model showing a typical plane from which strain results were taken.

3.2.2 Model Testing

A number of tests were carried out to assess the suitability of this idealised single tooth model. First, a model without a PDL was developed to highlight the importance of including the PDL in dental FE models. As well as testing the results from a no PDL model, four key issues were investigated with respect to model testing: boundary conditions, mesh convergence, model validation, and sensitivity to changes in the PDL. The details of this model testing are given here.

No PDL Model

The primary aim of this research is to investigate the significance of including the fibres of the PDL in FE models. However, some models do not include PDL at all, yet alone model its fibrous structure, *i.e.* they assume the teeth are attached directly to bone. This is especially the case in models of whole mandibles or crania, (*e.g.* Marinescu *et al.*, 2005; Boryor *et al.*, 2008). Although almost all single tooth models do include the PDL, in order to show the importance of modelling the PDL in dental FE models, a model was developed without a PDL. This no PDL model was developed directly from the solid PDL model, through appropriate changes in the material properties. The same shape was used but the material assigned to some of the volume meshes was changed. The tooth, cortical shell and trabecular bone region from the solid PDL model were left the same. In order to remove the PDL, the PDL volume from the solid PDL model was remeshed to be alveolar bone, while the alveolar bone volume was remeshed to be trabecular bone. The boundary conditions were left the same and a 500 N occlusal load was applied. The results from the no PDL model were then compared to the solid PDL model to show the importance of including a PDL. To compare the results, the trabecular bone region was cut in the buccolingual direction and then the strains in this region were compared visually for the two models.

Boundary Conditions

Boundary conditions applied to FE models have the potential to greatly influence the results obtained and so a model was also developed to test the suitability of the boundary conditions applied to the single tooth model. The boundary conditions applied around the edges of the single tooth model were designed to replace the rest of the mandibular bone, which has not been modelled, and so to represent the increase support which would be given to a tooth as part of the whole mandible. In order to test whether

or not the boundary conditions applied are appropriate, two additional simple “U-shaped” models were developed: a solid PDL U-shaped model and a fibrous PDL U-shaped model. The fibrous PDL U-shaped model is shown in Figure 3.4. As in the case of the single tooth model, the only difference between these two U-shaped models is how the PDL is modelled.

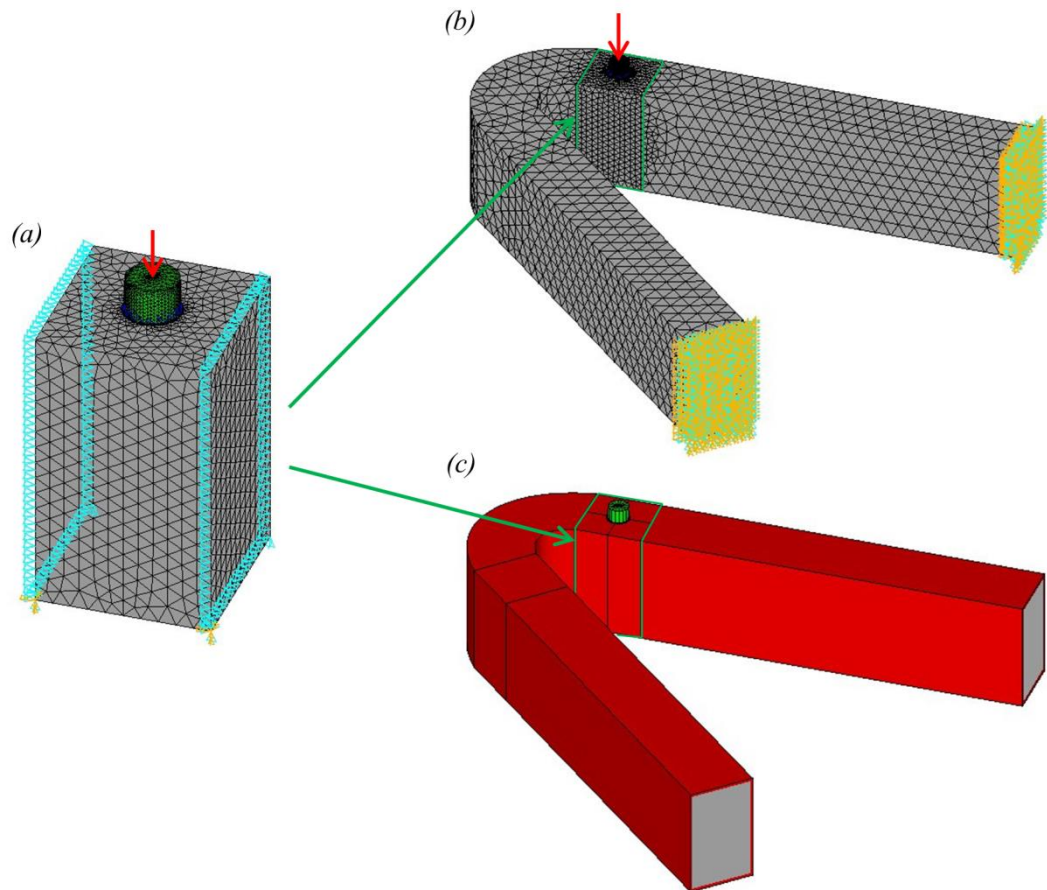


Figure 3.4 Original single tooth model and U-shaped tooth model: (a) original single tooth model showing load and boundary conditions; (b) finite element mesh for U-shaped model showing the location of the original model within the U-shaped model along with the vertical occlusal load and boundary conditions applied; (c) area plot showing areas meshed with shell elements.

To create the U-shaped models, additional bone was added to the original models to approximately represent the remainder of the mandible. The dimensions of the U-shaped models were chosen to approximate the size and shape of a typical human mandible from a superior view (Figure 3.5). For the U-shaped models, the single tooth model was assumed to represent the first lower right premolar. The additional bone gave the model a further 20,904 elements. These elements included 17,522 high-order

tetrahedral elements (SOLID187) (Kohnke, 2009) and 3,382 shell elements (SHELL281) (Kohnke, 2009). The total number of elements in the solid PDL U-shaped model was 123,758, with there being an additional 448 link elements (LINK10) (Kohnke, 2009) in the fibrous PDL model. A 500 N occlusal load was applied in the same way as the single tooth model. All nodes on the two end faces of the model, which are away from the region of interest around the tooth, were fixed in all degrees of freedom. The loading and boundary conditions applied to the model can be seen in Figure 3.4.



Figure 3.5 Superior view of a replica human mandible used to approximate the dimensions for the U-shaped models.

In order to test the influence of the boundary conditions on the single tooth model, results from the single tooth model were compared to those from the U-shaped model for both solid and fibrous PDLs. Two sets of results were compared: firstly, the vertical tooth displacement, and secondly, the minimum principal strain in the trabecular bone region of the single tooth model and the corresponding region in the U-shaped model.

Convergence

A mesh convergence test was also performed for both solid and fibrous PDL models. The model was remeshed using a smaller element size thus increasing the number of elements in the model from approximately 100,000 to just over 1.9 million. The tooth displacements from these two models were then compared to determine whether the models had converged.

Validation

Since this is a very simplified model, stresses and strains would be expected to differ from those in a real tooth and so direct validation of these against experimental results is not possible. However, it would still be expected that the tooth displacement observed would be comparable to previously published data. Therefore, to validate the model, the tooth displacement was compared to previously report values in the literature.

Sensitivity Study

A sensitivity analysis was carried out to assess the effect of altering the material properties assigned to the PDL component using the fibrous PDL model. Five values required to specify the PDL were tested, namely: Young's modulus and Poisson's ratio of the solid component, and Young's modulus, cross-sectional area and initial strain of the link elements. These values were each varied individually, keeping all other values the same, and the subsequent tooth displacements produced were compared.

3.2.3 Solid PDL versus Fibrous PDL

The aim of this study was to investigate the effect of including the fibrous structure of the PDL in FE models when applying either occlusal or orthodontic loads. After all model testing was completed, the results obtained from the solid PDL model were compared to the results obtained from the fibrous PDL model. As explained in Section 3.2.1, the tooth displacement and thus the overall elastic modulus of the PDL was defined as the same for both models so that the strain results could be compared. To provide an initial comparison of the results contour plots were produced so that the magnitude and distribution of strains in the two models could be compared by eye. Following this, to provide a more precise comparison of the results nodal strain graphs were plotted.

Nodal strain results were taken from three regions within the model: the inside surface of the alveolar bone (*i.e.* adjacent to the PDL), the outside surface of the alveolar bone (*i.e.* adjacent to the trabecular bone) and a line through the trabecular bone itself. For the occlusal load and buccolingual orthodontic load the results were taken along a line of nodes through the centre of the tooth model in the buccolingual direction (see Figure 3.3). Similarly, for the mesiodistal orthodontic load the results were taken along a line of nodes through the centre of the tooth model in the mesiodistal direction.

The FE mesh was identical for both the solid and fibrous PDL models and so the same nodes were used to plot the results for both models. The nodes were selected as follows. For the inside surface of the alveolar bone, all non-midside nodes along the chosen plane were selected. Those nodes to which link elements were connected were then removed, since strains at these points were expected to be artificially high. Similarly, nodes at the top of the model, near to the shell elements, and nodes at the apex were also removed from consideration to avoid any boundary artefacts. The remaining nodes were used to plot the results. For the outside surface of the alveolar bone, all non-midside nodes along this line were used to plot the results, except for at those at the top near the shell elements and at the apex. Finally, for the line through the trabecular bone, suitable non-midside nodes were selected (approximately 1 mm from the alveolar bone) by eye since there was no smooth line of nodes through this region. However, since these nodes were the same in all models, the strain distributions could still be compared with confidence.

Maximum and minimum principal strains were extracted along each of these regions for both solid and fibrous PDL models and these results were plotted against each other for visual comparison. For the solid PDL model, the nodal results were plotted and a smooth line was drawn connecting the points. However, for the fibrous PDL model, strain results obtained at the inside and outside surfaces of the alveolar bone were not smooth but rather contained fluctuating values due to strain concentrations developing at the location of the link elements. In a real PDL these high peak strains would not develop due to the much greater number of PDL fibres than represented in this model which would cause a smoother distribution of strain. Since these peak strains are not biologically realistic, rather than simply connecting the points, a third order trend line was plotted through the data to smooth out the results. This was performed for the results from the inside and outside surface of the alveolar bone for the fibrous PDL model in all three load cases. This smoothing was not necessary for the

trabecular bone nodal results from the fibrous PDL model, as these nodes were sufficiently far away from the location of the link elements to not be effected by the local stress concentrations.

3.3 Results

3.3.1 Model Testing

Five key issues were investigated with respect to model testing: no PDL model, boundary conditions, mesh convergence, model validation and sensitivity to changes in the PDL. The results from these five tests are presented here.

No PDL Model

Figure 3.6 shows the strain in the mandibular bone for the no PDL and solid PDL models. From visually comparing the two plots it can be seen that including the PDL in models alters both the magnitude and distribution of strain in the trabecular bone region especially in the region surrounding the alveolar bone. The presence of the PDL reduces the strain around the whole of the alveolar bone, especially in the alveolar crest and apex regions.

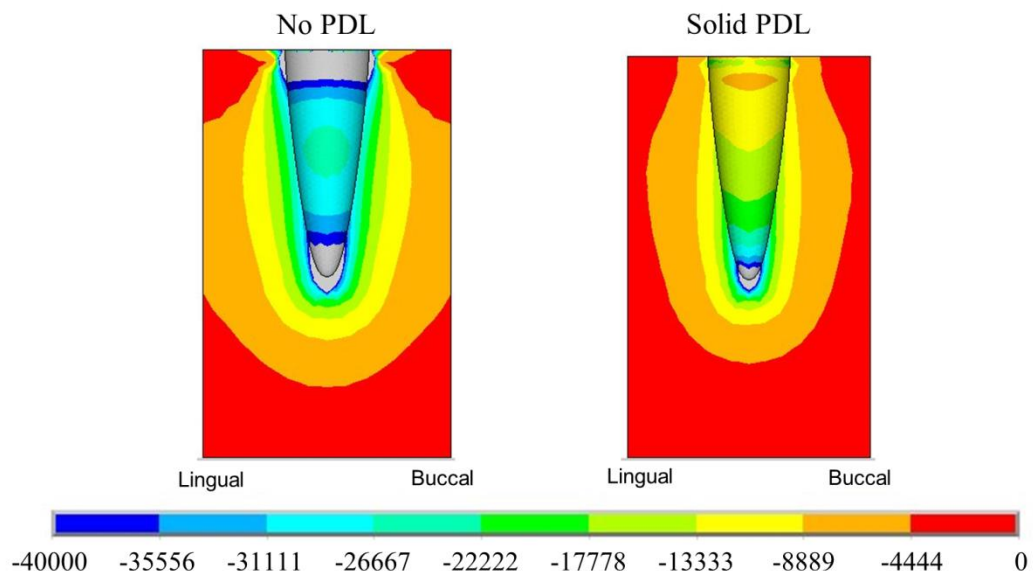


Figure 3.6 Contour plots showing the minimum principal microstrain in the trabecular bone region of the no PDL and solid PDL models due to the 500 N occlusal load.

Boundary Conditions

The results from the boundary conditions testing are shown in Table 3.2. These results show that the vertical tooth displacement, defined as the change in distance between the most apical node on the tooth root and the corresponding node on the alveolar bone, was very similar between the two models: for both solid and fibrous PDLs there was less than 2 % reduction in the vertical tooth displacement.

Table 3.2 Vertical tooth displacement results for original models and u-shaped mandible models.

Test	Model	Vertical Displacement (mm)			Width of Tooth Socket after Displacement (mm)	Vertical Tooth Displacement (mm)
		Tooth Apex	PDL Apex	Tooth Socket Apex		
Solid PDL	Original	-0.205	-0.134	-0.134	0.200	0.070
	U-Shaped	-0.448	-0.379	-0.378	0.200	0.069
Fibrous PDL	Original	-0.207	-0.137	-0.137	0.200	0.070
	U-Shaped	-0.451	-0.381	-0.381	0.200	0.069

^a Katona & Qian (2001)

The minimum principal strain results, shown in Figures 3.7 and 3.8, show that the boundary conditions do influence the results in the regions near to them. In both Figures 3.7 and 3.8, the top row of plots illustrate that the boundary conditions influence both the magnitude and distribution of strain in the outer regions of the trabecular bone. However, the bottom row in both figures show that in the region of interest, near to the alveolar bone, there is little difference between the two models suggesting that the boundary conditions do not adversely affect the results here.

Convergence

Tooth displacement results were compared for both solid and fibrous PDL convergence models and were seen to only vary by around 1 % compared to the original.

Validation

To validate these models, tooth displacement results from the original solid and fibrous PDL models (0.0703 mm) were compared to those reported in literature. In a finite element study, Borák *et al.* (2011) reported a vertical intrusion of 0.12 mm for a healthy human mandibular premolar tooth under a maximum bite force, based on an

experimental study conducted by Kato (1982). Similarly, Ichim *et al.* (2007) conducted a finite element study with a whole human mandible and adjusted the value of the PDL in their model until the canine intrude 0.3 mm, based on *in vivo* tooth mobility data reported by Mühlemann (1967). For the models used in this study, tooth displacement is calculated as the change in distance between the most apical node on the tooth root and the corresponding node on the alveolar bone (Katona & Qian, 2001). This is essentially measuring the change in thickness of the PDL at the tooth apex, therefore it gives a maximum possible value of 0.2 mm for the tooth displacement in these models. This is not how tooth displacement is measured *in vivo* and so it is difficult to compare this value with those values determined experimentally. However, since the tooth displacement for these models (0.0703 mm) was seen to be of a similar order of magnitude to experimental values used with other finite element models (0.12 mm and 0.3 mm), it was concluded that these models gave a reasonable tooth displacement for the purpose of this study.

Sensitivity Study

The sensitivity analysis to investigate the effect of altering the material properties assigned to the PDL component was only conducted with the fibrous PDL model. The results of this are shown in Table 3.3. The sensitivity analysis results show that the value assigned to Poisson's ratio of the solid PDL component does not have much influence on the results. Conversely, all four of the other parameters considered do appear to have a noticeable impact on the results obtained. Altering the value assigned to Young's modulus of the solid PDL component has more influence on the results as the value gets higher. A 10 times increase in this value from 0.1 MPa to 1 MPa causes approximately a 9 % reduction in the vertical tooth displacement, whereas a 10 fold increase from 10 MPa to 100 MPa causes almost a 90 % reduction in displacement. Likewise, the influence of adjusting the Young's modulus of the link elements becomes greater as its value increases. Both the cross sectional area and the initial strain assigned to the link elements also have an important influence on the tooth displacement. Doubling the cross sectional area approximately halves the tooth displacement and a 10 times increase in initial strain causes almost a 60 % reduction in tooth displacement.

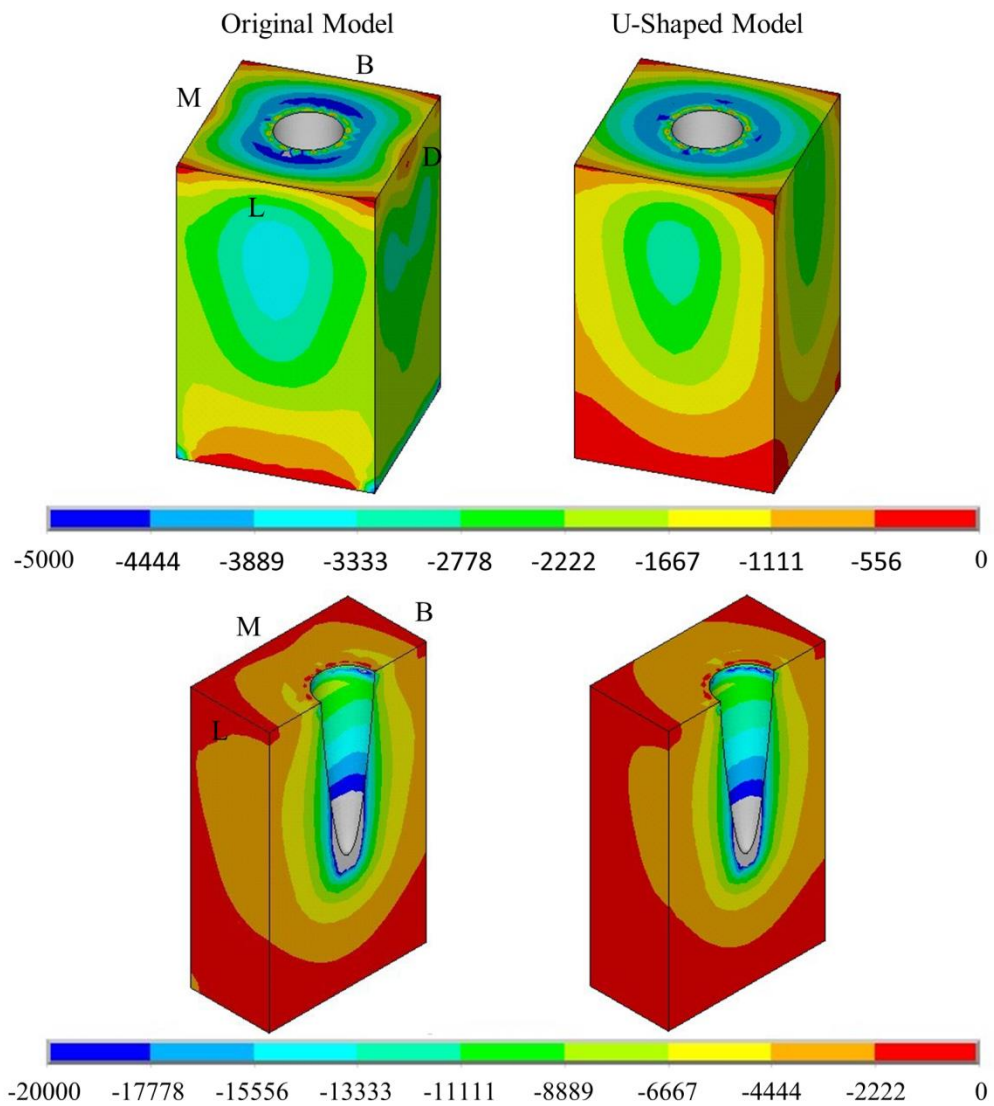


Figure 3.7 Solid PDL model: the minimum principal microstrain distribution in the trabecular bone region of the original single tooth model and the corresponding region of the U-shaped model for the solid PDL models due to the 500 N occlusal load. Directions are shown only on the original model plots but can be inferred for the U-shaped model plots. Directions are represented by M for mesial, D for distal, B for buccal and L for lingual.

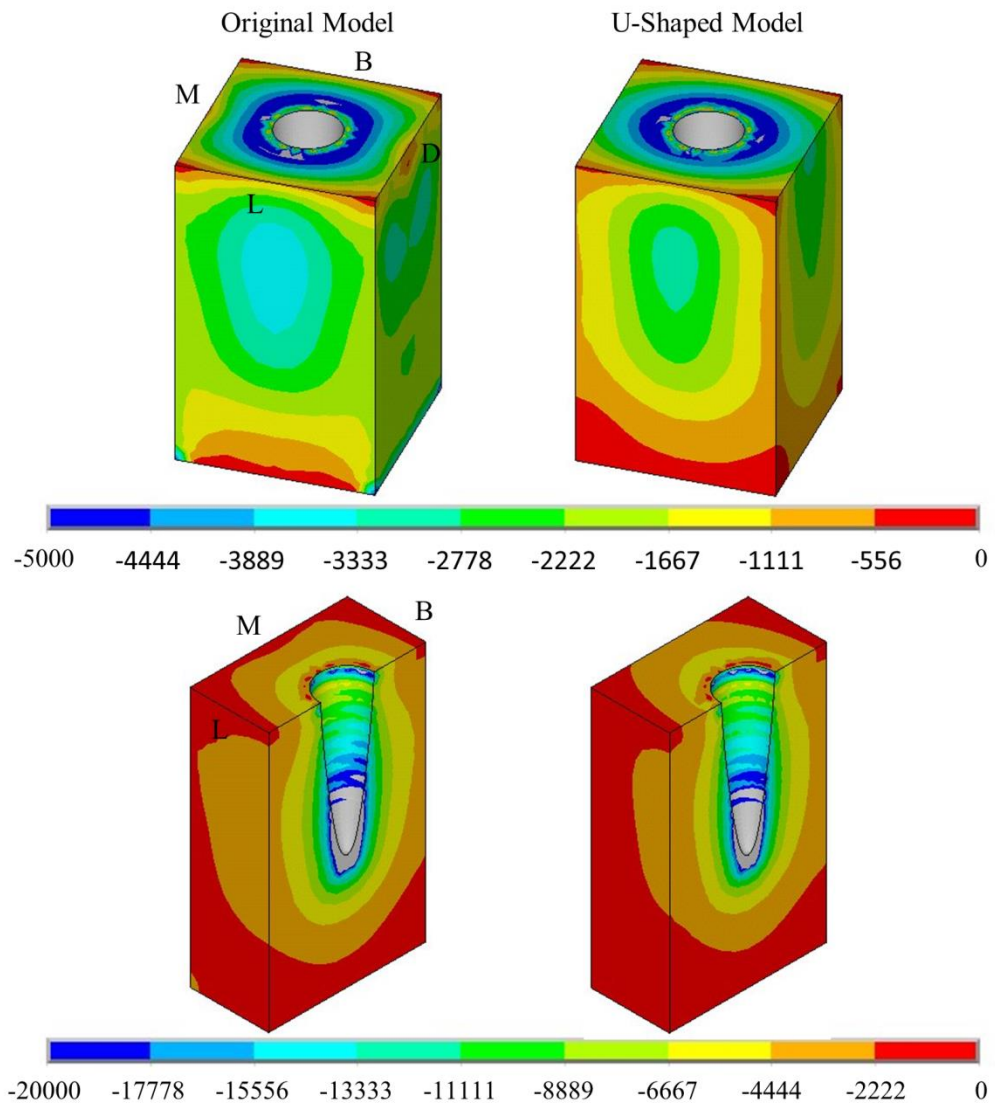


Figure 3.8 Fibrous PDL model: the minimum principal microstrain distribution in the trabecular bone region of the original single tooth model and the corresponding region of the U-shaped model for the fibrous PDL models due to the 500 N occlusal load. Directions are shown only on the original model plots but can be inferred for the U-shaped model plots. Directions are represented by M for mesial, D for distal, B for buccal and L for lingual.

Table 3.3 Results from sensitivity analysis with fibrous PDL model (numbers in bold represent the original model with the material properties shown in Table 3.1).

Test	Value	Vertical displacement (mm)			Width of tooth socket after displacement (mm)	Vertical tooth displacement (mm) ^a
		Tooth apex	PDL apex	Tooth socket apex		
Young's modulus of PDL Matrix (E_{PDL})	$E_{PDL} = 0.1$	-0.215	-0.138	-0.138	0.200	0.077
	$E_{PDL} = 1$	-0.207	-0.137	-0.137	0.200	0.070
	$E_{PDL} = 10$	-0.169	-0.133	-0.133	0.200	0.036
	$E_{PDL} = 100$	-0.128	-0.123	-0.123	0.200	0.005
Young's modulus of PDL fibres (E_{LINK})	$E_{LINK} = 30$	-0.861	-0.139	-0.139	0.200	0.722
	$E_{LINK} = 300$	-0.346	-0.140	-0.140	0.200	0.206
	$E_{LINK} = 1\ 000$	-0.207	-0.137	-0.137	0.200	0.070
	$E_{LINK} = 3\ 000$	-0.157	-0.132	-0.132	0.200	0.025
Poisson's ratio of PDL matrix (ν_{PDL})	$\nu_{PDL} = 0.3$	-0.208	-0.137	-0.137	0.200	0.071
	$\nu_{PDL} = 0.45$	-0.207	-0.137	-0.137	0.200	0.070
	$\nu_{PDL} = 0.49$	-0.203	-0.137	-0.137	0.200	0.066
Cross sectional area of link elements (CSA_{LINK})	$CSA_{LINK} = 0.04$	-0.241	-0.138	-0.138	0.200	0.103
	$CSA_{LINK} = 0.06$	-0.207	-0.137	-0.137	0.200	0.070
	$CSA_{LINK} = 0.08$	-0.189	-0.136	-0.136	0.200	0.053
Initial strain of link elements (ϵ_0)	$\epsilon_0 = 0$	-0.207	-0.137	-0.137	0.200	0.070
	$\epsilon_0 = 0.01$	-0.190	-0.136	-0.136	0.200	0.054
	$\epsilon_0 = 0.1$	-0.114	-0.092	-0.093	0.201	0.022

^a Katona & Qian (2001)

3.3.2 Solid PDL versus Fibrous PDL

Contour plots of maximum and minimum principal strain in the alveolar bone due to the 500 N occlusal load are shown in Figure 3.9. These contour plots show that omitting the fibrous structure from the PDL does have an effect on the distribution of strain in the alveolar bone. Figure 3.9 shows strain on the outside surface of the alveolar bone. Although the link elements are only attached at the inside surface of the alveolar bone, high strain concentrations around the link elements are clearly visible. To remove the effect of these strain concentrations, third order polynomials were plotted through the nodal results from the fibrous PDL model in the alveolar bone in Figures 3.10, 3.11 and 3.12.

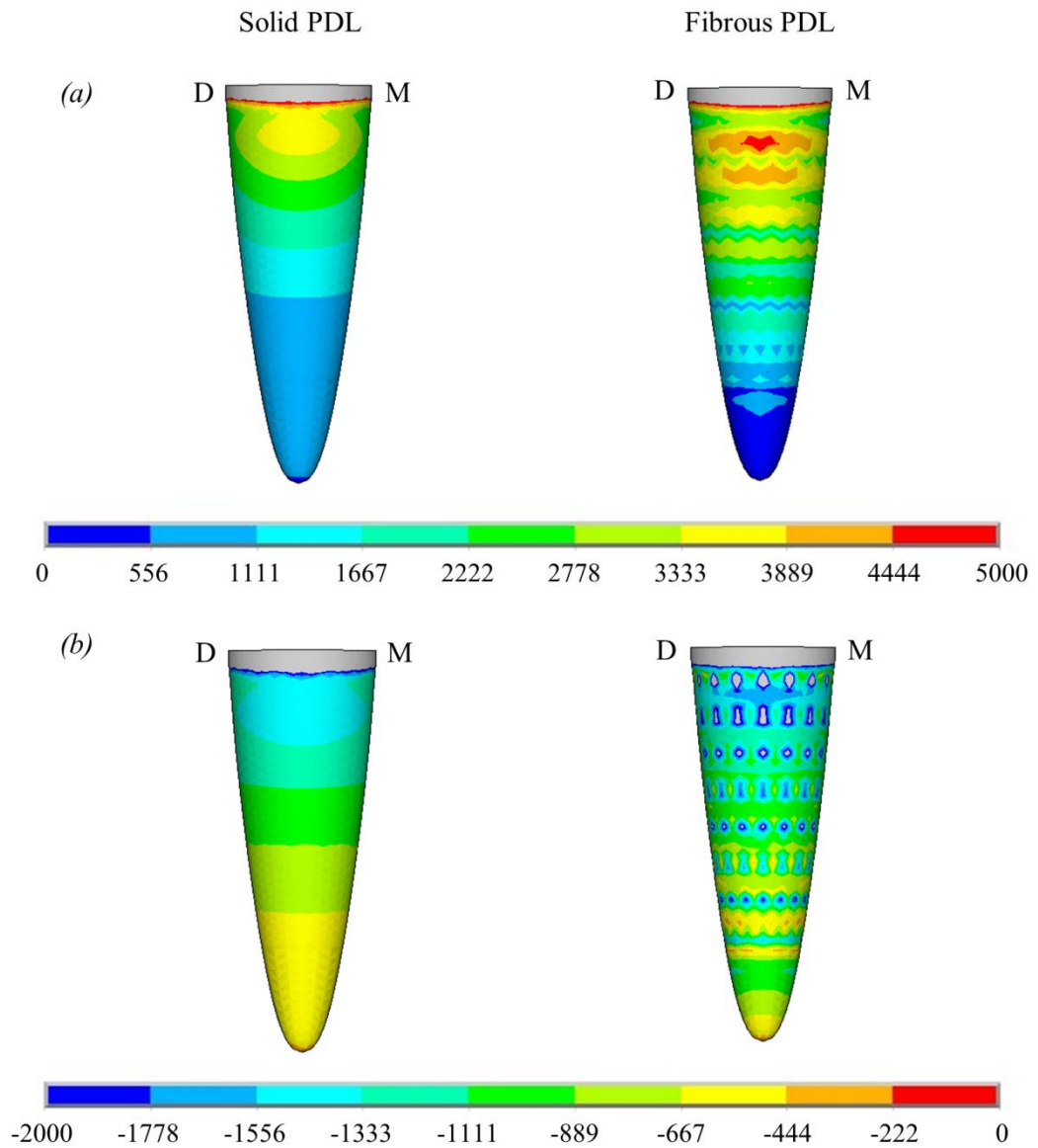


Figure 3.9 Contour plots showing nodal solutions for the principal microstrains on the outside surface of the alveolar bone for the solid PDL and fibrous PDL models due to the 500 N occlusal load: (a) maximum principal microstrain; (b) minimum principal microstrain. Directions are represented by M for mesial and D for distal.

Figures 3.10, 3.11, and 3.12 compare the nodal strain results from the solid and fibrous PDL models for the three load cases. For all graphs of alveolar bone strain, it can be seen that including the PDL fibres in the model affects the results. Similarly, the PDL fibres affect strain in the trabecular bone region for both of the orthodontic load cases. Conversely, for the occlusal load, strain in the trabecular bone region appears unaffected by the inclusion of the fibres.

Occlusal Load

In the case of the occlusal load (Figure 3.10), the PDL fibres increase maximum principal strain (the most tensile strain) in the upper region of the alveolar bone when compared to the solid PDL model. This effect is then reversed in the apex region where the PDL fibres reduce the tensile strain. A similar pattern can be seen for minimum principal strain (the most compressive strain) in the alveolar bone where again the PDL fibres increase the strain along the majority of the tooth root apart from the apex region where the strain becomes higher in the solid PDL model. The plots are symmetric because of the symmetry in the loading, but both sides are included for ease of comparison with the plots from the other load cases.

Orthodontic Load

For both orthodontic loads (Figures 3.11 and 3.12) the strains in the alveolar bone for the solid PDL model are all highest towards the tip of the tooth and then decrease towards the apex. Conversely, for the mesiodistal load (Figure 3.11) the fibrous PDL model shows almost uniform strain on the mesial side of the alveolar bone. A similar pattern is seen with the fibrous PDL model on the buccal side due to the buccolingual load (Figure 3.12) although the strains are not as uniform in this case. Whilst the strains at the apex are always low in the solid PDL model with the orthodontic loads, the strains are usually comparatively high at this location in the fibrous PDL model.

For both orthodontic loads the difference in strain between the solid and fibrous PDL models is most noticeable on the opposite side of the bone to the direction of tooth movement (*i.e.* on the mesial side in Figure 3.11 and the buccal side in Figure 3.12). In the direction of tooth movement there is little difference between the two models except in the apex region where strain is noticeably higher in the fibrous PDL model.

The buccolingual load is directed through the centre of the tooth and so causes translation of the tooth with very little rotation about its long axis. For this load, the fibrous PDL model allows a greater amount of tipping of the tooth. There is approximately 30 % greater displacement of the tooth crown in this model compared to the solid PDL model, along with around 11 % decrease in movement of the tooth apex. Conversely, the mesiodistal load causes both rotation of the tooth about its long axis as well as mesiodistal translation. Compared to the solid PDL model, the fibrous PDL model allows around 31 % increase in axial rotation at the tooth crown as well as 56 % greater displacement of the tooth apex.

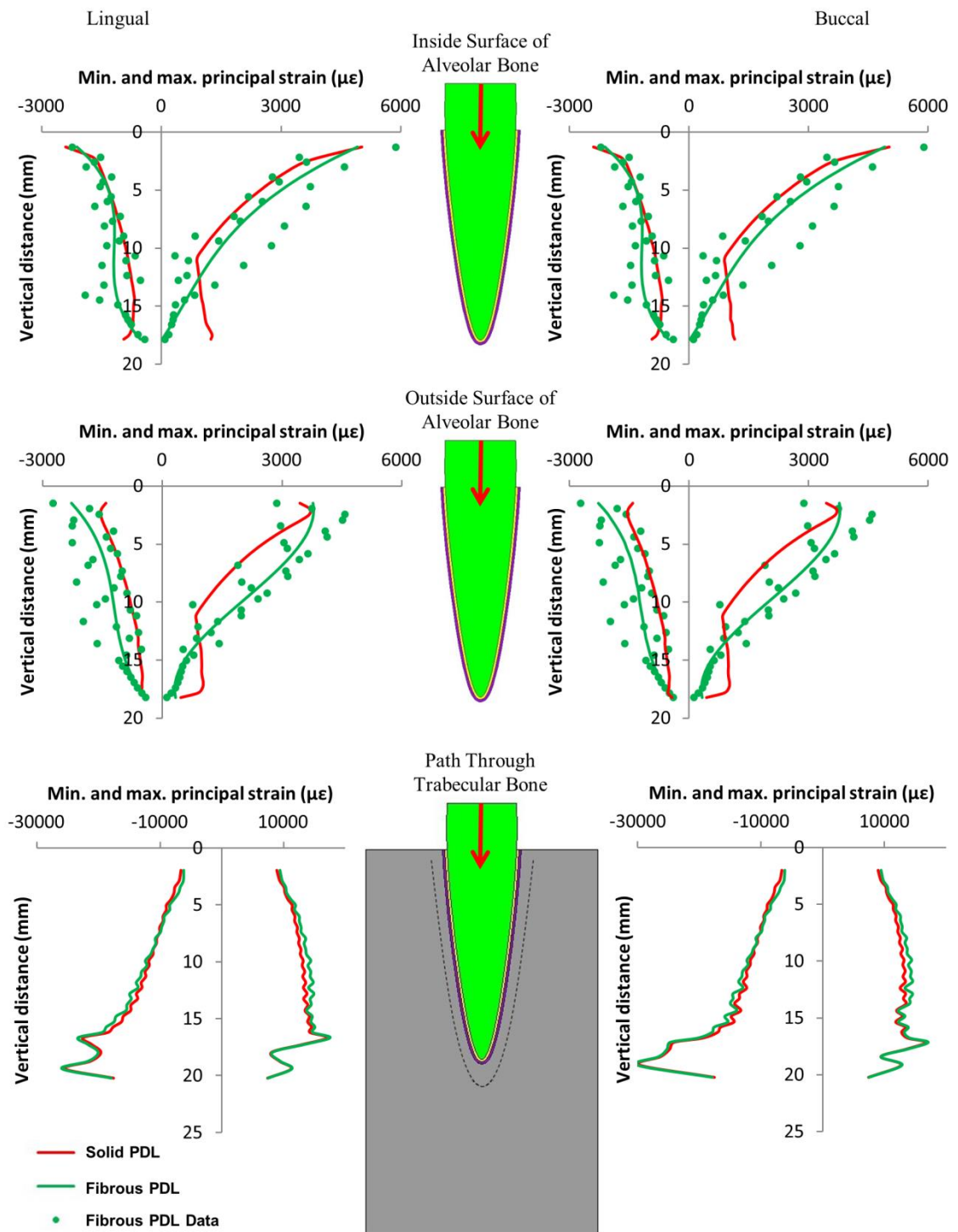


Figure 3.10 Maximum and minimum principal strains on the buccal and lingual sides of the tooth model from the 500 N occlusal load, along three regions within the model. The graphs relate strain to the vertical distance away from the top of the tooth socket.

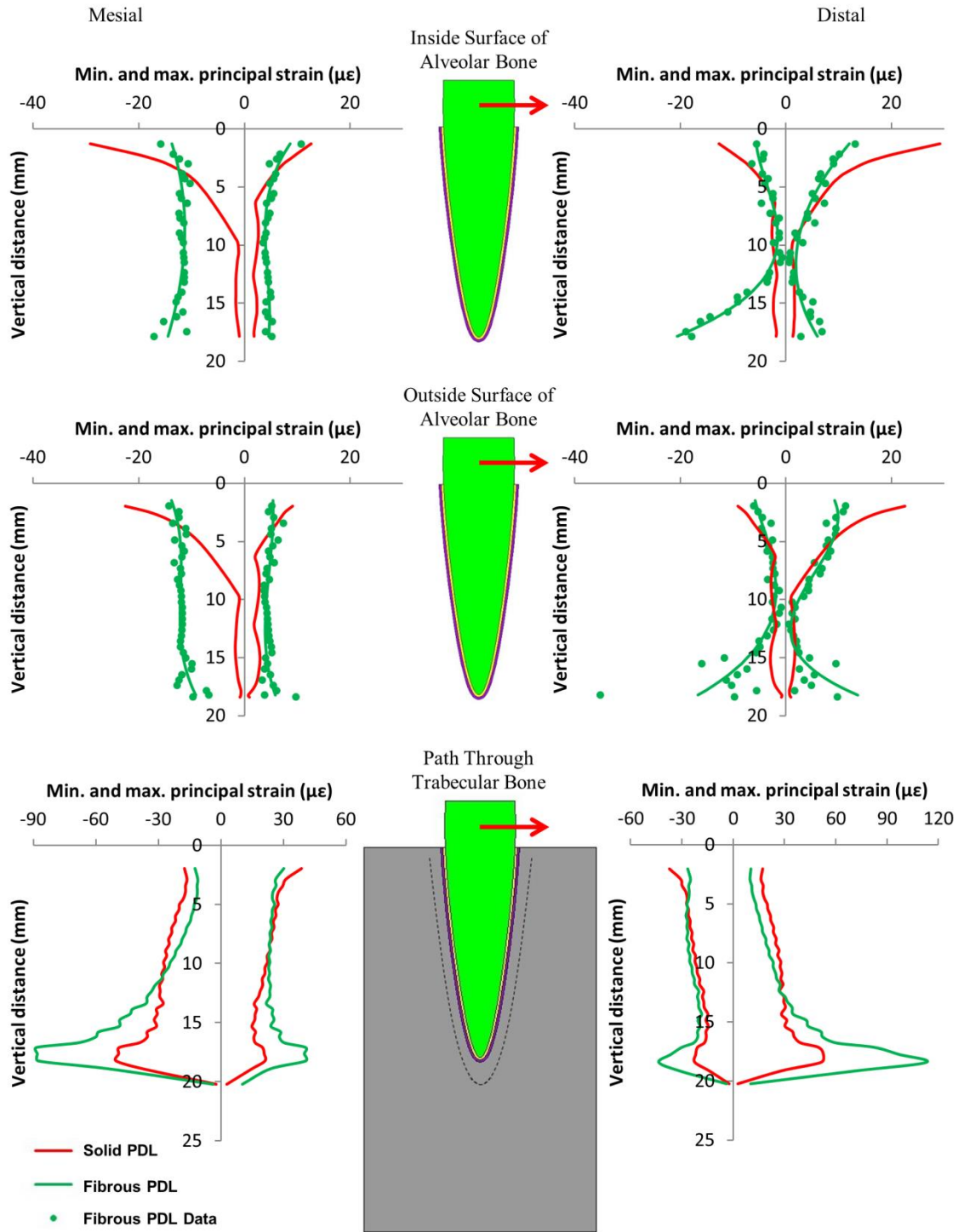


Figure 3.11 Maximum and minimum principal strains on the mesial and distal sides of the tooth model from the 1 N orthodontic load in the mesiodistal direction, along three regions within the model. The graphs relate strain to the vertical distance away from the top of the tooth socket.

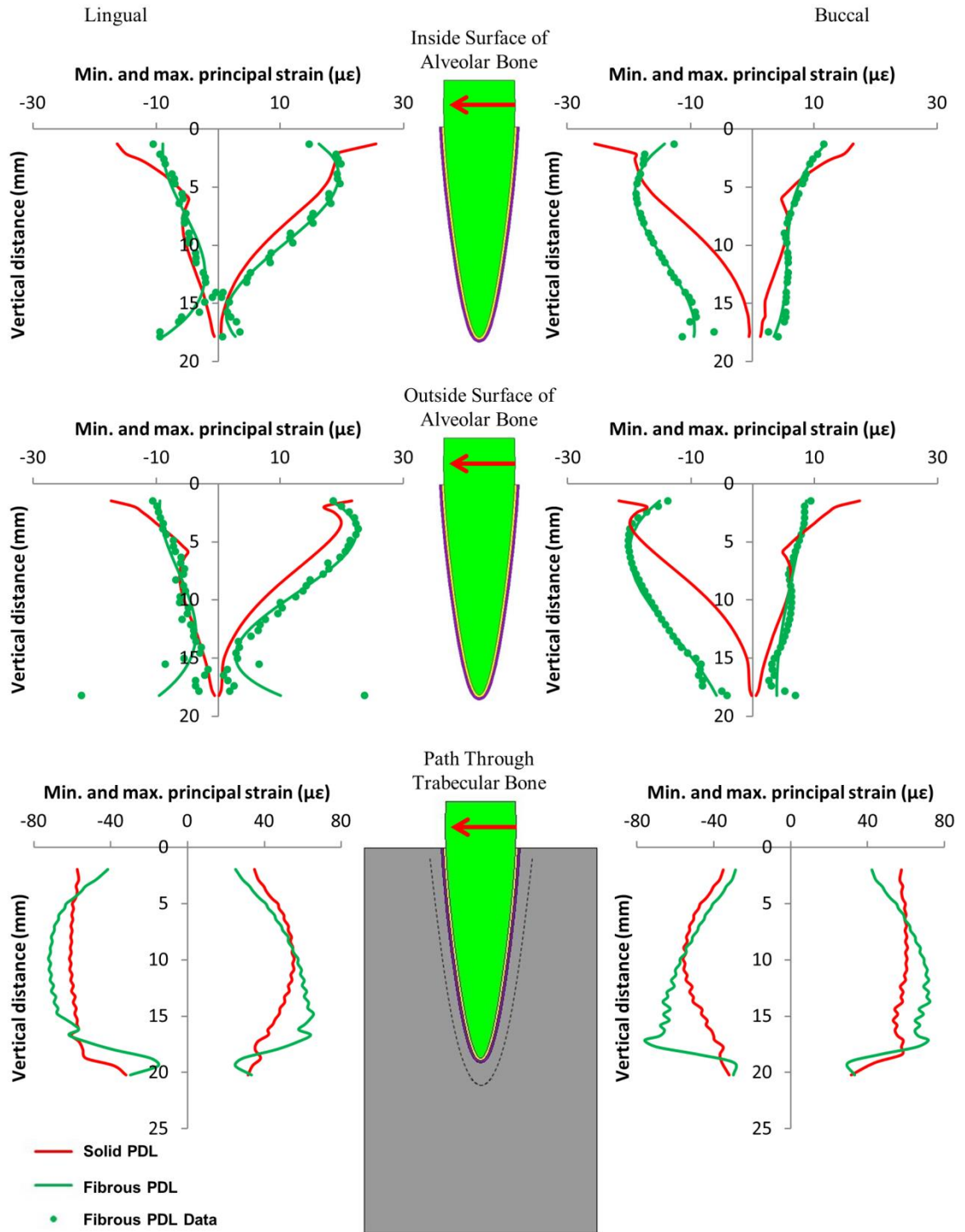


Figure 3.12 Maximum and minimum principal strains on the buccal and lingual sides of the tooth model from the 1 N orthodontic load in the buccolingual direction, along three regions within the model. The graphs relate strain to the vertical distance away from the top of the tooth socket.

3.4 Discussion

Comparing the predicted maximum and minimum principal strains between the solid and fibrous PDL model reveals that inclusion of the PDL fibres influences the strain in the alveolar bone for both occlusal and orthodontic loads. The influence of PDL fibres is not so pronounced in the trabecular bone region, particularly in the occlusal load case where there is very little difference between the results for the two models. The results from the no PDL model confirmed that the presence of the PDL is important in reducing the local bone strain in the region surrounding the tooth root. The sensitivity analysis reveals that adjusting the material property values assigned to the PDL can have a substantial influence on the results obtained (Table 3.3).

3.4.1 Model Testing

The results from the no PDL test (Figure 3.6) confirmed that the presence of the PDL is important when considering the strains around the tooth socket and so it should be included in dental finite element models, at least when strains in the alveolar bone are being examined.

In the boundary conditions test, due to bending of the additional bone, the overall nodal displacements are larger for the U-shaped model (Table 3.2). However, it is the local tooth displacement which is of concern here and the results show this is not greatly affected by the boundary conditions. Additionally, the strains were not seen to be greatly affected around the tooth socket (Figure 3.7 and 3.8). From these tests it can be concluded that the boundary conditions applied to the simplified section of mandible are acceptable for the purposes of this study. As expected, the boundary conditions applied alter results in the region of the tooth model near to them. However, they do not greatly influence the local tooth displacement or the strain in the region of interest near to the alveolar bone.

The tooth displacements from the two convergence models were only slightly different to the original models and so it could be concluded that the models had converged. As these tooth displacements were seen to be of a similar magnitude to previously reported values it was also determined that this model was a reasonable simplification of a real tooth and was acceptable for use here to compare the different types of PDL.

Adjusting the values of Young's modulus for the solid PDL component, Young's modulus of the link elements, the cross sectional area of the link elements or

the initial strain of the link elements, all had a noticeable influence on the vertical tooth displacement (Table 3.3). Conversely, altering the Poisson's ratio of the PDL matrix had a comparatively small effect on the tooth displacement. However, this may be due to there being a smaller range of possible values for the Poisson's ratio compared to the Young's modulus. The influence of Young's modulus of both the solid component and link elements increased as their value increased. The solid component in this model represents the soft matrix surrounding the collagen fibres in the physiological PDL and so its Young's modulus is likely to be well below that of the fibres. Therefore, the value chosen for the matrix may be less important than the values assigned to the fibres when fibres are modelled. It would appear particularly important to choose appropriate values for the cross sectional area, initial strain and Young's modulus of the link elements. However, since there are very little reliable data available from which to choose these, it is important to conduct sensitivity analyses when including PDL fibres in future FE models.

3.4.2 Solid PDL versus Fibrous PDL

Occlusal Load

The oblique orientation of the principal fibres in the PDL means they have a function as a suspensory ligament supporting the tooth root within the alveolar bone. Consequently, vertical forces on the tooth may be transmitted as lateral tension to the alveolar wall (Atmaram & Mohammed, 1981). This also helps to prevent high stresses occurring at the apex of the tooth root. However, if the PDL is modelled as a continuous solid structure these effects may be lost. Figure 3.10 shows that the effect of the PDL fibres on the distribution of strain from the tooth to the alveolar bone is noticeable between these two models. At both the inside and outside surfaces of the alveolar bone, the tensile strain is higher for the fibrous PDL model in the upper section of the bone, and then lower towards the apex compared to the solid PDL model. This is how the fibrous PDL would be expected to affect the strain, compared to the solid PDL, as fibres in the upper section of the bone would be in tension while those in the apex region would be in compression under an occlusal load. Although the PDL fibres have been included in this model in a highly schematic representation of their real structure, they do appear to be functioning as predicted. These results, therefore, agree with Qian *et al.* (2001) who concluded that it may be better to include simplistic PDL fibres than not to include the fibres at all.

However, although the fibres had a substantial influence on the strains observed in the alveolar bone, almost no difference was observed between the two models in the trabecular bone region. The magnitudes of the strains in this region were also far higher than would be expected. Frost (1987) suggested that bone modelling occurs at approximately $1500-3000\mu\epsilon$. However, the strains recorded in the trabecular bone in these models were around a full order of magnitude greater than that. It is likely that both of these problems are due to the highly simplified geometry and material properties in these models. Since this is a simplified model, the actual strain values are not the primary concern but rather the relative differences between the two models is of interest. Altering the Young's modulus of the trabecular bone may decrease the trabecular bone strain but it would have little effect on the behaviour of the tooth in its socket. Similarly, it is possible that the effects of the PDL fibres would be different in the trabecular bone region if the geometry of the trabecular network had been considered.

Orthodontic Load

For both orthodontic loads, the strains at the apex of the tooth socket, on both the inside and outside surfaces, were higher for the fibrous PDL model than for the solid PDL model (Figures 3.11 and 3.12). This is the opposite of what was observed in this region for the occlusal load where the fibrous PDL model showed less strain. This is understandable since the fibres only exert force in tension, not in compression. When a vertical load is applied the fibres at the apex are not stretched and so only the soft PDL matrix resists the tooth at this point. However, when an orthodontic load is applied, translation and rotation of the tooth occur which would stretch the apical fibres causing them to exert a force on the alveolar bone at this location.

For both orthodontic load cases, strain in the solid PDL model is always highest at the top of the alveolar bone and then decreases towards the apex of the tooth on both sides of the model. This is not the case for the fibrous PDL model. In this model, there is a more uniform distribution of strain along the length of the alveolar bone on the side of the tooth away from the direction of tooth movement. This is particularly obvious with the mesiodistal load. On the side to which the tooth is moved, there is less difference between the solid and fibrous PDL models except at the apex. This is due to the fact that the PDL fibres only exert force in tension and so on this side the fibrous PDL behaves similarly to a solid PDL.

Compared to the solid PDL model, the fibrous PDL model allows for a greater amount of tooth movement with both orthodontic loads. The crossed structure of the PDL fibres (Figure 3.2) ensures that some fibres are always in tension and therefore resisting tooth movement, regardless of the direction of an applied load (Berkovitz, 1990). However, this also means that some fibres are in compression and thus not playing any role in resisting the tooth movement. It is therefore not surprising that the fibrous PDL model allows for greater rotation and tipping of the tooth compared to the solid PDL model.

The strain results in Figures 3.11 and 3.12 can be interpreted in light of the three hypotheses shown in Figure 3.1. Neither set of results agree with the pressure-tension hypothesis. This hypothesis predicts that there should be compression on the side to which the tooth is moved and tension on the opposite side. Neither set of results show distinct regions of compression and tension as predicted. For the buccolingual load this situation is reversed with the buccal side being primarily in compression and the lingual side being primarily in tension. This is true for both the solid and fibrous PDL models. The strains from the mesiodistal load also don't agree with this prediction especially on the mesial side in the fibrous PDL model which is primarily in compression along the full length of the alveolar bone.

The alveolar bending hypothesis predicts both compression and tension occurring in the bone on each side of the tooth but on opposite surfaces of the alveolar bone, *i.e.* tension on the inside surface and compression on the outside surface or vice versa. However, for both the mesiodistal and buccolingual orthodontic loads (Figures 3.11 and 3.12) the type of stress occurring, either compressive or tensile, is the same at the inside and outside surfaces of the alveolar bone on both sides of the tooth. This suggests that perhaps the bone is not bending as predicted. Alternatively, since the strain results are very similar at the inside and outside surfaces, this may be due to the alveolar bone being very thin in this model. Consequently, the bending may involve the trabecular bone and so the sign change, *e.g.* from compression to tension, may occur in this region rather than in the alveolar bone region. This appears to be the case for the buccolingual load (Figure 3.12) where on the lingual side the alveolar bone is predominantly in tension while the trabecular bone is slightly more in compression, and on the buccal side the alveolar bone is in compression while the trabecular bone is in tension.

The mesiodistal load causes both tilting of the tooth in the mesiodistal direction and rotation of the tooth about its long axis which is not taken into consideration in the

alveolar bending hypothesis (Figure 3.1). A closer inspection of the direction of strains in the alveolar bone indicates that the tensile strains on the distal side and the compressive strains on the mesial side (which are predicted by the alveolar bending hypothesis) are predominantly orientated in the axial direction (*i.e.* parallel to the long axis of the tooth). This suggests that if the model was only being considered in two dimensions, the alveolar bending hypothesis may appear correct. However, in three dimensions, simple cantilever bending of the alveolar bone is not the only cause of strain in the alveolar bone.

For the buccolingual load, the lingual side is predominantly in tension as predicted. Additionally, the tensile strains are mostly orientated in the axial direction. Conversely, the compressive strains, which are not predicted by the alveolar bending hypothesis, are orientated in the hoop (*i.e.* directed around the tooth within the horizontal plane) and radial (*i.e.* directed away from the long axis of the tooth within the horizontal plane) directions. Similarly, on the compression side, the compressive strains are mostly orientated in the axial direction whereas the tensile strains on that side are mostly in the hoop and radial directions. These results also provide some support for the alveolar bending hypothesis, although again strain must be considered in all directions.

Unlike the pressure-tension hypothesis and the alveolar bending hypothesis, the stretched fibre hypothesis does not consider whether the bone is in compression or tension, but is mainly concerned with whether bone is in high strain or low strain. This hypothesis is also the one that should be most affected by whether or not fibres are included in the FE model. For both the mesiodistal load and the buccolingual load, strain is higher in the fibrous PDL model than the solid PDL model on the side which the tooth is moved away from (the mesial side in Figure 3.11 and the buccal side in Figure 3.12). This provides some support to this hypothesis which predicts that strains should be high on this side due stretching of the PDL fibres.

Whilst there is some support for the stretched fibre hypothesis on the side which bone is formed, it is not clear whether resorption on the other side is due to low strains. For the buccolingual load the magnitude of strain on the lingual side is not greatly different to that on the buccal side. For the mesiodistal load there is almost uniform strain on the mesial side (the side from which the tooth is moved away). Conversely, on the distal side (the side to which the tooth is moved) the strains are reasonably low in the upper portion of the alveolar bone but get much higher towards the apex. In neither case are the strains particularly low in the direction of tooth movement to suggest that bone resorption is due to under-loading.

For both orthodontic loads, the strains observed in the alveolar bone are all far below those values typically thought to cause bone remodelling (Frost, 1987). However, it should be emphasised that this is a simplified model and so the absolute values of strain in the model cannot be assumed to be accurate. Nevertheless, this agrees with the results of other authors who also found very low strains in the alveolar bone (*e.g.* Middleton *et al.*, 1996a; Jones *et al.*, 2001). The low strains commonly observed in the alveolar bone have led to the proposal that the stimulus for orthodontic tooth movement comes from the PDL rather than the alveolar bone (*e.g.* Chen *et al.*, 2014). However, if the PDL is responsible for controlling orthodontic tooth movement, the mechanical stimulus for this is still unclear. For example, Qian *et al.* (2010) used normal strain in the PDL to drive tooth movement whereas Chen *et al.* (2014) chose hydrostatic stress in the PDL.

One of the main reasons why the PDL is thought to mediate orthodontic tooth movement is because of the low alveolar bone strains observed. However, it has also been suggested that, rather than all bones responding to the same levels of strain, it may be the case that resorption and formation are triggered at different strain levels in different bones (Currey, 1984). Also, the alveolar bone is thought to be one of the most physiologically active bones in mammals (Hall, 2005). Therefore, whilst the strain in the alveolar bone may not be at the level known to cause remodelling in other bones, it may still be sufficiently high to cause remodelling here. Therefore, the fact that strains are low in the alveolar bone does not completely eliminate the possibility that the alveolar bone itself provides the stimulus for orthodontic tooth movement.

The results from these models are inconclusive in regards to which of the proposed hypotheses for orthodontic tooth movement may be correct. The results do not appear to provide any support for the pressure-tension hypothesis but provide some support for each of the other two. Regions of compression and tension correspond roughly to where they would be expected from the alveolar bending hypothesis. The results also show that including the PDL fibres is particularly important for increasing strain on the bone formation side as predicted by the stretched fibre hypothesis. It is possible that the exact mechanism responsible for orthodontic tooth movement is a combination of these two hypotheses along with regulation from the PDL itself.

These results show that including the fibrous structure of the PDL are important in FE models when investigating orthodontic loads. Compared to the fibrous PDL model, the solid PDL model restricts the amount of tooth movement observed. The fibres also help to distribute the load throughout the alveolar bone compared to the solid

PDL model where most of the load is supported by the upper portion of the bone. Unsurprisingly, the fibres have most effect on the side of the bone from which the tooth is moved away, since they will mostly be in tension, whereas they will be mostly in compression on the opposite side.

Of course, care must be taken when interpreting these results due to the highly simplified geometry and material properties in the model. However, as we were mainly concerned with the relative difference between the results from two models, the results clearly show that including the PDL fibres influences both the magnitude and distribution of the strain produced in the surrounding bone. With the limitations of this model in mind, it will be interesting to investigate the role of PDL fibres in morphologically accurate models based on microCT scans of real human mandibles. Nevertheless, since the purpose of this study was to investigate the effects of including the PDL fibres in FE models when investigating mandibular functional morphology or orthodontic tooth movement, these models provide useful results. Adjusting the material properties and geometry of the model would obviously alter the absolute values of the results obtained. In particular, the sensitivity analysis results in Table 3.3 indicate that even small adjustments to the material properties of the PDL may have a substantial impact on the magnitude of the results. Still, it is clear that including the PDL fibres does have an influence on both the magnitude and distribution of the strain produced in the surrounding bone. Since the distribution of strain is altered, these differences observed could not be accounted for simply by adjusting the material properties of the PDL in the solid PDL model.

Chapter 4

Human Molar Region Finite Element Models

4.1 Introduction

In the previous chapter a novel method of including the fibrous structure of the periodontal ligament (PDL) in finite element models was introduced. The fibrous PDL was then compared to solid PDL and no PDL representations in a simplified model of an individual tooth. This chapter builds upon the previous one, using a similar technique for representing the fibrous structure of the PDL, but using a finite element model with realistic geometry based on the molar region of a real human (*Homo sapiens*) mandible.

Briefly, the results of the previous study indicated that the way in which the PDL is modelled affects strains in the tooth socket. However, since this was a simplified single tooth model, the results clearly could not reveal how the inclusion of the PDL affects strains elsewhere in the mandible. In this current study, the same three different methods of modelling the PDL (fibrous, solid and no PDL) are compared, using a finite element model of a human molar region, with strains examined both adjacent to and further from the tooth socket of the loaded tooth. Although the fibrous structure of the PDL was only included around one molar tooth, this is the first time the fibrous structure of the PDL has been included in such an FE model of more than just a single tooth. Additionally, this is the first time a fibrous PDL has been included in a model with realistic, rather than simplified, tooth and bone geometry.

In addition to further investigating the PDL in finite element models, this study also investigated two different methods of modelling the trabecular tissue. Ideally, the individual trabeculae, and therefore the real structure of the trabecular network, should be included in finite element models (Gröning *et al.*, 2012b). However, since the mean thickness of individual trabeculae in a human mandible is approximately 0.1 mm (Giesen & Van Eijden, 2000; Fanuscu & Chang, 2004), very high resolution scans and very many elements are required in order to include trabeculae in finite element models (Gröning *et al.*, 2012b). Therefore, for practical reasons, most previous mandibular finite element models have represented the trabecular tissue as a homogeneous bulk

material (e.g. Tanne et al., 1993; Koriath & Hannam, 1994; Ichim et al., 2006, 2007; Gröning *et al.*, 2011b, 2012b). This current study focused on the molar region of a human mandible. By reducing the field of view to just the molar region, rather than the whole mandible, a higher resolution scan could be performed allowing the structure of the trabecular network to be included in the finite element models. This was then compared to the usual way of representing the trabecular tissue as a bulk (homogeneous) material.

Therefore, in this study, two different representations of the trabecular tissue are considered; as a trabecular structure and bulk material. For clarity, the term ‘trabecular bone’ is used in the following to refer to the material forming the individual trabeculae; the term ‘trabecular filling’ is used to refer to the material in the pores surrounding the individual trabeculae; and the term ‘trabecular tissue’ is used to refer to the trabecular bone and trabecular filling combined. These terms are illustrated in Figure 4.1.

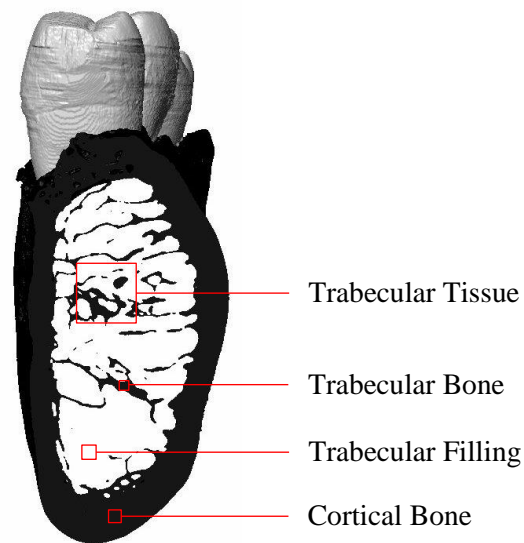


Figure 4.1 Schematic representation of a cross section through mandibular bone. Trabecular bone refers to the material forming the individual trabeculae. Trabecular filling refers to the material in the pores surrounding the trabeculae. Trabecular tissue refers to the combination of trabecular bone and trabecular filling. Cortical bone refers to the dense bone around the outer surface of the mandible.

The material properties of cortical bone and of the bone forming the individual trabeculae are generally thought to be very similar (Currey, 1989, 2002). Therefore, in models where the trabecular tissue is modelled as a detailed trabecular structure, the trabecular bone and cortical bone are given the same material properties, with the trabecular filling being given a very low Young’s modulus value. In models where the

trabecular tissue is modelled as a bulk material, both the trabecular bone and trabecular filling are given the same material properties, with a Young's modulus value much lower than that of cortical bone.

So, the aim of this study was to investigate three different ways of modelling the PDL (fibrous PDL, solid PDL and no PDL), and two different ways of modelling the trabecular tissue (trabecular structure and bulk material). Combining the three different types of PDL with the two different types of trabecular tissue meant six different types of models were created:

- Fibrous PDL and Trabecular Structure
- Fibrous PDL and Bulk Trabecular Tissue Material
- Solid PDL and Trabecular Structure
- Solid PDL and Bulk Trabecular Tissue Material
- No PDL and Trabecular Structure
- No PDL and Bulk Trabecular Tissue Material

All six types of models had the same finite element mesh, with or without the addition of the PDL fibres, which allowed them to be compared directly with each other. This was achieved using three different types of loading: an occlusal load, and two different orthodontic loads. All six types of models were tested with all three load cases.

For the occlusal load, the strains in the cortical bone were compared for the different models to investigate how the PDL representation affects strains away from the tooth socket. For the orthodontic loads, the strains in the alveolar bone were compared since this is the region where bone adaptation occurs during orthodontic tooth movement. Three different hypotheses for the biomechanical driver of orthodontic tooth movement were discussed in Chapter 3: the “pressure-tension hypothesis”, the “alveolar bending hypothesis” and the “stretched fibre hypothesis” (see Figure 3.1). The results obtained from the orthodontic load models are discussed in relation to these three hypotheses in the main discussion in Chapter 6.

The remainder of this chapter is divided into four sections. First, Section 4.2 describes in detail how the different types of models were created and loaded. The results obtained are then presented in Section 4.3 and discussed in Section 4.4. Finally, Section 4.5 summarises the findings.

4.2 Materials and Methods

All six models were created from the same finite element mesh by varying the material properties assigned to different elements, with additional link elements included in the fibrous PDL models. All finite element analyses were performed using ANSYS software (version 14.5, ANSYS Inc., Canonsburg, PA, USA) following image segmentation and tetrahedral mesh generation using AVIZO software (version 6.3, FEI Visualization Sciences Group, Berlin, Germany).

4.2.1 Mesh Generation

Micro-computed Tomography Scanning

A microCT scan of a dry adult human right hemi-mandible specimen was obtained using an X-Tek HMX160 microCT scanner (X-Tek Systems Ltd., Tring, UK) at the University of Hull. The microCT data set was exported as a stack of 8-bit TIFF (tagged image file format) images with a voxel size of 0.040 mm in all three directions, and imported into AVIZO.

Thresholding and Manual Segmentation

Since a detailed representation of the three-dimensional geometry of the trabeculae was to be included in the finite element models, the Ray Casting Algorithm (RCA) method (Scherf & Tilgner, 2009) was used for automatic thresholding of the grey scale values. The RCA method was developed by Scherf and Tilgner (2009) specifically for segmenting fine scale bone structures and they found it to be superior to traditional methods such the half-maximum height thresholding protocol (Spoor *et al.*, 1993; Fajardo *et al.*, 2002; Coleman & Colbert, 2007) or the adaptive iterative thresholding method (Ryan & Ketcham, 2002a, 2002b; Fajardo *et al.*, 2007).

After thresholding, the hemi-mandible was cropped to just the molar region, containing the second premolar and first and second molars. Pre-mortem loss of the third molar meant it was not present in this specimen, and could, therefore, not be included in these models.

Further manual segmentation was then required to separate different materials within the model. First, points of contact between adjacent teeth were removed so that the three teeth were completely separate from each other. All the teeth were also separated manually from the surrounding alveolar bone. Where there were points of

contact between the teeth and the alveolar bone, the teeth were edited rather than the bone, so as not to reduce the volume of bone present.

After separating the teeth, a material was added to fill the space between each individual tooth and alveolar bone, to represent the PDL. To do this, a border was first created between the tooth and alveolar bone, at approximately the cervical margin of each tooth. There were some gaps in the alveolar bone which were then filled manually so that the space between the tooth and alveolar bone, up to the border at the cervical margin, could be flood-filled with material representing the PDL. This meant the PDL material completely surrounded the tooth root and joined the tooth root to the alveolar bone for all three teeth.

To facilitate definition of the PDL fibres, the PDL material around the middle tooth (first molar) was further divided into two materials every ten slices down its length, *i.e.* first ten slices PDL material one, second ten slices PDL material two, third ten slices PDL material one, and so on, as shown in Figure 4.2. This was done so that after the creation of the finite element mesh, there would be a plane of nodes at each PDL material intersection, which could then be used for creating link elements to represent the PDL fibres in the fibrous PDL models (see Section 4.2.2 for more details).

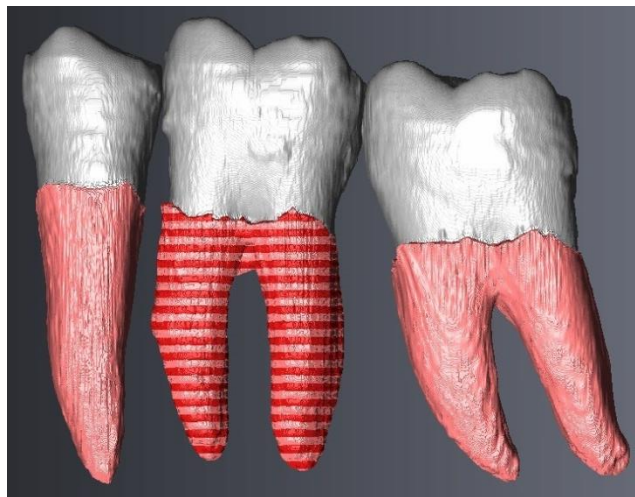


Figure 4.2 Surface model showing three teeth and surrounding PDL, including the two materials forming the PDL around the middle tooth, viewed from the lingual side. From left to right: second premolar, first molar and second molar.

Next, cortical and trabecular bone regions were separated from each other in AVIZO. In this process, the alveolar bone was considered to have the same material properties as cortical bone and left as one material, with the trabecular bone as a separate material. A material was then added to fill the space between the trabeculae

within the trabecular bone tissue, as shown in Figure 4.3. This was done so that after meshing, the same finite element model could be used for both the trabecular structure and bulk material models by adjusting the material properties assigned to the two trabecular materials within the model.

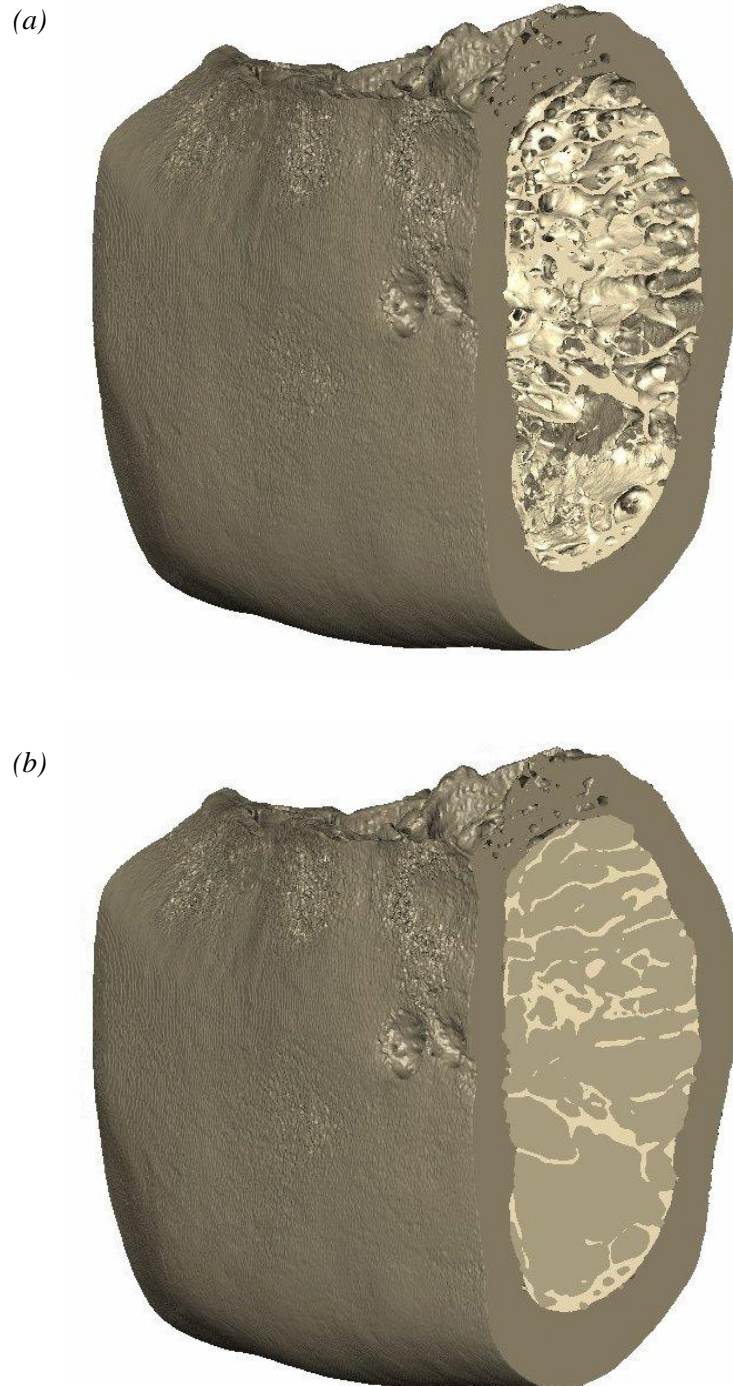


Figure 4.3 Surface models showing the buccal side and the cut mesial surface of the mandibular bone: (a) cortical bone and trabecular bone without trabecular filling; (b) cortical bone and trabecular bone with trabecular filling.

Mesh Generation

The solid model was then complete, as shown in Figure 4.4, and ready to be converted into a finite element mesh. The solid model was smoothed before generating a polygon surface model which was simplified further to reduce the number of faces and ultimately the number of elements generated when the model was meshed. Some automatic surface fixes in AVIZO were performed to sort problems with the surface model, such as intersecting faces, before a tetrahedral mesh was generated. This was then converted into a text file which was imported into ANSYS as a finite element mesh.

The process of converting the solid model into a tetrahedral mesh in AVIZO was performed twice, with different simplifications each time, to create two finite element models, one with 1,338,931 elements and one with 4,245,791 elements to allow model convergence to be examined as described in Section 4.2.2. The subsequent finite element modelling was then undertaken primarily with the 1 million element model.

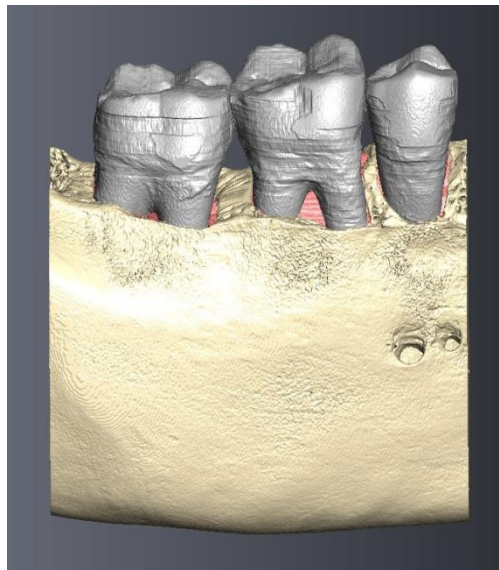


Figure 4.4 Surface model showing the final human molar region model including teeth, bone and PDL (in pink), viewed from the buccal side.

4.2.2 Model Development

The mesh generated in AVIZO was imported into ANSYS for finite element analysis. Solid 10-noded high-order tetrahedral elements (SOLID187) (Kohnke, 2009) were used throughout the model. The model contained five different materials: cortical bone,

trabecular bone, trabecular filling, teeth and PDL. Additional elements representing PDL fibres were added later. As explained in Section 4.2.1, the solid PDL around the middle tooth (first molar) was separated into two materials (Figure 4.2). However, this was only done to aid in the creation of the PDL fibres. Both materials had the same properties and were otherwise treated the same throughout. To avoid confusion, the solid PDL material is referred to as one material when discussed below.

Initial Model Testing

To check for any problems with the finite element mesh, an initial test solve was performed. All nodes on the two cut surfaces at the mesial and distal ends of the model were constrained in all degrees of freedom, and a point load of 500 N was applied to the occlusal surface of the middle tooth. All materials were given a Young's modulus of 17 GPa with a Poisson's ratio of 0.3. This initial test solve produced some errors due to poorly connected elements within the mesh. These elements arose, for example, when only one edge (between two corner nodes) of an element was connected to the rest of the model, so it could effectively rotate about that edge. These elements were identified by looking for nodes with excessively large displacements, identifying and deleting elements attached to these nodes, and then resolving the model. This process was repeated until all insufficiently constrained elements were removed. In total, only 19 elements were removed in this way, therefore the final number of elements in the model was 1,338,912.

Boundary Conditions

Boundary conditions should represent the loads, displacements and constraints which the structure normally experiences. The boundary conditions applied to this model, for the occlusal load case, are shown in Figure 4.5. All of the nodes on the two cut surfaces at the mesial and distal ends of the model were constrained in the mesiodistal direction to represent the adjacent bone in this direction in a whole mandible. A small number of nodes at the base of each edge were also constrained in all degrees of freedom to prevent rigid body translation of the model, especially in the coronal and buccolingual directions. In addition, a selection of nodes on each of the mesial and distal sides of the exterior surface of the tooth crown on the middle tooth were constrained in the mesiodistal direction to represent the points of contact between adjacent teeth, which would limit movement in this direction, but allow buccolingual

displacement. Finally, a total occlusal load of 500 N was distributed over a small area around the centre of the occlusal surface of the crown of the middle tooth, directed in the corono-apical direction. A load of 500 N was chosen to represent a maximal human bite force (Daegling & Hylander, 1997; O'Connor *et al.*, 2005; De Abreu *et al.*, 2014).

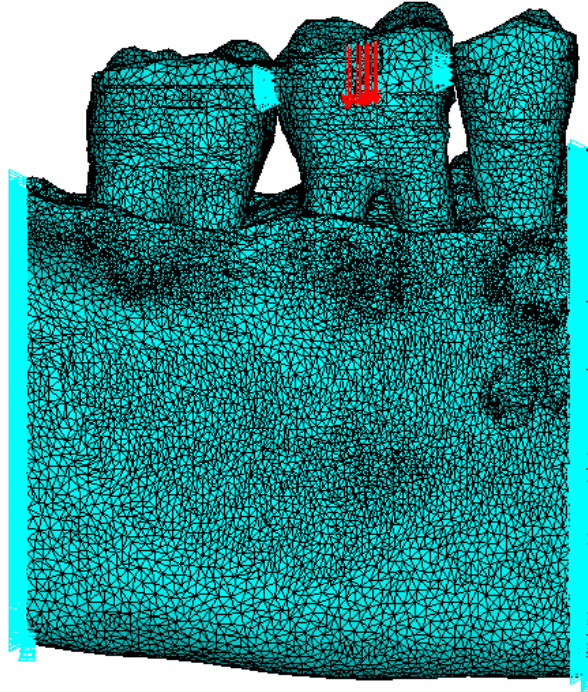


Figure 4.5 Finite element model, viewed from the buccal side, showing loading and boundary conditions applied for the occlusal load case, where light blue triangles represent constraints and red arrows represent applied forces.

Initial Material Properties for the Convergence Study

Having defined the boundary conditions, the six different models were created by varying the material properties assigned to different elements, with or without the addition of PDL fibres. The first model to be developed was the most anatomically accurate fibrous PDL and trabecular structure model. The material properties for the other models were then determined by optimisation, so the tooth displacement for each model was matched to that of the Fibrous PDL Trabecular Structure model. As this is explained in more detail later, only the process of developing the Fibrous PDL Trabecular Structure model is described in this section.

Cortical bone, trabecular bone and, for simplicity, teeth were all assigned a Young's modulus of 17,000 MPa with a Poisson's ratio of 0.3 (Gröning *et al.*, 2011a). The teeth were not separated into different components but were modelled entirely as dentin, which has similar properties to bone (Currey, 2002). It was not necessary to

include enamel since the strains within the teeth are not of interest in this study. An initial Young's modulus value of 12.2 MPa and Poisson's ratio of 0.45 were used, based on the solid PDL model in Chapter 3. The PDL fibres were not considered in the convergence study as it would be too time consuming to create them in each model.

The purpose of including the trabecular filling was to allow the same finite element mesh to be used for both the trabecular structure and bulk material models. To ensure the filling had a negligible effect in the trabecular structure model, the filling was given a very low Young's modulus. To determine a suitable value, the Young's modulus was varied (by orders of magnitude) between 1 MPa and 1×10^{-6} MPa with a Poisson's ratio of 0.3. For each value, the maximum principal strain, minimum principal strain and Von Mises strain were recorded at five selected nodes on the outer surface of the cortical bone, as shown in Figure 4.6. The final Young's modulus chosen for the trabecular filling was 1×10^{-4} MPa, the value below which no further changes in any of the strain values were observed.

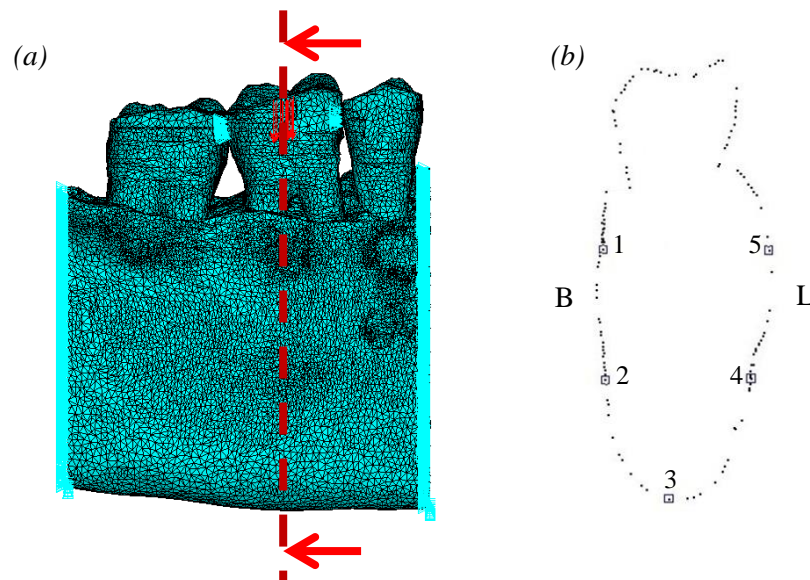


Figure 4.6 Nodes on the outer surface of the cortical bone selected for the convergence test and for choosing the Young's modulus value for the trabecular filling: (a) finite element model, viewed from the buccal side showing the approximate location of the plane from which nodes were selected; (b) nodes from the plane shown in (a), viewed from the mesial side, around the outer surface of the tooth and cortical bone indicating the location of the five nodes selected. The red arrows indicate the viewing direction in (b) compared to that in (a).

Convergence Test

A number of studies of whole human mandibles using tetrahedral finite element meshes have included convergence tests (*e.g.* Zhao *et al.*, 2001; Al-Sukhun *et al.*, 2007; Ramos

et al., 2011), and typically found that convergence was reached with much fewer elements, typically 100,000 elements, which is much less than that used in this model of just the molar region. A detailed convergence study was thought unnecessary, but a quick test was performed by comparing the results from this model (with 1.3 million elements) to one with 4.2 million elements.

The 4.2 million element model again used solid 10-noded high-order tetrahedral elements (SOLID187) (Kohnke, 2009). As with the smaller model, the first solution initially produced errors due to poorly connected elements which were removed in the same way as before. In total, 97 elements were removed, so the final number of elements in the model was 4,245,694.

The same boundary conditions were applied to the 4 million element model as to the 1 million element model, as shown in Figure 4.7, and described above. The same material properties were used, *i.e.* cortical bone, trabecular bone and teeth were all given a Young's modulus of 17,000 MPa with a Poisson's ratio of 0.3, the trabecular filling was given a Young's modulus of 1×10^{-4} MPa with a Poisson's ratio of 0.3, and the PDL was given a Young's modulus of 12.2 MPa with a Poisson's ratio of 0.45.

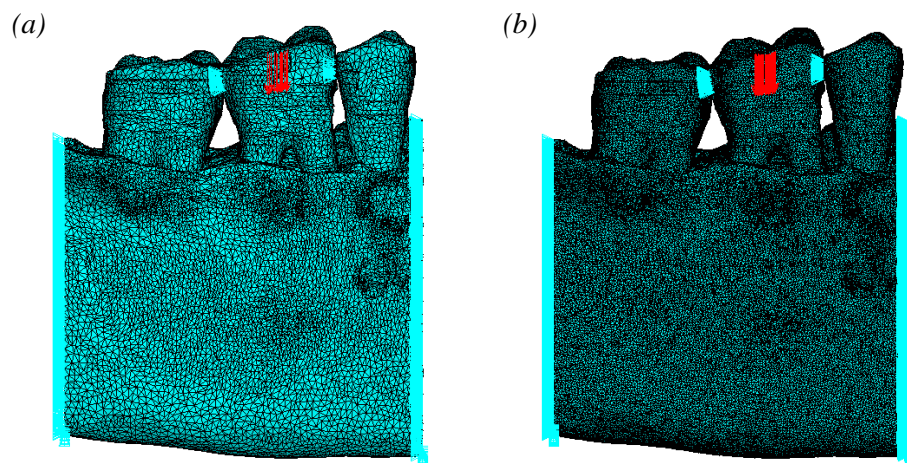


Figure 4.7 Finite element models used for the convergence test, viewed from the buccal side, showing loading and boundary conditions applied, where light blue triangles represent constraints and red arrows represent applied forces: (a) 1.2 million element model; (b) 4.2 million element model.

To compare the two models, maximum principal strain, minimum principal strain and Von Mises strain values were recorded from five locations on the outer surface of the cortical bone. For the 1 million element model, the same five nodes were selected as used previously when determining the material properties for the trabecular

filling. For the 4 million element model, nodes were selected with coordinates as close as possible to the locations of those five nodes.

PDL Fibres

The fibre-reinforced matrix structure of the PDL was represented in these models in a similar method to that used with the simplified single tooth model (see Chapter 3). Although the models contain three teeth, fibres were only added to the PDL around the middle tooth since this is the tooth on which the loads were applied. The PDL fibres were represented by tension-only three-dimensional spar elements (LINK10) (Kohnke, 2009). These link elements connected nodes on the interface between the alveolar bone and the PDL with corresponding nodes on the interface between the tooth root and PDL.

Each PDL fibre was added manually by selecting two nodes to be joined by a link element. Each link element was crossed by another link element to represent the criss-cross structure of the PDL fibres found in real PDLs (Berkovitz, 1990; Schroeder, 2000). The alternating materials forming the PDL around the middle tooth (see Figure 4.2), created planes of nodes which were used to add the PDL fibres, as shown in Figure 4.8. The orientation of the link elements in different regions of the PDL were chosen to represent crestal, horizontal, oblique and apical PDL fibres. In total, 2,112 link elements were added, as shown in Figure 4.9.

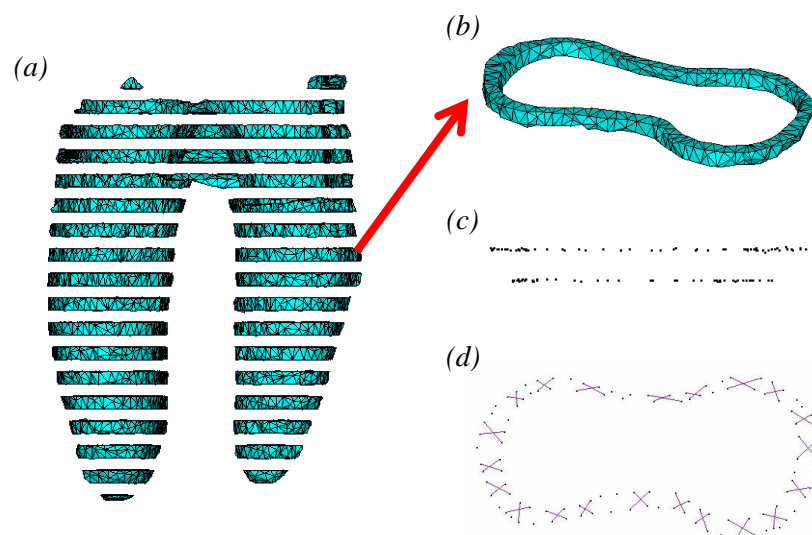


Figure 4.8 Details of how the link elements representing the PDL fibres were added: (a) buccal side view of one of the two materials making up the PDL around the middle tooth; (b) one ring of elements selected as indicated by the red arrow; (c) buccal side view of nodes selected from the outer surface on the top of the ring, *i.e.* adjacent to the alveolar bone, and the inner surface on the bottom of the ring, *i.e.* adjacent to the tooth, for creating oblique PDL fibres; (d) superior view of nodes showing nodes through which link elements were created.

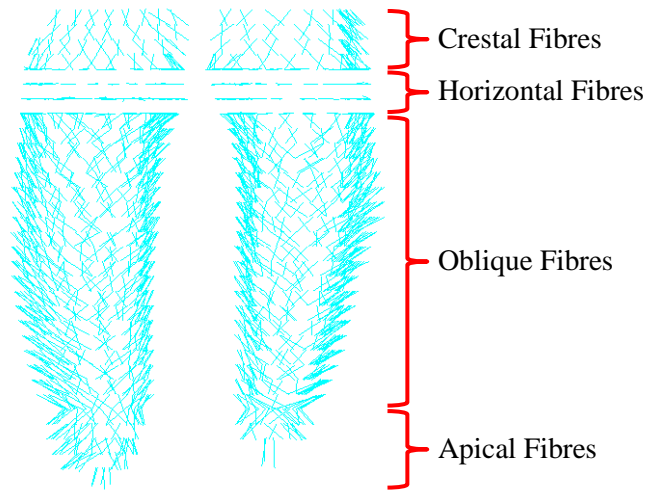


Figure 4.9 Buccal side view of 2,112 link elements, added to the fibrous PDL models, connecting the alveolar bone to the tooth root through the PDL.

For the fibrous PDL models, the material properties of the PDL matrix and PDL fibres were chosen to be the same as those used previously for the simplified single tooth model (see Chapter 3), which were obtained from previous studies. Thus, the PDL matrix was given a Young's modulus value of 1 MPa with a Poisson's ratio of 0.45, and the PDL fibres were given a Young's modulus value of 1,000 MPa, with a Poisson's ratio of 0.35.

However, for the PDL fibres, it was also necessary to specify the cross-sectional area and (optional) initial strain of the link elements. Approximately 50 to 75 % of the PDL tissue volume is made up of the PDL fibres (Dorow *et al.*, 2003). Therefore, the cross-sectional area of the link elements was calculated so that the combined volume of the link elements would be between 50 and 75 % of the PDL volume in the model. The total volume of the PDL around the middle tooth is 137.56 mm³ and the total length of the link elements is 1371.04 mm. From this, the cross-sectional area of the link elements would need to be between approximately 0.05 mm² and 0.075 mm². Therefore, the cross-sectional area was chosen to be 0.06 mm². This value is approximately middle of the range. It is also the same as the value used for the cross-sectional area of the link elements in Chapter 3. As before, this value makes the link elements one to two orders of magnitude thicker than the collagen fibres found *in vivo* (Berkovitz, 1990; Meyer *et al.*, 2010), but it has to be considered that the number of modelled PDL fibres is significantly less than the number in real PDL material. As no data was available in the literature to suggest a suitable value for any initial strain of the link elements, this value was defined as zero.

Optimisation

In summary, the material properties of the Fibrous PDL Trabecular Structure model are presented in Table 4.1. The remaining models were then produced by altering the material properties assigned to different materials and optimising the necessary Young's modulus value in order to match the tooth displacement of the new model to that of the Fibrous PDL Trabecular Structure model. For this, tooth displacement was defined as the average vertical displacement of the nodes to which the occlusal load had been applied. For the occlusal force of 500N, the tooth displacement for the Fibrous PDL Trabecular Structure model was found to be 0.0593 mm. This value is similar to the tooth displacement calculated for the simplified single tooth model (0.0703 mm, see Chapter 3), and seems reasonable when compared to the value of 0.12mm cited by Borák *et al.* (2011) from an experiment by Kato (1982).

Table 4.1 Mechanical properties assigned to each material in the original Fibrous PDL Trabecular Structure model.

Component	Young's Modulus (MPa)	Poisson's Ratio
Cortical bone ^a	17,000	0.30
Trabecular bone ^b	17,000	0.30
Trabecular filling	1×10^{-4}	0.30
Teeth ^a	17,000	0.30
PDL matrix ^c	1	0.45
PDL fibres ^d	1,000	0.35

^a Gröning *et al.* (2011a).

^b Currey (1989, 2002).

^c Jones *et al.* (2001), Qian *et al.* (2001).

^d Gautieri *et al.* (2012), Katona and Qian (2001), Meyer *et al.* (2010), Rees and Jacobsen (1997).

The purpose of this study was to investigate three different ways of modelling the PDL (fibrous PDL, solid PDL and no PDL), and two different ways of modelling the trabecular tissue (trabecular structure and bulk material). Each of the PDL types were modelled with both of the two trabecular tissue types meaning there were a total of six different models created. So, the only difference between a trabecular structure model and a bulk material model, with the same PDL, was the way in which the trabecular tissue was modelled. Similarly, the only difference between fibrous PDL, solid PDL and no PDL models, with the same trabecular tissue, was the way in which the PDL was modelled. The tooth displacement for the two fibrous PDL models and the

two solid PDL models were matched by a series of optimisations, summarised in Figure 4.10. Since the majority of tooth displacement is due to deformation of the PDL (Naveh *et al.*, 2012b), tooth displacement was not matched to the original for the no PDL models.

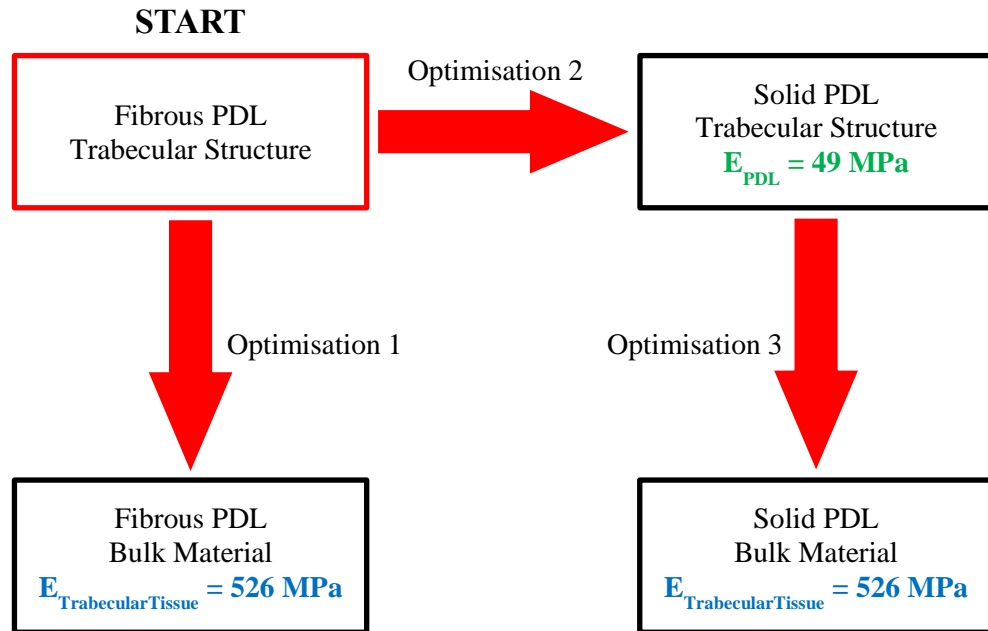


Figure 4.10 Schematic diagram summarising the steps involved in the optimisation process to match the tooth displacements, as described in the text.

The process was as follows (see Figure 4.10). The first optimisation was used to create the Fibrous PDL Bulk Material model. For this bulk material model, the trabecular bone and trabecular filling material were assigned the same material properties and their Young's modulus value then varied until the tooth displacement for the new model matched that of the original model. To achieve the same displacement, it was found necessary to use a Young's modulus value of 526 MPa for the two materials. This value is within the range of reported values for Young's modulus of trabecular bone (Van Eijden, 2000) and is similar to values used in other finite element models (*e.g.* Gröning *et al.*, 2012b).

The second optimisation was to create the Solid PDL Trabecular Structure model. This model differs from the original model only in how the PDL is modelled. For this model, the link elements representing the PDL fibres were removed from the model leaving only a solid material to represent the PDL. The Young's modulus value assigned to the PDL was varied until the tooth displacement for this model matched that

of the original model. To get the same displacement, it was found necessary to use a Young's modulus value of 49 MPa. This value is within the range of reported values for Young's modulus of PDL (Rees, 2001; Fill *et al.*, 2011) and is similar to values used in other finite element models (*e.g.* Rees & Jacobsen, 1997).

The third optimisation was to create the Solid PDL Bulk Material model. In the second optimisation, the effective elastic modulus of the solid PDL was matched to that of the fibrous PDL, so this value was used again for this model. The trabecular bone and trabecular filling were then assigned the same material properties and their Young's modulus value was varied until the tooth displacement matched that of the original Solid PDL Trabecular Structure model. To get the same displacement, it was found necessary to use a Young's modulus value of 526 MPa for the two materials. This was the same value found in the first optimisation, and thus the overall effective elastic modulus of the trabecular tissue was the same for these two models.

The final two models were the No PDL Trabecular Structure and No PDL Bulk Material models. These models were simply created from the corresponding solid PDL models by changing the material properties of the PDL material to be the same as cortical bone. This is the same method as that used to create the no PDL models in Chapter 3, and is the same method adopted by Gröning *et al.* (2011a) to compare no PDL and solid PDL models.

Final Models

In summary, the material properties assigned to each material for each of the models are shown in Table 4.2.

Table 4.2 Mechanical properties assigned to each material in all six different models.

Material		Finite Element Model					
		Fibrous PDL, Trabecular Structure	Fibrous PDL, Bulk Material	Solid PDL, Trabecular Structure	Solid PDL, Bulk Material	No PDL, Trabecular Structure	No PDL, Bulk Material
Cortical Bone	Young's Modulus (MPa)	17,000	17,000	17,000	17,000	17,000	17,000
	Poisson's Ratio	0.3	0.3	0.3	0.3	0.3	0.3
Trabecular Bone	Young's Modulus (MPa)	17,000	526	17,000	526	17,000	526
	Poisson's Ratio	0.3	0.3	0.3	0.3	0.3	0.3
Trabecular Filling	Young's Modulus (MPa)	1×10^{-4}	526	1×10^{-4}	526	1×10^{-4}	526
	Poisson's Ratio	0.3	0.3	0.3	0.3	0.3	0.3
Teeth	Young's Modulus (MPa)	17,000	17,000	17,000	17,000	17,000	17,000
	Poisson's Ratio	0.3	0.3	0.3	0.3	0.3	0.3
PDL Matrix	Young's Modulus (MPa)	1	1	49	49	17,000	17,000
	Poisson's Ratio	0.45	0.45	0.45	0.45	0.3	0.3
PDL Fibres	Young's Modulus (MPa)	1,000	1,000	N/A	N/A	N/A	N/A
	Poisson's Ratio	0.35	0.35	N/A	N/A	N/A	N/A

4.2.3 Model Loading

Three different loading scenarios were considered: an occlusal load and two different orthodontic loads. To assess the effect of the way in which the PDL was modelled, the results were compared between models with different types of PDL but the same type of trabecular tissue, *e.g.* Solid PDL Trabecular Structure versus Fibrous PDL Trabecular Structure. Similarly, to assess the effect of how the trabecular tissue was modelled, results were compared between models with different types of trabecular tissue, but with the same type of PDL, *e.g.* Solid PDL Trabecular Structure versus Solid PDL Bulk Material.

Occlusal Load

As before, an occlusal load of 500 N was distributed over a small area around the centre of the occlusal surface of the crown of the middle tooth, directed in the corono-apical direction (Figure 4.5).

To provide a straightforward visual assessment of the results from the different models, pair-wise comparisons were made by subtracting the element strains in one model from those in a second model, and presenting the results as colour-coded difference plots. This was done for both maximum (tensile) and minimum (compressive) principal strains.

To provide a more precise comparison of the results, maximum and minimum nodal principal strains were also plotted and compared for the different models. Results were taken from nodes on the outer surface of the cortical bone along a plane in the buccolingual direction through the centre of where the 500 N load was applied. Results were not plotted from nodes along the superior side of the mandible, but only around the buccal and lingual sides, from the top down to the lowest node on the inferior surface. The same plane was used for the convergence test (see Figure 4.6).

Orthodontic Load

Two separate orthodontic loads were also applied to each of the six different types of model, one directed in the distomesial direction, and one in the buccolingual direction (Figure 4.11). For these models, the boundary conditions on the two cut surfaces at the mesial and distal ends of the model remained the same. The 500 N occlusal load was removed, as were the constraints on the mesial and distal sides of the middle tooth since rotation of the tooth may occur during orthodontic tooth movement. A 1 N load was distributed over a small area around the centre of the buccal surface of the crown of the middle tooth (Figure 4.11). The value of 1 N was chosen to represent a typical load used during orthodontic treatment (Van Driel *et al.*, 2000).

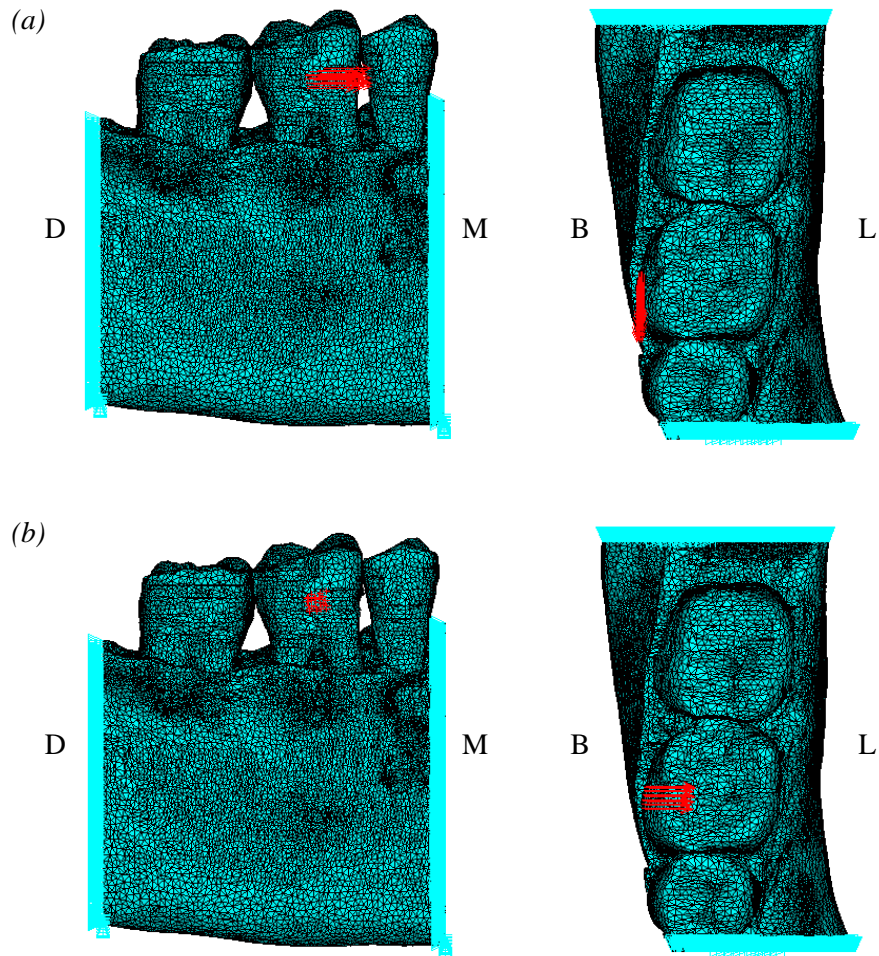


Figure 4.11 Finite element models showing loading and boundary conditions applied for the two orthodontic load cases, where light blue triangles represent constraints and red arrows represent applied forces: (a) two views of the distomesial orthodontic load; (b) two views of the buccolingual orthodontic load. Directions are represented by D for distal, M for mesial, B for buccal and L for lingual.

To compare the results from the orthodontic loads, nodal strain values were used from the inside surface of the alveolar bone, *i.e.* adjacent to the PDL, around both the mesial and distal roots of the middle tooth. For the distomesial load, results were obtained from nodes on the distal and mesial sides of each tooth root. Similarly, for the buccolingual load, results were obtained from nodes on the buccal and lingual sides of each tooth root. In both cases, results were obtained from all nodes on the inside surface of the alveolar bone, in a plane approximately through the apex of the tooth roots. Maximum and minimum principal strains were extracted from each of the nodes and were plotted against those from other models.

4.3 Results

The results are divided into three sections. First, the results from the model convergence test are presented in Section 4.3.1, followed by the analyses of the occlusal load and two orthodontic loads in Sections 4.3.2 and 4.3.3 respectively.

4.3.1 Model Development – Convergence Test

The convergence test compared nodal strains between the 1 million and 4 million element models at five locations around the outside of the cortical bone (Figure 4.6). The variations in the maximum principal strain, minimum principal strain and Von Mises strain results are shown in Figure 4.12, and show that the results from both models are similar at all five locations for all three types of strain. The largest errors occur at location four, with approximately a 15 % difference in strains between the two models. This is due to location four having the lowest absolute strain values. At this point, the absolute difference in strain between the two models is comparable to the absolute strain difference at other locations, but since the values are smaller the percentage difference is higher. However, most differences are less than 5 %, and so it was considered that the model had converged. (Remember that the node locations may not be identical in the two models).

4.3.2 Occlusal Load

The results from the occlusal load are divided into two sections: trabecular tissue modelling and PDL modelling. In order to study the effect of altering different features, one feature was varied while all others were kept constant.

Trabecular Tissue Modelling

Difference plots comparing maximum principal strains and minimum principal strains for bulk material and trabecular structure models are shown in Figure 4.13 and 4.14 respectively. For all difference plots in the two figures, the strain from the trabecular structure model is subtracted from the strain in the bulk material model. Therefore, in Figure 4.13, maximum principal strain, a negative value means the tensile strain is greater in the trabecular structure model and a positive value means the tensile strain is greater in the bulk material model. Conversely, in Figure 4.14, minimum principal strain, a negative value means the compressive strain is greater in the bulk material

model and a positive value means the compressive strain is greater in the trabecular structure model. Figure 4.15 compares the actual nodal strain values on the buccal and lingual surfaces of the cortical bone for the trabecular structure and bulk material models for each of the three PDL types.

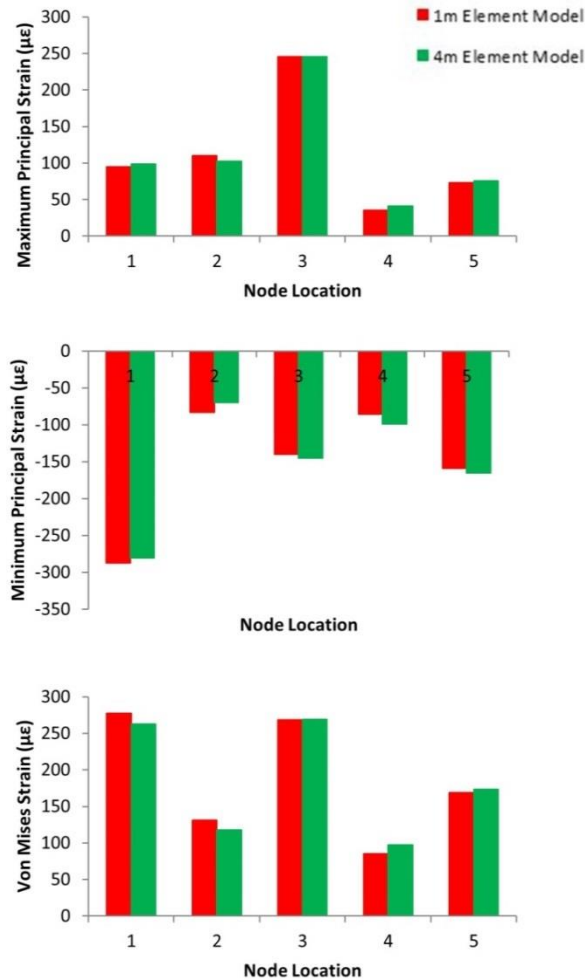


Figure 4.12 Strain graphs showing maximum principal strain, minimum principal strain and Von Mises strain results from the convergence test models.

In both Figures 4.13 and 4.14, the difference plots are similar for each of the three PDL types. Both figures clearly indicate that the way in which the trabecular tissue is modelled significantly affects the strain throughout the mandible section, and is not confined to a particular area, *e.g.* around the loaded tooth. Generally speaking, tensile strain (Figure 4.13) is greater in the trabecular structure model, although there are regions where it is greater in the bulk material model. This general trend is also seen in Figure 4.15. The results from the compressive stain (Figure 4.14) are more varied. Compressive strain is generally higher in the trabecular structure model around the alveolar process and around the inferior portion of the mandible, whereas it is generally higher in the bulk material model around the mandibular body. However, Figure 4.15

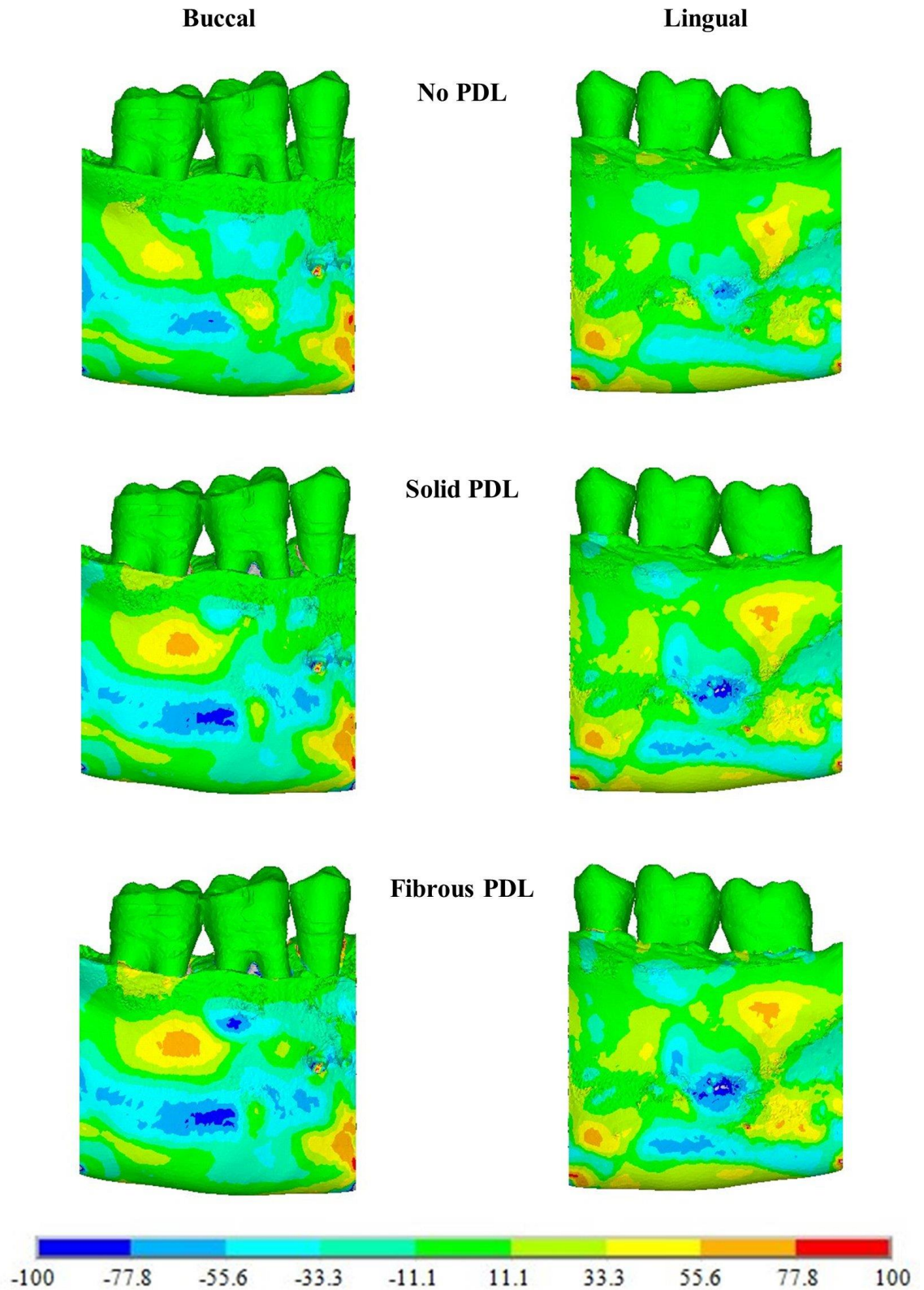


Figure 4.13 Maximum principal strain difference plots for the strain differences, in microstrain, between the trabecular structure and bulk material models with each of the three PDL types.

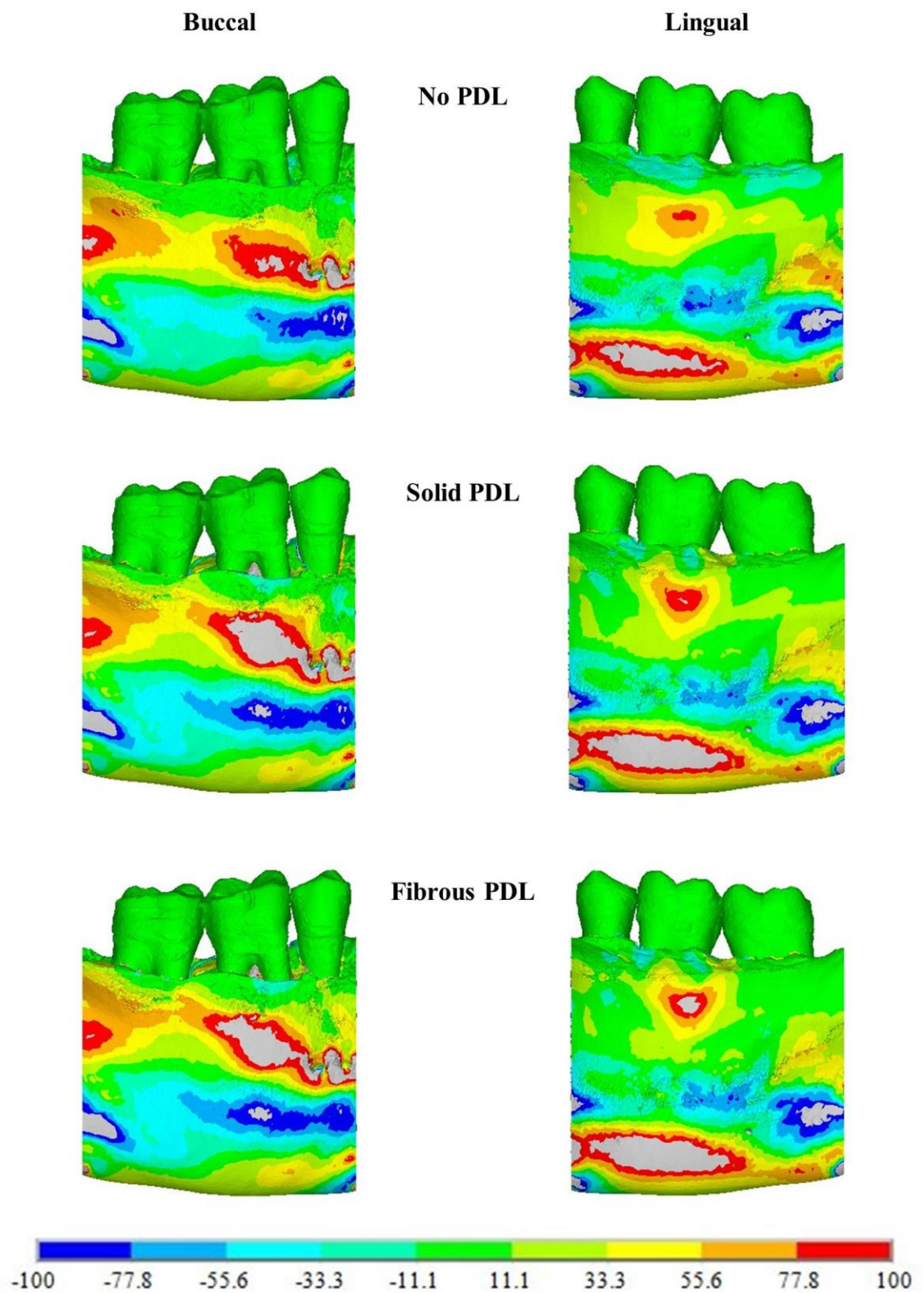


Figure 4.14 Minimum principal strain difference plots for the strain differences, in microstrain, from trabecular structure and bulk material models with each of the three PDL types.

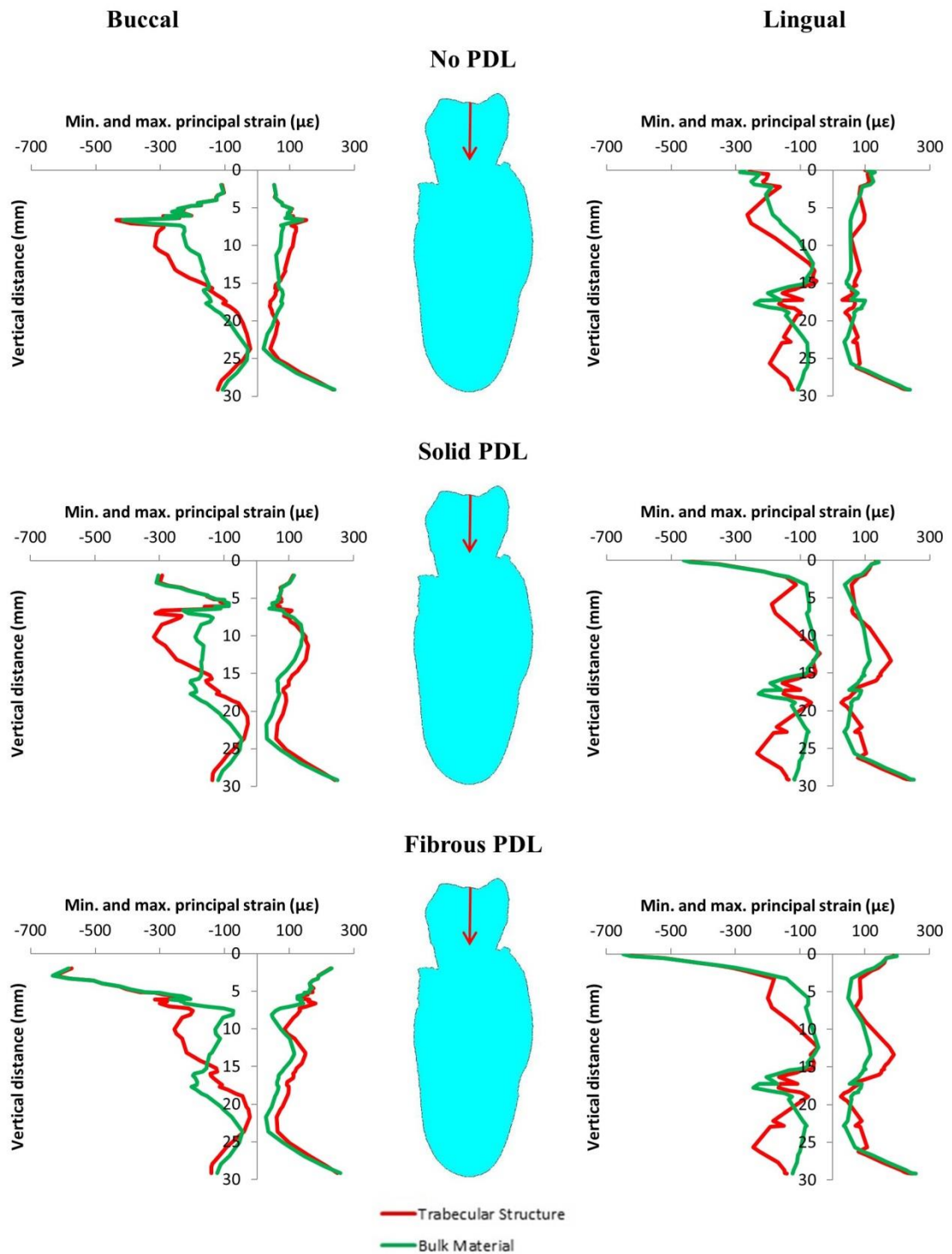


Figure 4.15 Vertical strain profiles for maximum and minimum principal strains on the buccal and lingual surfaces of the cortical bone from the 500 N occlusal load. Graphs compare results from trabecular structure and bulk material models for each of the three PDL representations. The red arrows indicate the direction of the applied load.

shows that for both trabecular structure and bulk material models, compressive strain is generally highest towards the superior part of the mandibular corpus, and decreases further down, though it increases again towards the base of the corpus.

PDL Modelling

Difference plots comparing maximum principal strains and minimum principal strains for each of the three PDL types, all with bulk material trabecular tissue, are shown in Figures 4.16 and 4.17 respectively. Similarly, difference plots comparing maximum principal strains and minimum principal strains for each of the three PDL types, all with trabecular structure trabecular tissue, are shown in Figures 4.18 and 4.19. Although there are three types of PDL, only two models can be compared at a time, *e.g.* no PDL vs solid PDL. In each case, strains in the second model have been subtracted from strains in the first model. Similar to Figures 4.13 and 4.14, for maximum principal strain difference plots, a negative value means the tensile strain is greater in the second model, whereas for minimum principal strain difference plots, a negative value means compressive strain is greater in the first model. Figure 4.20 compares nodal strain results from each of the three PDL types, for both of the two trabecular tissue types.

The two maximum principal strain figures (Figure 4.16 and Figure 4.18) are similar to each other, as are the two minimum principal strains figures (Figure 4.17 and Figure 4.19). In all four figures (Figures 4.16 to 4.19) the difference plots comparing the no PDL and solid PDL models are similar to those comparing the no PDL and fibrous PDL models. Generally speaking, tensile strain (Figures 4.16 and 4.18) is higher in models with a PDL, either solid or fibrous, than in the model with no PDL. However, compressive strain (Figures 4.17 and 4.19) appears generally higher around the alveolar process, not including the very top of the mandible, for the no PDL model, whereas it is generally comparatively higher around the body of the mandible for the two models with a PDL. This is also shown by the strain graphs in Figure 4.20, where, other than for compressive strain around the alveolar process, strain is generally lower in the no PDL model than in the two models with a PDL. In the superior part of the mandibular corpus, both compressive and tensile strain, though especially compressive strain, are much higher in models with a PDL than without, and even higher in the fibrous PDL model than in the solid PDL model. This is shown clearly by the strain graphs in Figure 4.20, as well as in the difference plots.

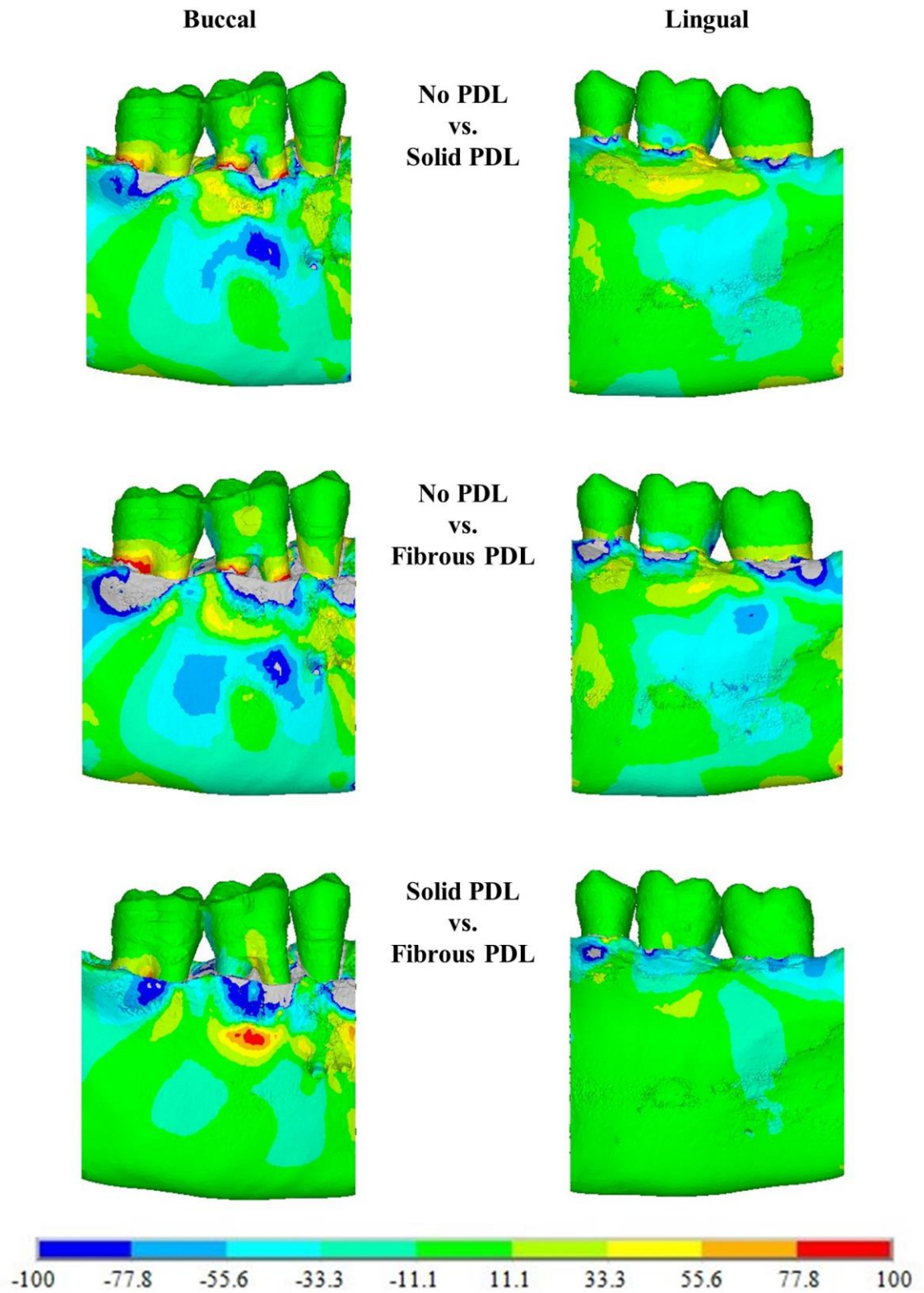


Figure 4.16 Maximum principal strain difference plots for the strain differences, in microstrain, between models with bulk material trabecular tissue but different PDLs as indicated.

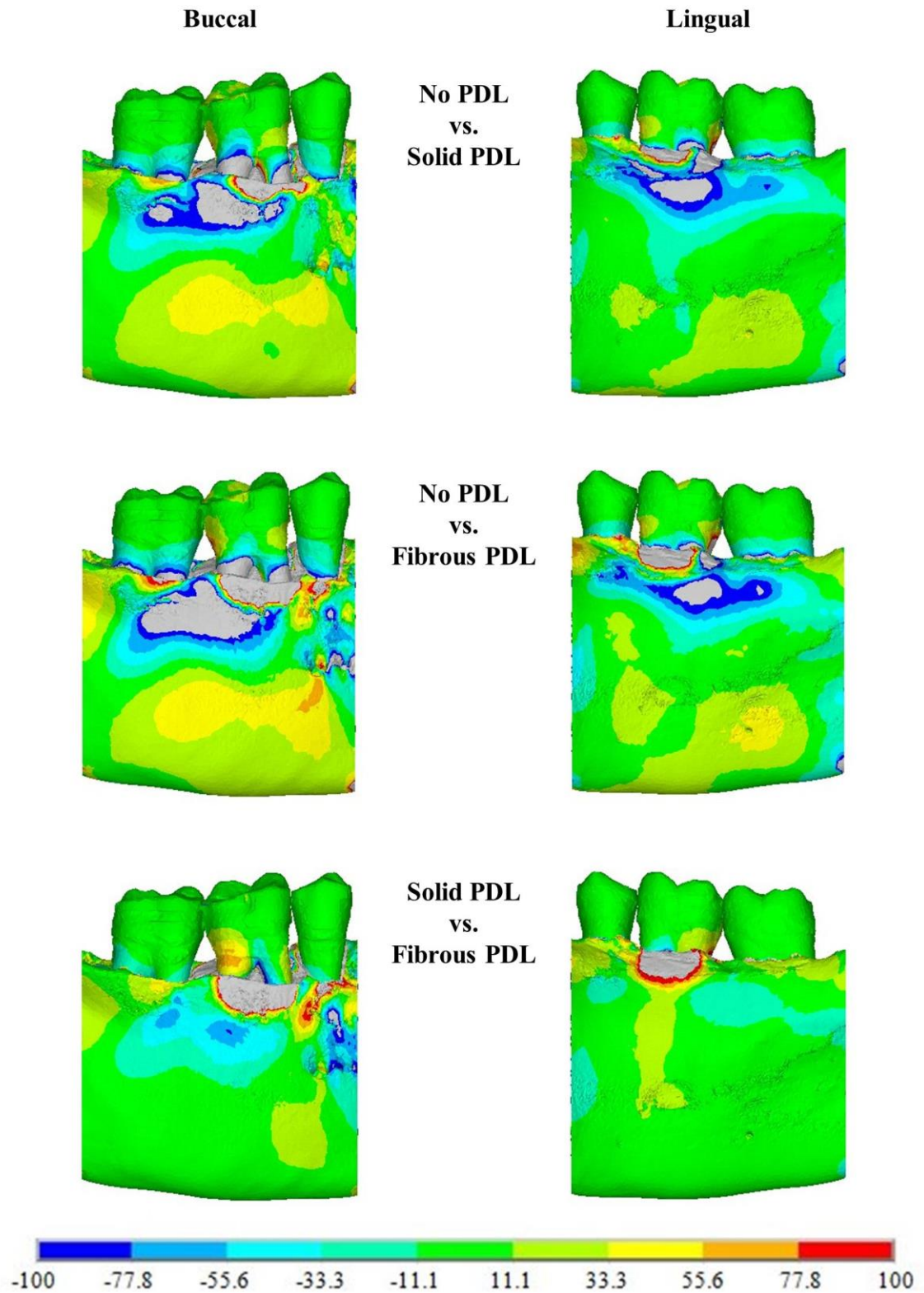


Figure 4.17 Minimum principal strain difference plots for the strain differences, in microstrain, between models with bulk material trabecular tissue but different PDLs as indicated.

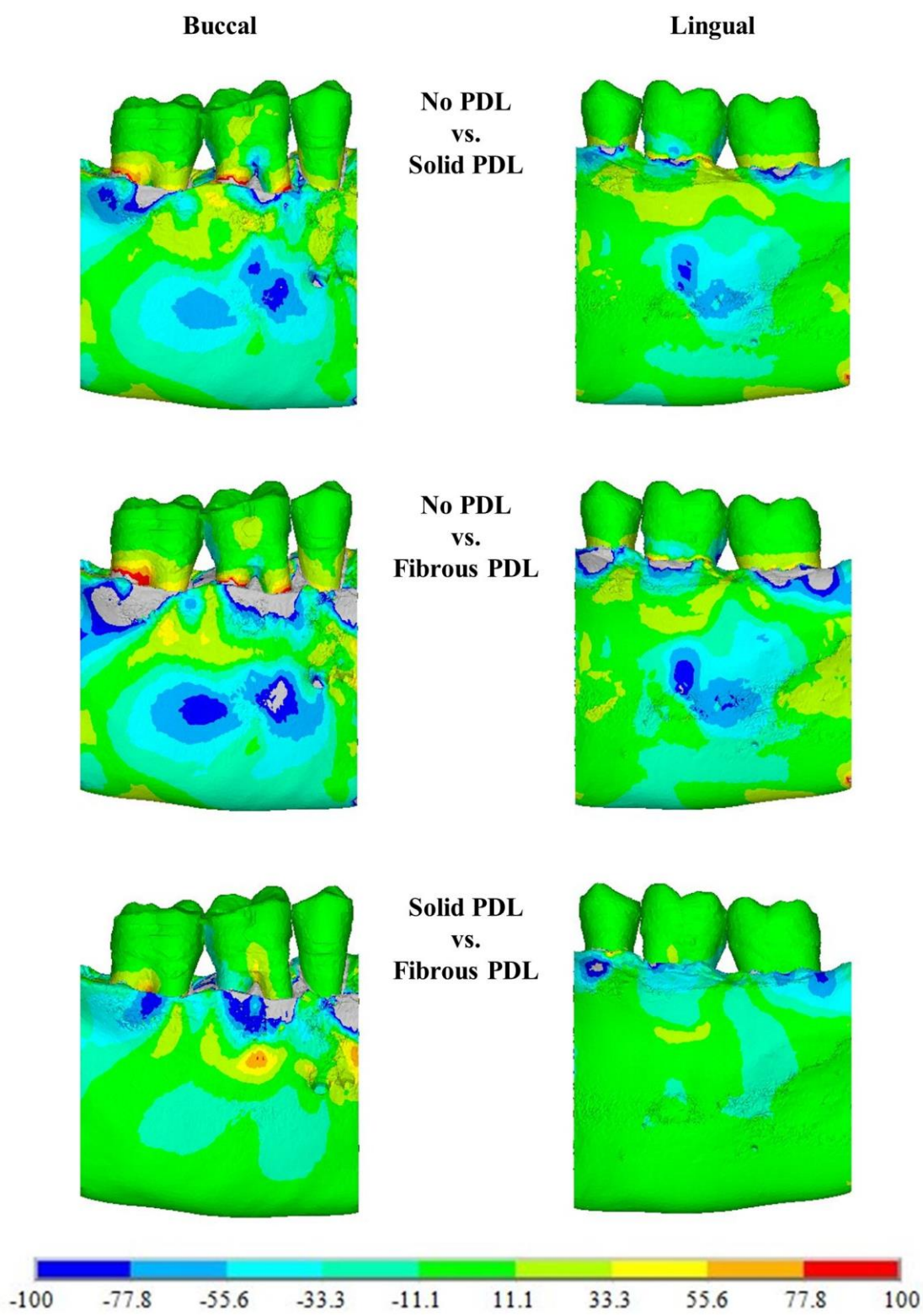


Figure 4.18 Maximum principal strain difference plots for the strain differences, in microstrain, between models with trabecular structure trabecular tissue but different PDLs as indicated.

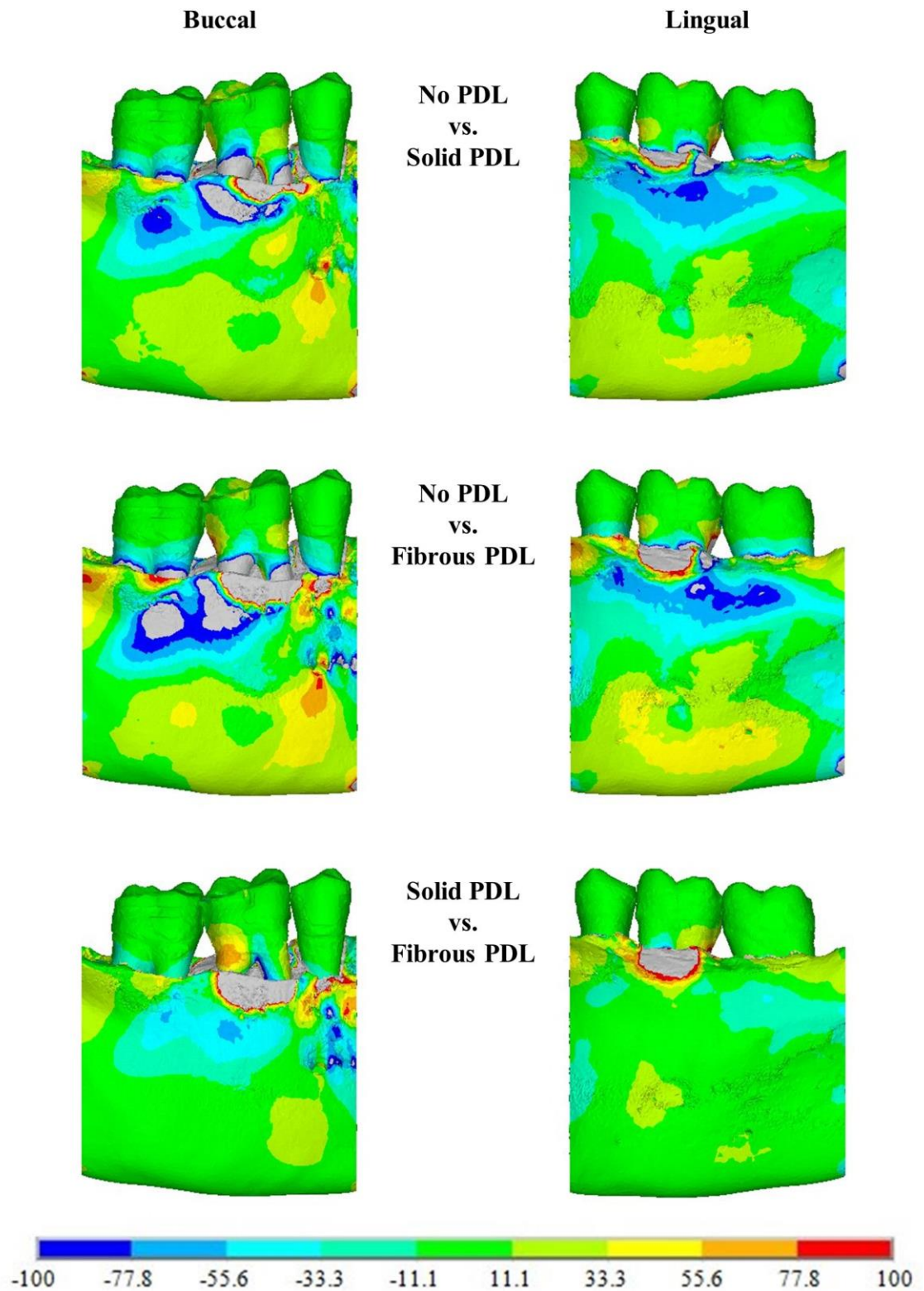


Figure 4.19 Minimum principal strain difference plots for the strain differences, in microstrain, between models with trabecular structure trabecular tissue but different PDLs as indicated.

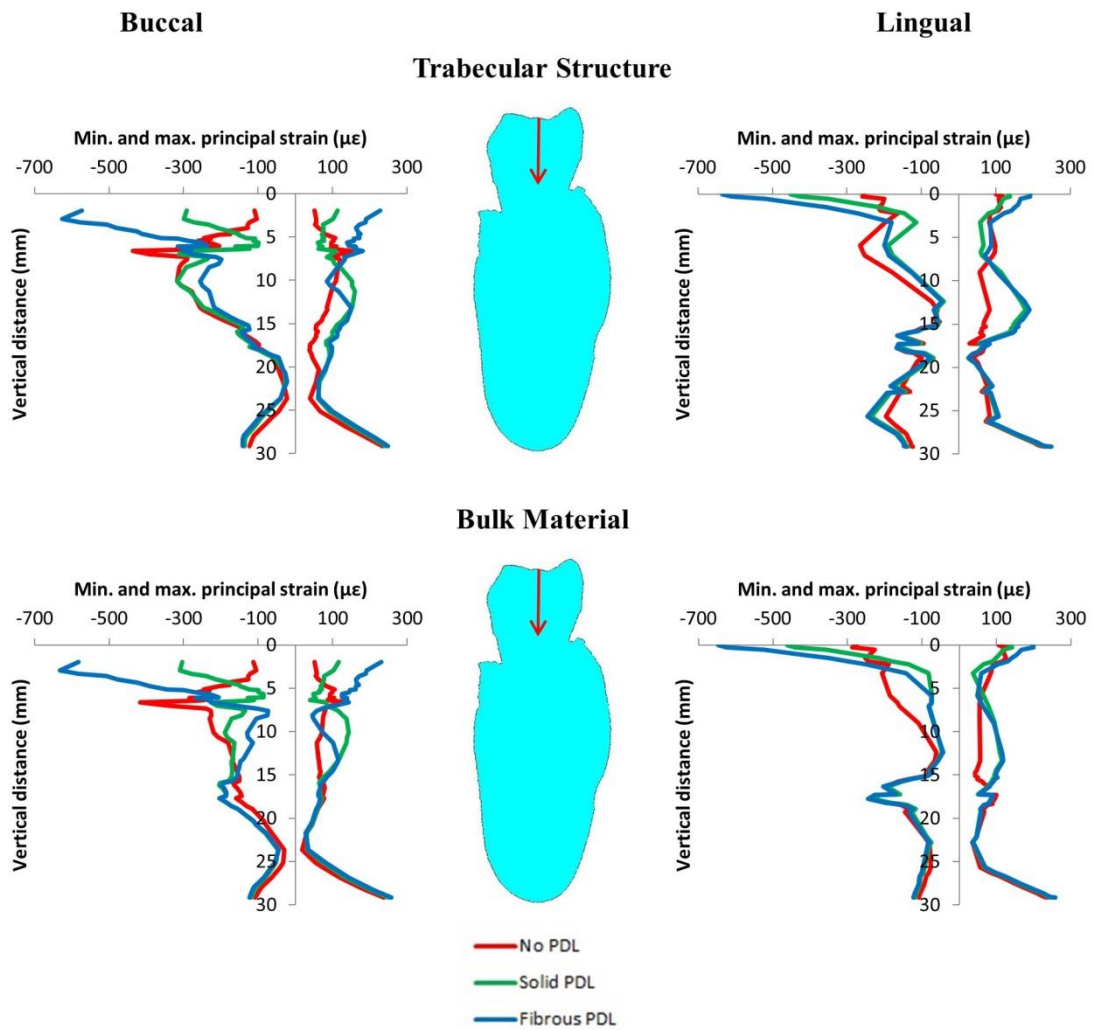


Figure 4.20 Vertical strain profiles for maximum and minimum principal strains on the buccal and lingual surfaces of the cortical bone from the 500 N occlusal load. Graphs compare results from no PDL, solid PDL and fibrous PDL models for both trabecular tissue types. The red arrows indicate the direction of the applied load.

Comparing the solid PDL and fibrous PDL models, there are large differences in the alveolar process with the fibrous PDL model generally having the higher strains. However, for the majority of the body of the mandible, especially on the lingual side, the strains are similar. So, generally speaking, the plots show that there is more difference between the no PDL model and either of the two models with a PDL (either solid or fibrous), than there is between the solid PDL and fibrous PDL models. This is also shown by the strain graphs in Figure 4.20, where, apart from the superior part of the mandibular corpus, the strains for the two PDL models are very similar although all 3 models appear very similar at the base of the mandible.

4.3.3 Orthodontic Load

The results from the orthodontic load are divided into two sections: results from the distomesial load and results from the buccolingual load. Within each of these sections, results are first presented to compare the two different methods of modelling the trabecular tissue, and then to compare the different methods of modelling the PDL. Nodal strains have been taken from the inside surface of the alveolar bone around the loaded tooth. As this tooth has two roots, a distal root and a mesial root, results are presented for strains around both roots for each of the two loads.

Distomesial Orthodontic Load

Figures 4.21 and 4.22 compare nodal strain results from the trabecular structure and bulk material models, for each of the three PDL types, around the distal root and mesial root respectively. [It is very important to note the scales of the x-axes in the different plots]. Figure 4.23 compares nodal strain results from each of the three PDL types, all with trabecular structure for the trabecular tissue, around both the distal and mesial roots.

Figures 4.21 and 4.22 show that for both roots there is very little difference in the results obtained from the trabecular structure and bulk material models. Therefore, rather than plotting results for both the trabecular structure model and bulk material model, only results from the former are considered, in Figure 4.23, when examining the effects of the different PDL models.

Looking at Figure 4.23, the strain magnitudes for each of the PDL representations are very different, therefore the three models are difficult to plot on the same graph (Figure 4.23). However, the distributions (in Figures 4.21 and 4.22) have some similarities in places, especially on the outside of the tooth roots, *i.e.* the distal side of the distal root (Figure 4.21) and the mesial side of the mesial root (Figure 4.22). The strains for the no PDL model in Figures 4.21 and 4.22 also show a similar trend to those in the solid PDL and fibrous PDL models, although there are more noticeable differences and the graphs are generally smoother.

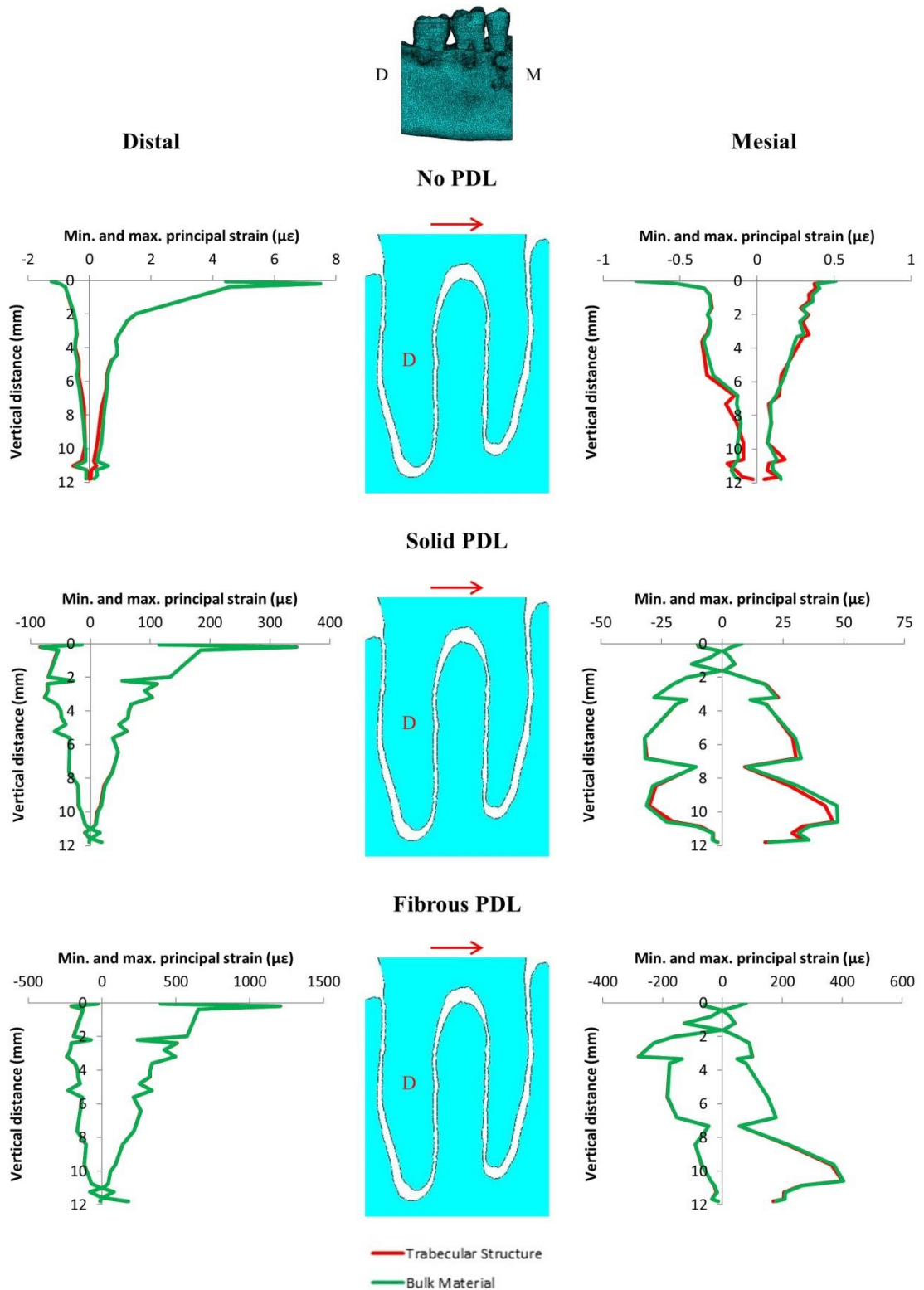


Figure 4.21 Vertical strain profiles for maximum and minimum principal strains on the distal and mesial surfaces of the alveolar bone around the distal (D) tooth root from the 1 N distomesial orthodontic load. Graphs compare results from trabecular structure and bulk material models for each of the three PDL types. The red arrows indicate the direction of the applied load. The Image at the top indicates the viewing direction for the results where D is distal side and M is the mesial side of the model. [Note the different scales of the x-axes].

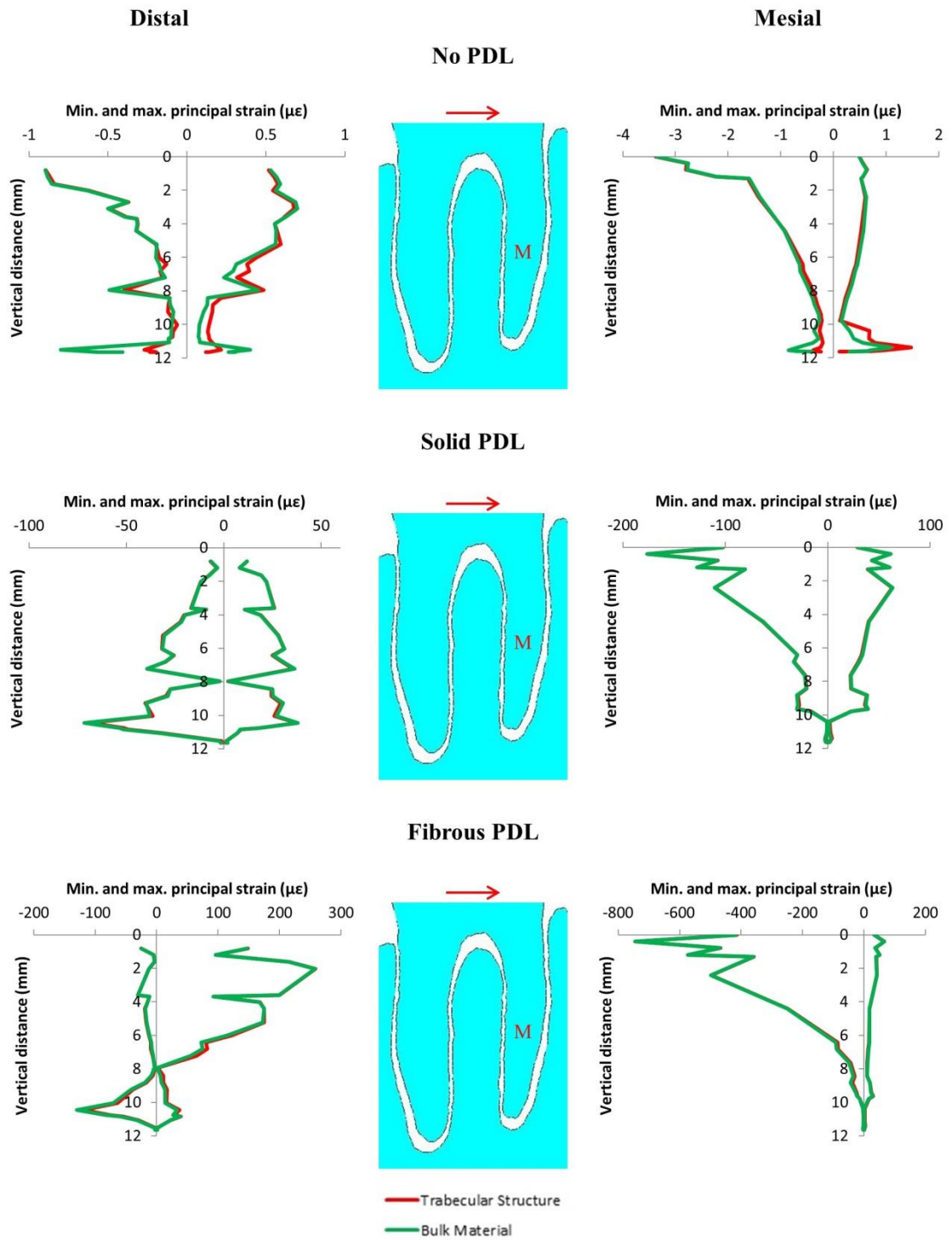


Figure 4.22 Vertical strain profiles for maximum and minimum principal strains on the distal and mesial surfaces of the alveolar bone around the mesial (M) tooth root from the 1 N distomesial orthodontic load. Graphs compare results from trabecular structure and bulk material models for each of the three PDL types. The red arrows indicate the direction of the applied load. [Note the different scales of the x-axes].

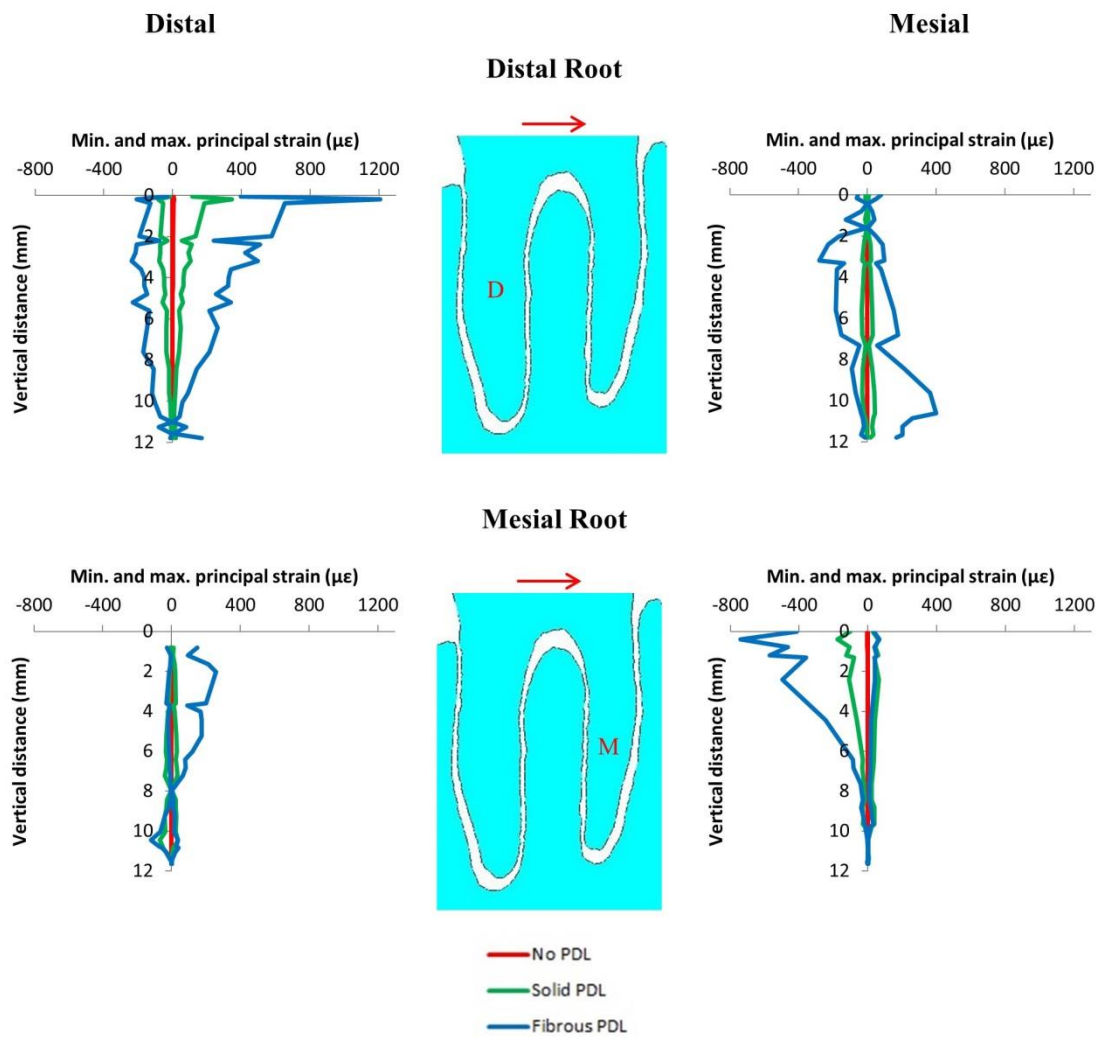


Figure 4.23 Vertical strain profiles for maximum and minimum principal strains on the distal and mesial surfaces of the alveolar bone around both the distal (D) and mesial (M) tooth roots from the 1 N distomesial orthodontic load. Graphs compare results from no PDL, solid PDL and fibrous PDL models each with trabecular structure trabecular tissue. The red arrows indicate the direction of the applied load.

Buccolingual Orthodontic Load

Figures 4.24 and 4.25 compare nodal strain results on the buccal and lingual surfaces of the alveolar bone around the distal root and mesial root respectively as predicted by the trabecular structure and bulk material models, for each of the three PDL types. Note that the strain results for the buccolingual load are taken from a different plane to the results for the distomesial load as indicated in Figures 4.21 and 4.24. Figure 4.26 compares nodal strain results from each of the three PDL types, all with trabecular structure for the trabecular tissue, around both the distal and mesial roots.

As with the results from the distomesial load (Figures 4.21 and 4.22), Figures 4.24 and 4.25 show that for both roots there is very little difference in the results obtained from the trabecular structure and bulk material models. Therefore, as for the distomesial load (Figure 4.23), the results for the three types of PDL were only plotted for trabecular structure models and are shown for both roots together (Figure 4.26).

Again, as was observed with the distomesial load, due to the large difference in strain magnitudes between the different models, it is difficult to compare the models when the results are all plotted on the same graph (Figure 4.26). However, looking again only at the distribution of the values in Figures 4.24 and 4.25, and ignoring the magnitude, the graphs for the solid PDL models are very similar to the graphs for the fibrous PDL models. This is true on both buccal and lingual sides of the model for both distal and mesial roots. Similarly to the distomesial load, the strain in the no PDL models also shows some similarity to the general shape of the graphs for the solid and fibrous PDLs although there are specific differences.

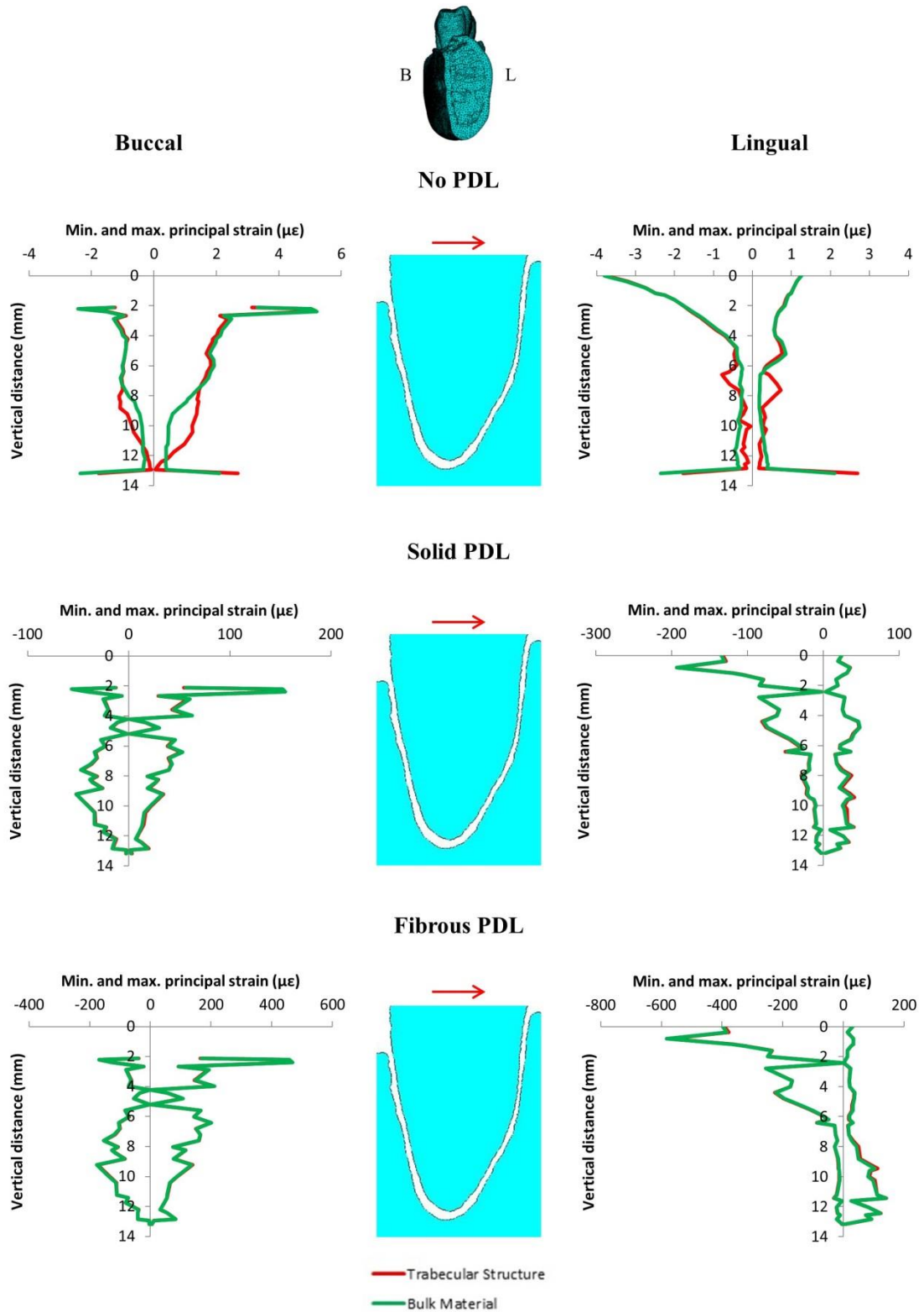


Figure 4.24 Vertical strain profiles for maximum and minimum principal strains on the buccal and lingual surfaces of the alveolar bone around the distal tooth root from the 1 N buccolingual orthodontic load. Graphs compare results from trabecular structure and bulk material models for each of the three PDL types. The red arrows indicate the direction of the applied load. The Image at the top indicates the viewing direction for the results where B is buccal side and L is the lingual side of the model. [Note the different scales of the x-axes].

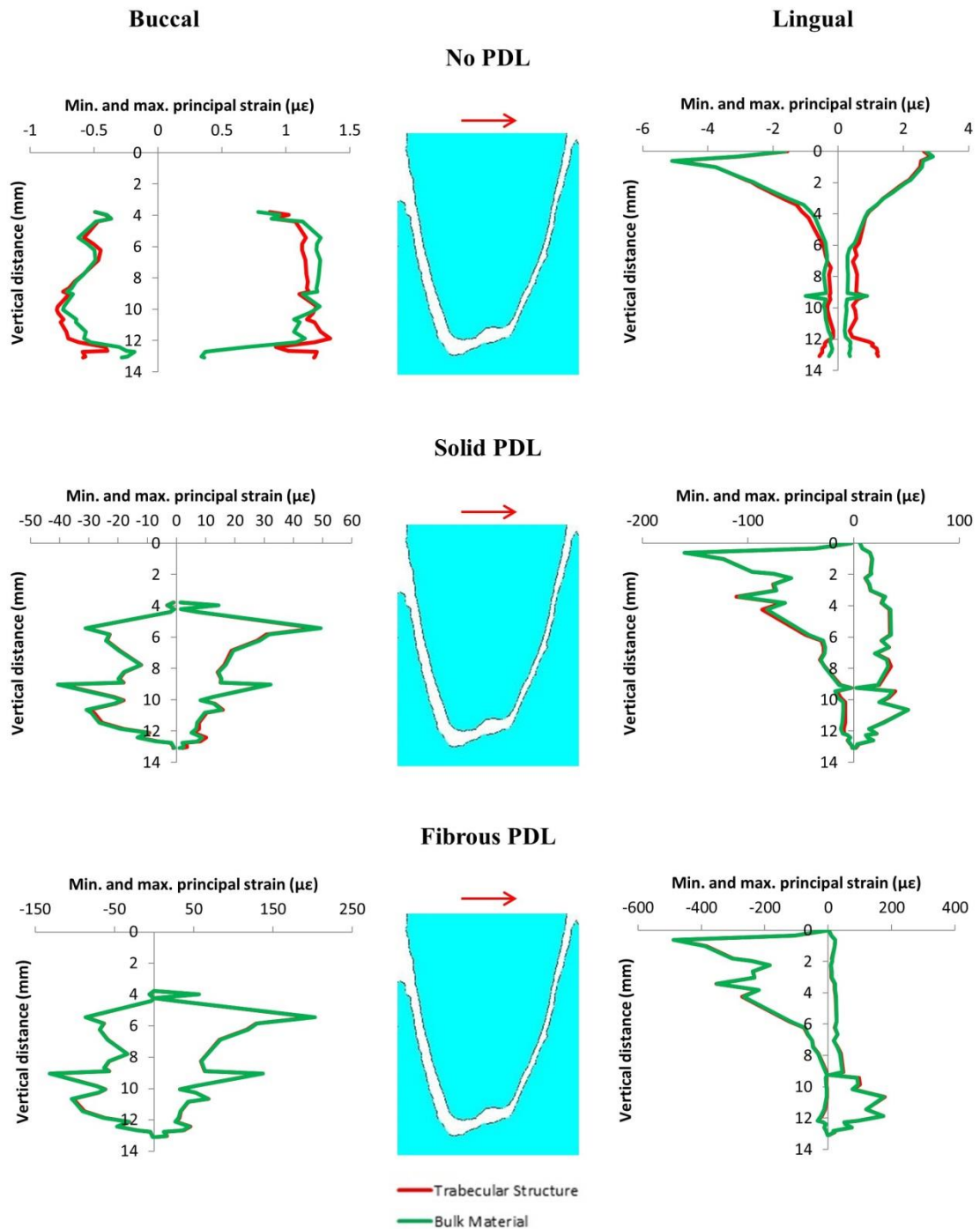


Figure 4.25 Vertical strain profiles for maximum and minimum principal strains on the buccal and lingual surfaces of the alveolar bone around the mesial tooth root from the 1 N buccolingual orthodontic load. Graphs compare results from trabecular structure and bulk material models for each of the three PDL types. The red arrows indicate the direction of the applied load. [Note the different scales of the x-axes].

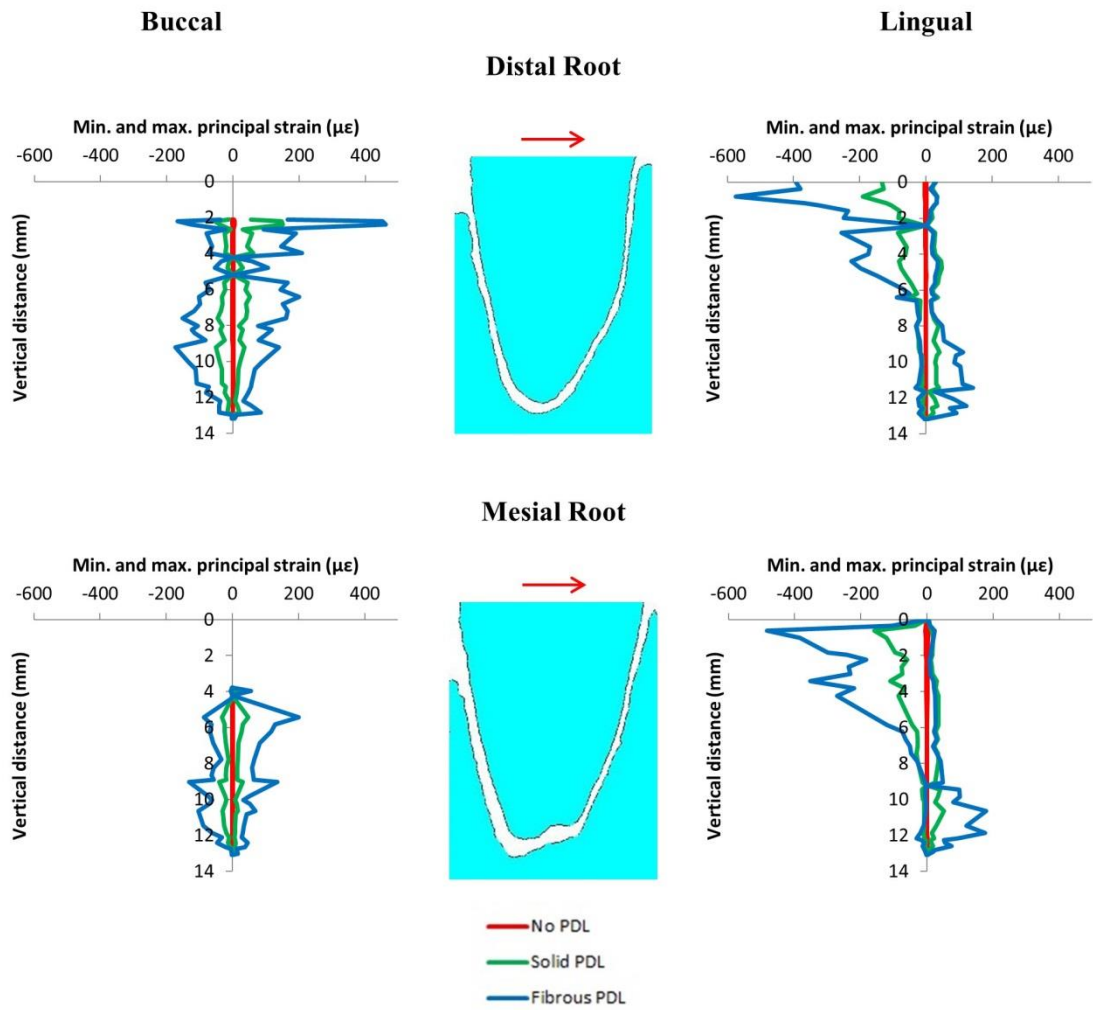


Figure 4.26 Vertical strain profiles for maximum and minimum principal strains on the buccal and lingual surfaces of the alveolar bone around both the distal and mesial tooth roots from the 1 N buccolingual orthodontic load. Graphs compare results from no PDL, solid PDL and fibrous PDL models each with trabecular structure trabecular tissue. The red arrows indicate the direction of the applied load.

4.4 Discussion

In this section the results presented in the previous sections are discussed. The relevance of the results to the overall aim of the research, their relationship to previous research in this field and their implications for orthodontic tooth movement are discussed in the main discussion in Chapter 6.

4.4.1 Model Development

As part of the model development process, a mesh convergence test was performed to confirm that the model had converged and was thus suitable for further analysis. Since including the PDL fibres manually is a very time consuming process, the convergence test was performed before they were added, so this only needed to be done once. The results from the convergence test (especially Figure 4.12) show that the model has converged since there is little difference between the strains in the 1 million and 4 million element models. Therefore, the 1 million element model was chosen for further analyses.

4.4.2 Occlusal Load

For the occlusal load, results have been plotted from the outer surface of the cortical bone. This is the region of the model furthest away from the PDL, and the trabecular bone, and therefore, results were compared here to see if the ways in which the PDL and trabecular tissue are modelled, affects the results throughout the mandible not just in the area local to the tissue.

The difference plots for the three PDL types are similar in both Figures 4.13 and 4.14 suggesting that the way in which the trabecular tissue is modelled does affect the strain results irrespective of how the PDL is modelled. In general, strain is higher for the trabecular structure models than for the bulk material models. Previous studies have suggested that it is the cortical bone rather than the trabecular bone which is primarily responsible for resisting masticatory loads in the mandible (Ralph & Thomas, 1988; Yaşar & Akgünlü, 2005). This is unsurprising when the volume of each is compared, but clearly the load transfer path between the tooth and cortical bone is critical and is dictated by the arrangement of the alveolar bone and trabecular bone, and the use of a bulk filler rather than trabeculae changes that load transfer path significantly.

For the different types of PDL, the results from both the difference plots (Figures 4.16 to 4.19) and the strain graphs (Figure 4.20) show that the strains are more

similar in the two models with a PDL (solid or fibrous) than in the no PDL model. This is especially shown in the difference plots. The difference plots comparing the no PDL and solid PDL models are very similar to the difference plots comparing the no PDL and fibrous models. However, the difference plots comparing the solid PDL and fibrous PDL models are noticeably different to the others and generally show less change in the strains between the two models. This suggests that whilst it may be important to include a PDL in mandibular finite element models, it may be unnecessary to include the fibrous structure. Other than for compressive strain around the alveolar process, strain is generally higher in the models with a PDL. This agrees with the findings of Gröning *et al.* (2011a) and Marinescu *et al.* (2005) which both found that not including the PDL increases the stiffness of the mandible and thus decreases the strains observed.

Although there are differences in strains observed with and without a PDL, Figure 4.20 shows that, other than the superior part of the mandibular bone, the strain distribution is generally quite similar for all three types of PDL, especially towards the base of the mandible furthest away from the PDL. This may be due to the boundary conditions applied. The loading applied to the section of mandible is similar to a three-point bending situation, with the two ends supported and a load applied in the middle. Therefore, the bending caused will put the mandible in tension at the bottom and compression at the top, as shown by the strains in Figure 4.20. Beam mechanics suggests that in this situation, the effect of including the PDL would be less than if the direction of bending was reversed (Gröning *et al.*, 2011a). Gröning *et al.* (2011a) found that including the PDL in human mandibular finite element models led to increased torsion of the mandible about the posterior-anterior axis compared to models without a PDL. In addition to this, Hylander (1984, 1985) found that, in non-human primates, wishboning was the main deformation type observed in the mandible during mastication. Since only a section of the molar region was included in this model, rather than the whole mandible, neither of these two types of deformation will be included here, which would reduce the potential impact that including the PDL could have on strains within the model.

4.4.3 Orthodontic Load

All of the results comparing trabecular structure and bulk material models for the orthodontic loads (Figures 4.21, 4.22, 4.24 and 4.25) show that there is very little difference between the results from the two types of trabecular tissue. This may be

because towards the superior portion of the tooth socket, the alveolar bone is surrounded by cortical bone rather than trabecular bone (see Figures 4.3 and 4.3). This is particularly true for the buccal side as the tooth is closer to that side of the mandible (see Figure 4.11). Therefore, part of the alveolar bone from which results were obtained is not attached to trabecular bone. Additionally, since the orthodontic loads are orientated in the transverse plane, the load does not pass as much through the trabecular bone as it does for the occlusal load.

The results show that there is a large difference in strain magnitude predicted for each of the three different types of PDL for both orthodontic loads (Figures 4.21 to 4.26). This is especially true for the no PDL model which has strains around two to three orders of magnitude lower than that of the fibrous PDL model. This is because without a PDL the tooth is fused with the alveolar bone creating a rigid structure. There is less difference between the solid PDL and fibrous PDL models, however, the strains in the fibrous PDL model are around two to three times greater than the strains in the solid PDL model. Therefore there is still quite a big difference between these two models.

For both orthodontic loads, the solid and fibrous PDL models produced very different results. Conversely, the results from the two models were very similar for the occlusal load. The Young's modulus for the solid PDL was optimised to match that of the fibrous PDL under the occlusal load since that would be the dominant load which occurs naturally, whereas orthodontic loads are not natural. The PDL fibres are primarily arranged to provide axial and torsional stability rather than stability in the buccolingual or mesiodistal directions. Shear forces resulting from transverse movements during chewing would cause some natural tooth movement in those directions, however, this would be combined with an occlusal load which would stiffen the PDL fibre system. So, the two models are similar under the physiological occlusal load, whereas the fibrous PDL provides less resistance in the case of the non-physiological orthodontic load.

Chapter 5

Other Species Molar Region Finite Element Models

5.1 Introduction

Chapter 4 investigated three different ways of modelling the periodontal ligament (PDL) using the molar region of a human mandible: no PDL, solid PDL and fibrous PDL. The results indicated that under an occlusal load, including the PDL reduced the overall stiffness of the model and thus increased the strain. Although there were some differences between the results from the solid and fibrous PDL models, greater differences were observed between the model without a PDL and those with a PDL, than between the two different types of PDL.

This study builds upon the previous one, investigating the effect of including the PDL in mandibular finite element models of different species. The purpose of this was to determine whether the findings from the previous study were specific to the human molar region, or whether they may be true for the mammalian mandible in general. Five species were chosen: domestic cats (*Felis silvestris*), wild cercocebus (*Cercocebus atys*), domestic pigs (*Sus scrofa*), wild rabbits (*Oryctolagus cuniculus*), and domestic sheep (*Ovis aries*). These species were chosen because they show a diverse range of molar shapes: cats have blade-shaped molars, cercocebus have molars with high cusps and ridges, pigs have flattened molars with rounded cusps, and rabbits and sheep have flattened molars with ridges. These species also have very different tooth root morphologies which may be important since this study is interested in the PDL which surrounds the tooth roots: cat and cercocebus molars have two roots, pig molars have five roots, rabbit molars have a single root, and sheep molars have two or three roots.

The aim of this study was to investigate the effect of including the PDL as a layer of solid material in mandibular finite element models. The PDL is difficult to visualise using computed tomography scans and is time consuming to include in finite element models, so many researchers have not included it (*e.g.* Marinescu *et al.*, 2005; Boryor *et al.*, 2008). A few sensitivity studies have previously tested how this lack of PDL might affect the results (*e.g.* Wood *et al.*, 2011; Gröning *et al.*, 2011a, 2012b).

Therefore, this study adds to the discussion about the importance of the PDL by investigating its effect in these five species. This was done using finite element models of the molar region of the five species, with and without a PDL, under the application of an occlusal load. To assess the effect of including the PDL, results from the models with and without a PDL were compared for each of the five species. In Chapter 4, two different methods of representing the trabecular tissue were also investigated. High resolution scans are required to include the structure of the individual trabeculae of the trabecular tissue in finite element models. For practical reasons, most mandibular finite element models, therefore, represent the trabecular tissue as a homogeneous bulk material (*e.g.* Tanne *et al.*, 1993; Koriath & Hannam, 1994; Ichim *et al.*, 2006, 2007; Gröning *et al.*, 2011b, 2012b). However, the results from Chapter 4 indicated that this simplification does affect the strains in the mandible, and so in this study the structure of individual trabeculae was included in all finite element models.

5.2 Materials and Methods

For this study, finite element models were created of the molar regions of five different species of mammals: cat (*Felis silvestris*), cercocebus (*Cercocebus atys*), pig (*Sus scrofa*), rabbit (*Oryctolagus cuniculus*) and sheep (*Ovis aries*). Two models were created for each species using data from the same individual: a no PDL model and a solid PDL model. For each individual, the two models were created from the same finite element mesh by varying the material properties assigned to the elements of the PDL. All finite element analyses were performed using ANSYS software (version 14.5, ANSYS Inc., Canonsburg, PA, USA) following image segmentation and tetrahedral mesh generation using AVIZO software (version 6.3, FEI Visualization Sciences Group, Berlin, Germany).

The Materials and Methods section describes first how the finite element meshes were generated (Section 5.2.1), followed by how the two different finite element models were developed for each of the five species (Section 5.2.2). All of the models were then tested with an occlusal load and the results obtained were used to compare the no PDL and solid PDL models for each species (Section 5.2.3). The methodology was similar for all five species and so they are all described in the same section, with differences mentioned when required.

5.2.1 Mesh Generation

This section describes how the finite element mesh was generated, from a micro-computed tomography (microCT) scan, using AVIZO.

Micro-computed Tomography Scanning

The five mandible specimens selected for this study were dissected and cleaned before a microCT scan was taken using an X-Tek HMX160 microCT scanner (X-Tek Systems Ltd., Tring, UK) at the University of Hull. The resulting microCT data sets were exported as stacks of 8-bit TIFF (tagged image file format) images and imported into AVIZO image segmentation software. The voxel size, in all three directions, for each of the five scans were as follows: cat 0.019 mm, cercocebus 0.071 mm, pig 0.071 mm, rabbit 0.019 mm, and sheep 0.057 mm. The resolutions varied because the smallest possible field of view was chosen for each specimen to achieve the maximum resolution. For the cat, pig, rabbit, and sheep, only the molar region was scanned, whereas for the cercocebus the whole mandible was scanned.

Thresholding and Manual Segmentation

A detailed representation of the three-dimensional geometry of the trabecular architecture was included in these finite element models. This was achieved using the Ray Casting Algorithm, which was developed specifically for segmenting fine scale bone structures using automatic thresholding of the grey scale values (Scherf & Tilgner, 2009). Thus, rather than defining specific grey scale values, this algorithm uses the three-dimensional grey value gradient for the image set, with structure boundaries defined by the maxima of the grey value gradients. Therefore, thresholding is unaffected by slight variations in brightness, which are a large source of error in conventional threshold-based methods (Scherf & Tilgner, 2009).

After thresholding, each model was cropped to just the molar region. These were taken from the right side of the mandible for the cat and cercocebus, and the left side of the mandible for the pig, rabbit and sheep. In each case, the model was cropped to just three teeth, except for the rabbit where five teeth were kept because the tooth roots curve backwards underneath one another, so it was impractical to crop to just three teeth. As a result, the rabbit model contained the first and second premolars, and the first, second and third molars. The sheep, pig and cercocebus models all contained the second premolar and first and second molars. The third molars were not present in the

pig mandible and were only partially erupted in the sheep mandible so these were not included in the models. In the cercocebus mandible, the third molar was present and fully erupted, but was cropped out so that the teeth used were consistent with the pig and sheep models. Therefore, the same three teeth were used in the cercocebus, pig and sheep models as were used in the human model for the previous study (Chapter 4). Additionally, the pig model contained two unerupted teeth, one underneath the premolar, and the other underneath the first molar. Finally, since cats only have one molar tooth in each tooth row, the cat model contained the first and second premolars, and the molar.

Further manual segmentation was then required to separate different materials within the models. Firstly, points of contact between adjacent teeth were removed, so that each tooth was completely separate from any other teeth to avoid unintended stiffening of the model and loading of the adjacent teeth. All of the teeth were also manually separated from the surrounding alveolar bone. Where necessary, at points of contact between the teeth and alveolar bone, the teeth were edited, rather than the bone, so as not to reduce the volume of alveolar bone present to avoid artificially high strains in the bone.

After separating the teeth, a material was added around the tooth roots to represent the PDL. This material was created by expanding the outer surface of the tooth roots to fill the gap between the tooth and the alveolar bone. This created a material completely surrounding the tooth root, and joining the tooth root to the alveolar bone, for all of the teeth. This was a different method to that used to add the PDL to the human model (Chapter 4), where a border was first created around the cervical margin of the tooth, between the tooth and alveolar bone, and then the space between the tooth and bone was flood-filled with a new material. However, both methods essentially have the same result, adding a material into the gap between the tooth and alveolar bone to represent the PDL. Additionally, there were also some areas in each of the models where there were gaps in the alveolar bone, which were manually filled in as required.

A few final edits were then made to some of the models. In the pig model, a layer of material was added around the outside of the unerupted teeth to prevent them from artificially stiffening the bone. This material was given the same material properties as the PDL so that there was a soft, rather than hard, material joining the unerupted teeth to the surrounding bone. Finally, due to the angle at which they were scanned, the occlusal plane of the teeth for the cat and sheep was not perpendicular to any of the three coordinate directions in the model. These models were therefore rotated

about the buccolingual axis and the bone re-cropped, so that the occlusal plane of the teeth was perpendicular to one of the three coordinate directions. This made the application of the occlusal load to the models easier, since the load could then be applied in one of the three coordinate directions, rather than having to apply the load at an angle.

Mesh Generation

The solid models for all five specimens were then complete, as shown in Figure 5.1, and ready to be converted into a finite element mesh. For each model, a smoothing algorithm was applied before generating a polygon surface model in AVIZO. These surface models were then simplified to reduce the number of faces, and some automatic surface fixes were performed before the tetrahedral meshes were generated. These meshes were converted into text files for the finite element analysis.

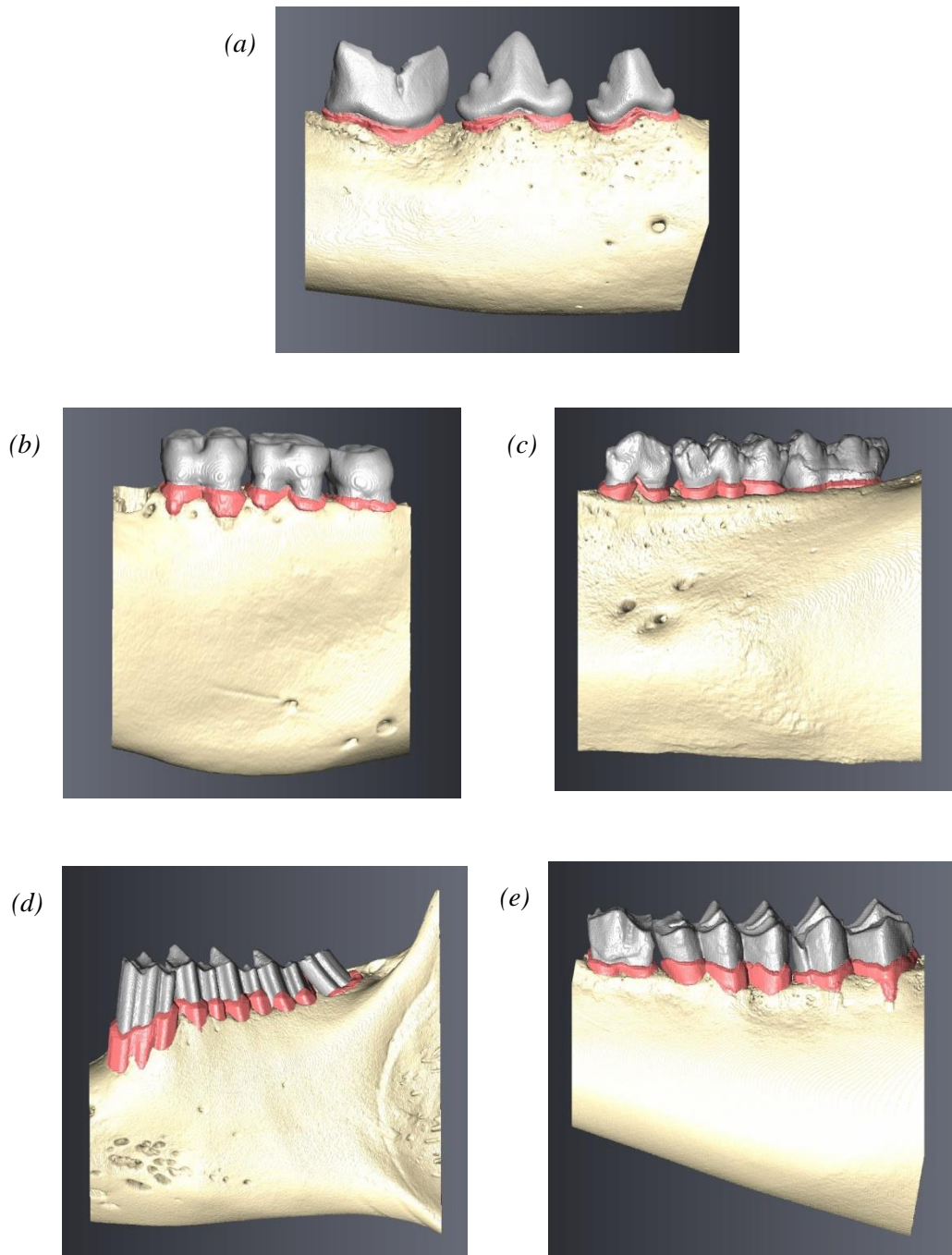


Figure 5.1 Surface models showing the five final models, all including teeth, bone, and PDL (in pink), viewed from the buccal side: (a) cat; (b) cercocebus; (c) pig; (d) rabbit; (e) sheep.

5.2.2 Model Development

The five meshes generated in AVIZO were imported into ANSYS for finite element analysis. Solid 10-noded high-order tetrahedral elements (SOLID187) (Kohnke, 2009) were used in all of the models. The cat, cercocebus, rabbit and sheep models, all contained three different materials: bone, teeth and PDL. The pig model also contained these three materials, along with two additional materials for the unerupted teeth and the soft layer around those teeth.

This section describes how these models were developed in ANSYS creating two models for each specimen: a no PDL model and a solid PDL model.

Initial Model Testing

To identify any problems with the finite element meshes, some initial tests were performed. For each specimen, all of the nodes on the two cut surfaces at the mesial and distal ends of the model were constrained in all degrees of freedom, and a point load of 100 N was applied to the occlusal surface of the middle tooth. All materials were given a Young's modulus value of 17,000 MPa with a Poisson's ratio of 0.3. These initial tests produced some errors due to poorly connected elements within the meshes. These elements were identified and deleted, and then the model was resolved. This process was repeated until all insufficiently constrained elements were removed. The final number of elements in each model, and the number of elements removed, is shown in table 5.1. Although the cercocebus and sheep required a much larger amount of elements to be removed than the other three models, the number of elements removed was still only a very small percentage of the total number of elements in the model, approximately 0.01 %. All five models contained more elements than the previous human model (Chapter 4) and so another convergence study was unnecessary.

Boundary Conditions

The boundary conditions applied were similar for all five specimens and were based on the boundary conditions applied to the human models in the previous study (Chapter 4), as shown in Figure 5.2.

Briefly, all of the nodes on the two cut surfaces at the mesial and distal ends of each model were constrained in the mesiodistal direction, with a small number of nodes at the base of each side being constrained in all degrees of freedom. For the cercocebus, pig, rabbit, and sheep models, a selection of nodes on each of the mesial and distal sides

of the exterior surface of the tooth crown on the middle tooth were also constrained in the mesiodistal direction. These constraints represent the points of contact between the loaded tooth and the adjacent teeth. They were not required in the cat model, since there is a gap between the teeth. Finally, for all five models, a total occlusal load of 100 N was distributed over a small area of the occlusal surface of the crown of the middle tooth. Thus, the cercocebus, pig, rabbit, and sheep models were all loaded on the first molar tooth, as was the case for the previous human model (Chapter 4), while the cat was loaded on the second premolar. This load was directed in the corono-apical direction, approximately perpendicular to the occlusal plane of the teeth. Since the aim of this study was to compare no PDL and solid PDL models (*i.e.* it is the relative strain difference between the two models that is of interest rather than the absolute strain values), the same load was used for all models, even though, for example, this would be a large load for a rabbit (Watson *et al.*, 2014) but a small load for a pig (Bousdras *et al.*, 2006).

Table 5.1 Final number of elements in each species model along with the number of insufficiently constrained elements which were removed.

Species Model	Final Number of Elements	Number of Elements Removed
Cat	1,344,802	1
Cercocebus	1,603,861	231
Pig	1,375,546	5
Rabbit	1,482,045	0
Sheep	1,414,472	158

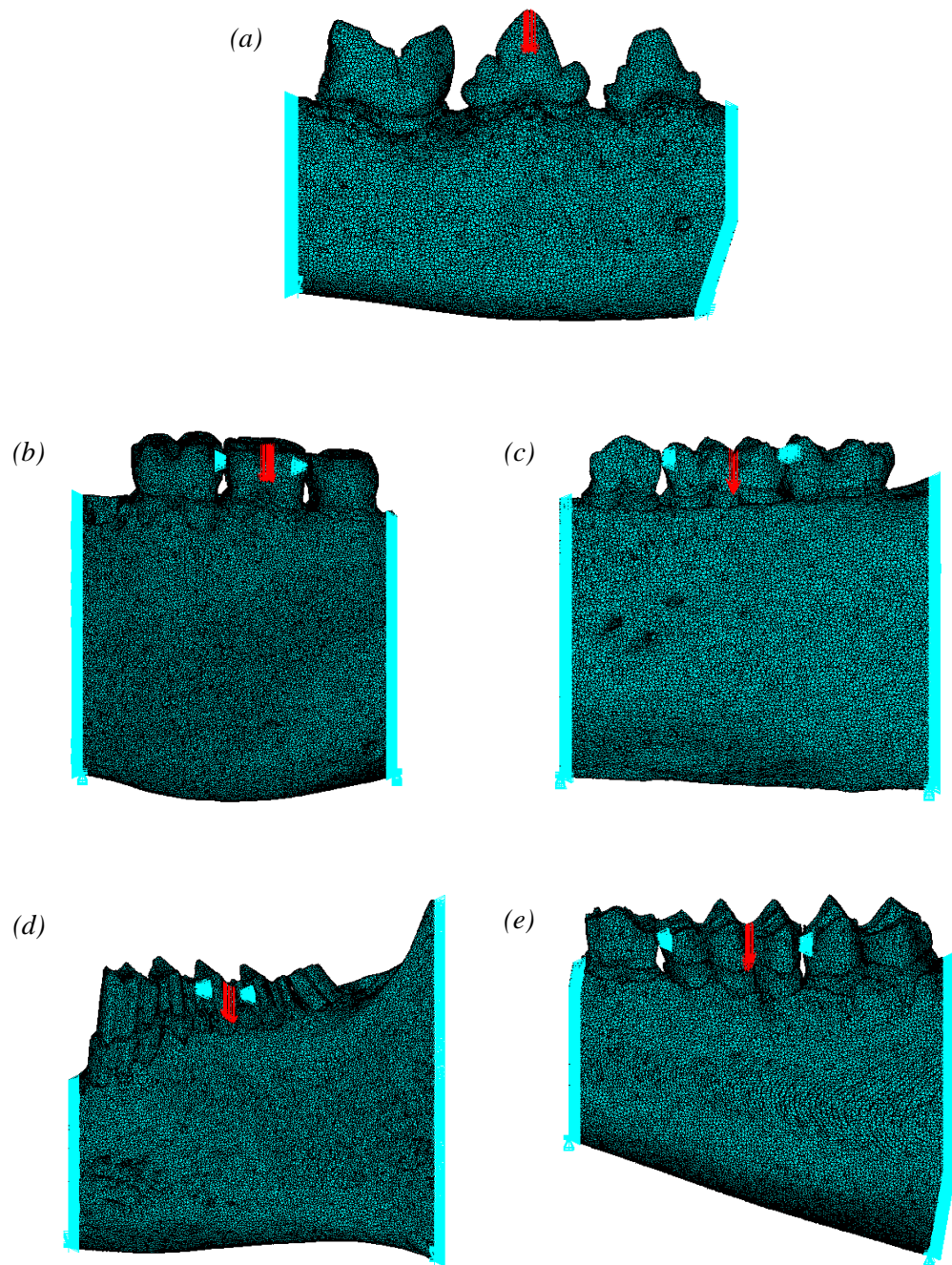


Figure 5.2 Finite element models, viewed from the buccal side, for each of the five mammals, showing loading and boundary conditions applied, where light blue triangles represent constraints and red arrows represent applied forces: (a) cat; (b) cercocebus; (c) pig; (d) rabbit; (e) sheep.

Material Properties

Two different models were created for each of the five specimens: a no PDL model and a solid PDL model. In each case, the two models were created from the same mesh by altering the material properties assigned to the PDL component. The material properties assigned to these models were obtained from previous studies. For the bone, the same material properties were assigned to the cortical bone, alveolar bone, and the trabecular bone, which included modelling the structure of the individual trabeculae (Currey, 2002).

In all models, bone and teeth were assigned a Young's modulus value of 17,000 MPa with a Poisson's ratio of 0.3 (Gröning *et al.*, 2011a). For the solid PDL models, the PDL was assigned a Young's modulus value of 49 MPa with a Poisson's ratio of 0.45. This value was the same as that used in the previous study in Chapter 4 and is within the range of Young's modulus values assigned to the PDL in other finite element models (Rees, 2001; Fill *et al.*, 2011). For the no PDL models, the PDL was assigned the same material properties as bone. Therefore, the only difference between the no PDL and solid PDL models was the material properties assigned to the elements of the PDL. Additionally, in the pig models, the unerupted teeth were assigned a Young's modulus value of 17,000 MPa with a Poisson's ratio of 0.3, and the layer of material around each of the unerupted teeth was assigned a Young's modulus value of 49 MPa and a Poisson's ratio of 0.45. It should be noted that the material properties of the soft material around the unerupted teeth were the same in both the no PDL and solid PDL models, so again the only difference between these two models was the material properties of the PDL.

5.2.3 No PDL versus Solid PDL

For each species, results were compared for models with and without a PDL to assess the effect of including the PDL in finite element models.

To provide an initial assessment of the results from each specimen, pair-wise comparisons were made by subtracting the element strains in the solid PDL model from those in the no PDL model for the same individual. These results were then presented as colour-coded difference plots allowing a visual comparison to be made of the strain differences between the two models. This was done for both maximum (tensile) and minimum (compressive) principal strains. Thus, for maximum principal strain difference plots, a negative value means the tensile strain was greater in the solid PDL

model, whereas for minimum principal strain difference plots, a negative value means compressive strain was greater in the no PDL model.

To provide a more precise comparison of the results, maximum and minimum principal strain graphs were also plotted and compared for both models for the same specimen. Nodal strain results were taken from nodes on the outer surface of the cortical bone along a plane in the buccolingual direction through the centre of where the 100 N load was applied. They were plotted from all nodes along the buccal and lingual sides, from the most superior nodes to the most inferior nodes on the base of the mandibular corpus.

5.3 Results

5.3.1 No PDL versus Solid PDL

For each of the five specimens, two figures are shown. One with difference plots comparing maximum principal strains and minimum principal strains for the no PDL and solid PDL models, and one with nodal strain graphs comparing the two models.

Difference plots for the no PDL and PDL cat models are shown in Figure 5.3, and nodal strain graphs comparing the two models are shown in Figure 5.4. The strain graphs in Figure 5.4 show that, in general, strain was higher in the PDL model than in the no PDL model. The most notable exception to this was for the compressive strain at the alveolar margin of the lingual side which was much higher in the no PDL model than in the PDL. The difference plots show that the strain in the PDL model was generally higher throughout the mandible section as well as just around the loaded tooth as shown in the strain graphs. This is especially true for the tensile strain, whereas for the compressive strain there were noticeable regions where strain is higher in the no PDL model, such as around the molar tooth.

Difference plots and nodal strain graphs for the no PDL and PDL cercocebus models are shown in Figure 5.5 and Figure 5.6 respectively. The difference plots show that there was more variation between the strains in the two models on the buccal side than on the lingual side. This is confirmed by the nodal strain graph which shows the very similar strains on the lingual side but more pronounced strain differences on the buccal side. In general, strains were higher in the PDL model, even on the lingual side where there is only a small difference between the two models.

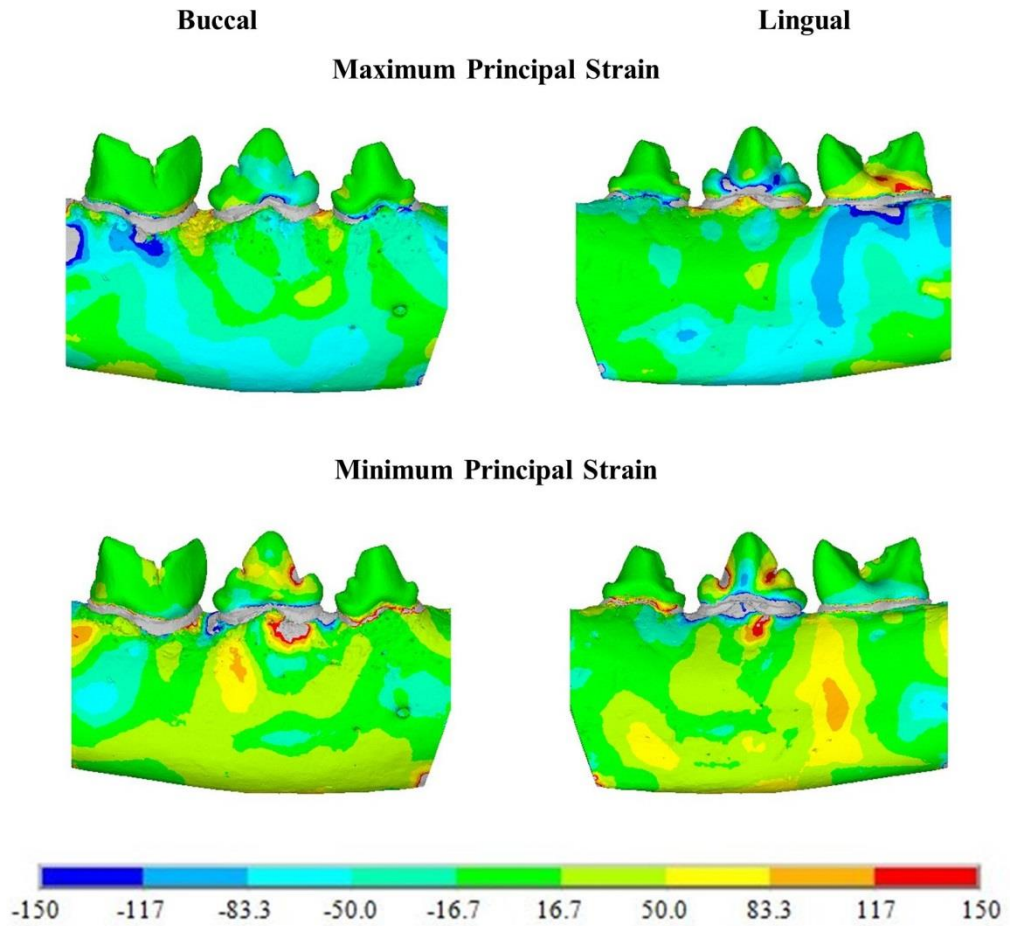


Figure 5.3 Maximum and minimum principal strain difference plots for the strain differences, in microstrain, between no PDL and solid PDL cat models.

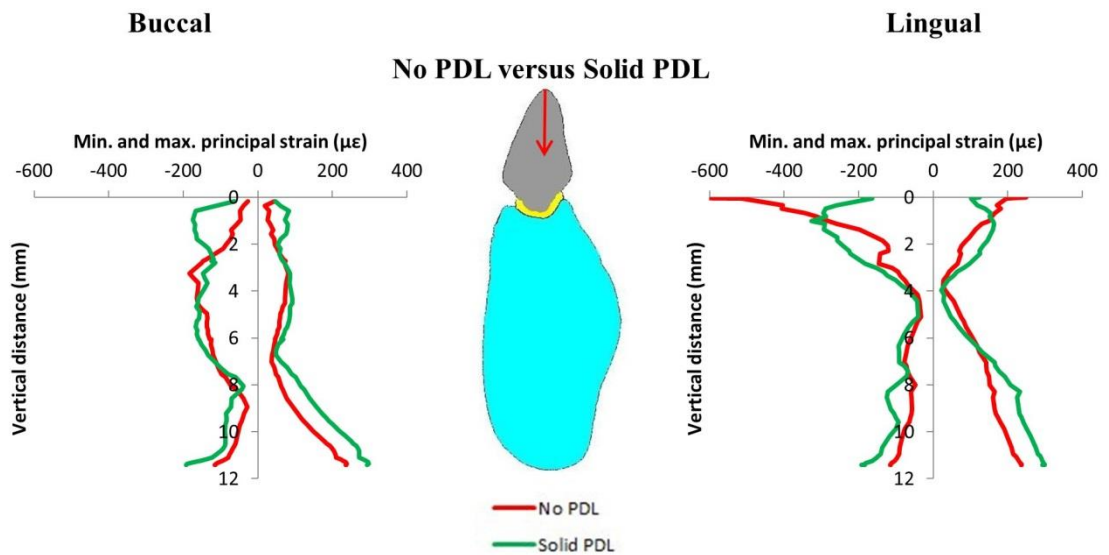


Figure 5.4 Vertical strain profiles for maximum and minimum principal strains on the buccal and lingual surfaces of the cortical bone around the middle tooth for the cat models. Graphs compare results from the no PDL and solid PDL models. The red arrow indicates the direction of the applied load.

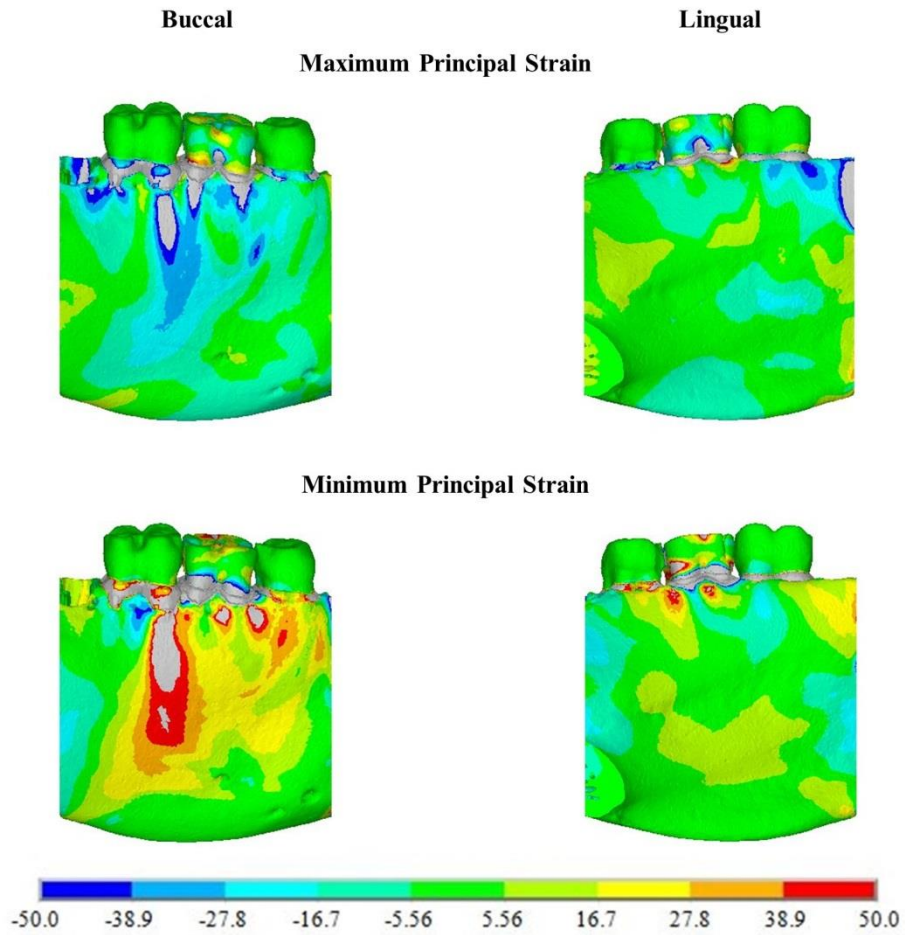


Figure 5.5 Maximum and minimum principal strain difference plots for the strain differences, in microstrain, between no PDL and solid PDL cercocebus models.

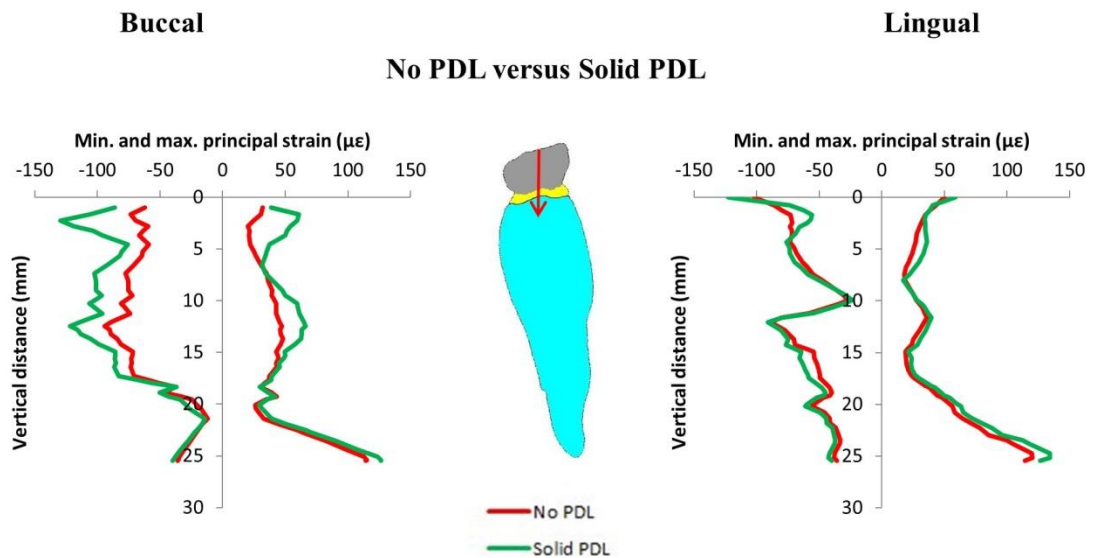


Figure 5.6 Vertical strain profiles for maximum and minimum principal strains on the buccal and lingual surfaces of the cortical bone around the middle tooth for the cercocebus models. Graphs compare results from the no PDL and solid PDL models. The red arrow indicates the direction of the applied load.

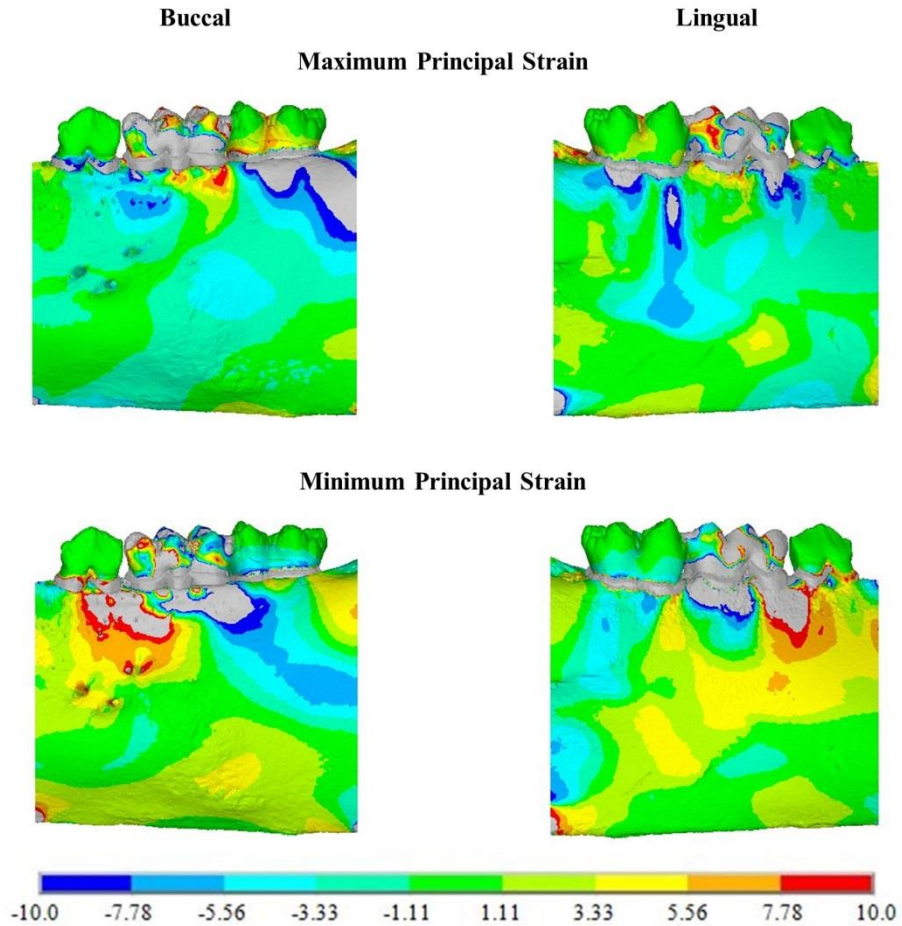


Figure 5.7 Maximum and minimum principal strain difference plots for the strain differences, in microstrain, between no PDL and solid PDL pig models.

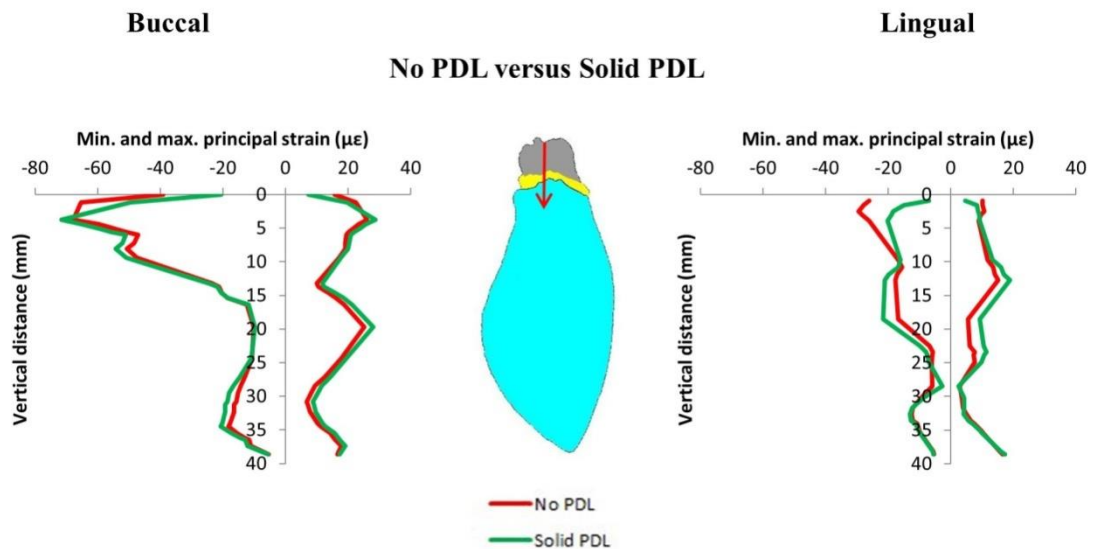


Figure 5.8 Vertical strain profiles for maximum and minimum principal strains on the buccal and lingual surfaces of the cortical bone around the middle tooth for the pig models. Graphs compare results from the no PDL and solid PDL models. The red arrow indicates the direction of the applied load.

Results from the pig models are shown in Figure 5.7 and 5.8. The difference plots (Figure 5.7) show that tensile strain was generally higher in the PDL model, although the strain graphs (Figure 5.8) show that strains in the two models were very similar. However, the compressive strain showed more variation between the two models, with strain in the PDL model being generally higher towards the mesial side of the mandible and strain in the no PDL model being generally higher towards the distal side. The difference plots show that these strain differences are small, with most differences being less than 10 microstrain. However, the strain graphs show that, with the exception of the relatively high compressive strain at the top of the buccal side, the strain magnitude was generally only around 20 microstrain, and so a difference of 10 microstrain would still be comparatively large. For example, the strain graphs show an increase in strain of up to 20 % for the PDL model on the buccal side, and up to 50 % on the lingual side.

Figures 5.9 and 5.10 show the difference plots and strains graphs respectively for the rabbit models. The difference plots show that generally both tensile and compressive strains were higher in the solid PDL model, although there is a section in the middle, around the loaded tooth, where the opposite is true. This region can be seen on the nodal strain graphs, which were taken from around the loaded tooth. These graphs show compressive strain at the top of the lingual side, and both strains around the middle of the buccal side, to be higher in the no PDL model. The difference plots show that the largest strain differences occurred towards the base of the mandible, in the regions near to the bases of the tooth roots.

Finally, the results for the sheep models are shown in Figures 5.11 (difference plots) and 5.12 (strain graphs). The difference plots show that tensile strain was generally higher on the buccal side for the PDL model, whereas the two models were quite similar on the lingual side. For the compressive strain, the strains in the PDL model were generally slightly higher on the buccal side, whereas the strains in the no PDL model were slightly higher on the lingual side. Although the differences were small, this trend was also shown on the strain graphs, with compressive strain being generally higher for the PDL model on the buccal side, and the no PDL model on the lingual side. However, the strain graphs show that the strains in the two models were actually very similar. This is particularly the case on the lingual side, whereas on the buccal side, the strain in the solid PDL model is generally higher.

For all five species, the results show that strain was generally higher in the PDL model, although there were several regions where the opposite was true. This was

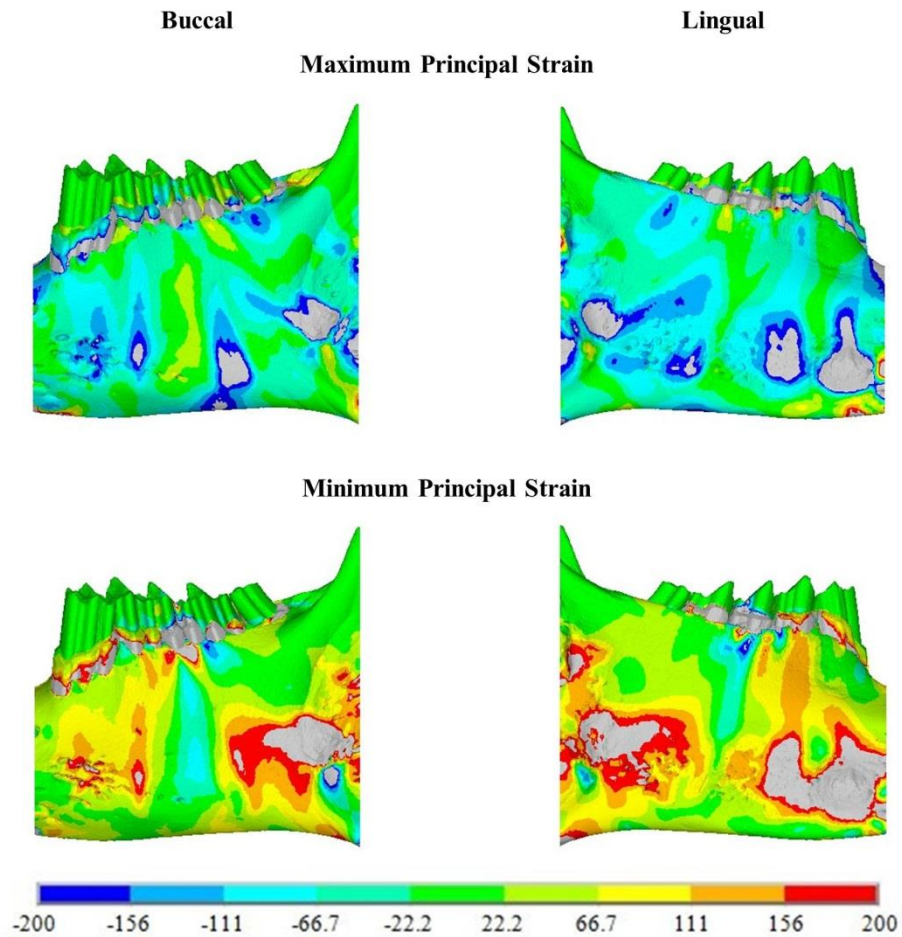


Figure 5.9 Maximum and minimum principal strain difference plots for the strain differences, in microstrain, between no PDL and solid PDL rabbit models.

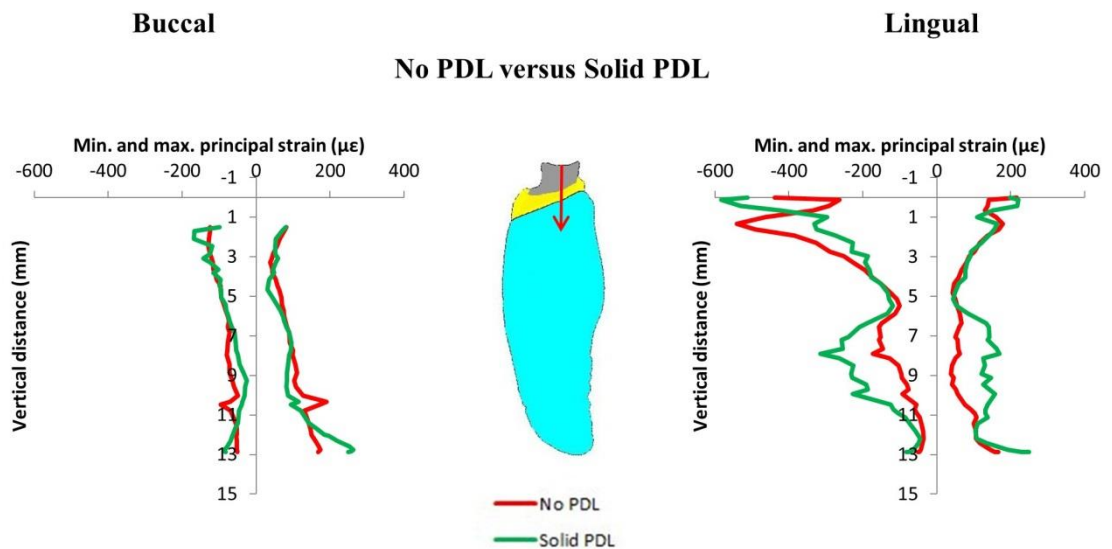


Figure 5.10 Vertical strain profiles for maximum and minimum principal strains on the buccal and lingual surfaces of the cortical bone around the middle tooth for the rabbit models. Graphs compare results from the no PDL and solid PDL models. The red arrow indicates the direction of the applied load.

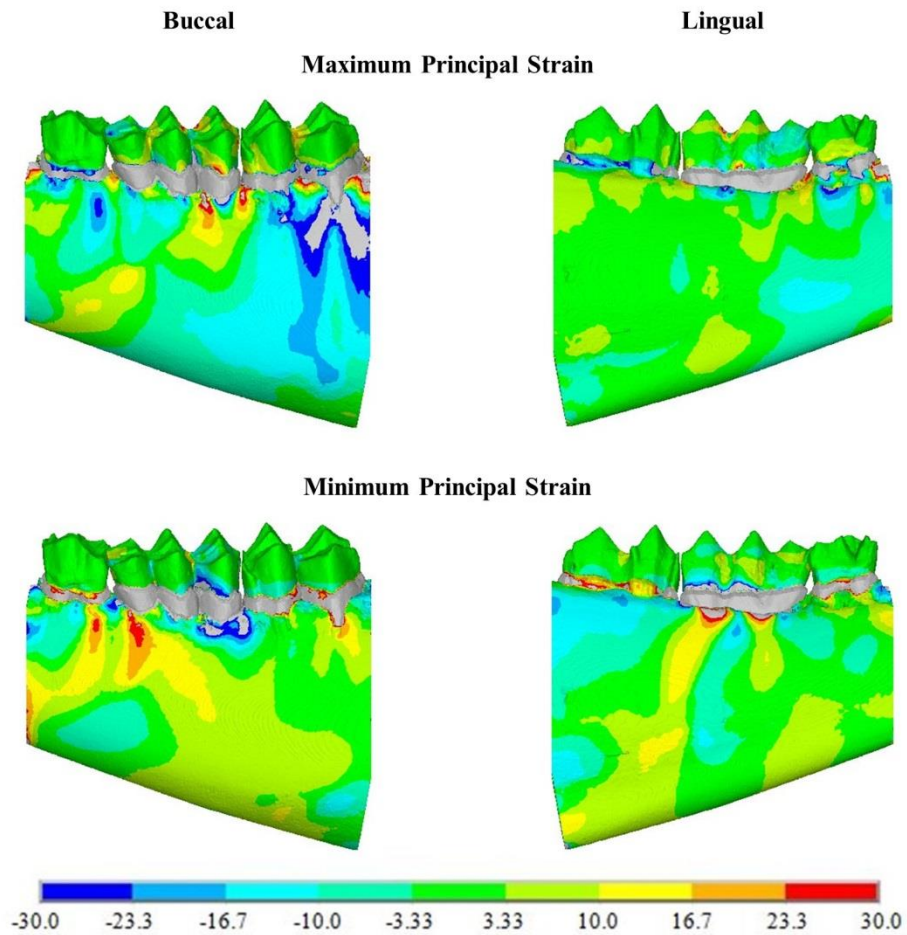


Figure 5.11 Maximum and minimum principal strain difference plots for the strain differences, in microstrain, between no PDL and solid PDL sheep models.

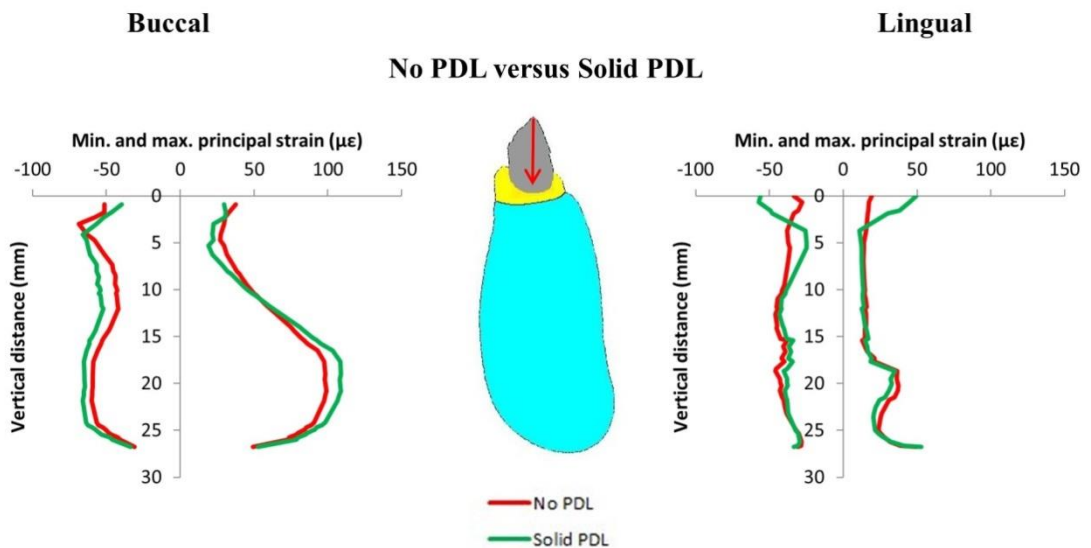


Figure 5.12 Vertical strain profiles for maximum and minimum principal strains on the buccal and lingual surfaces of the cortical bone around the middle tooth for the sheep models. Graphs compare results from the no PDL and solid PDL models. The red arrow indicates the direction of the applied load.

especially the case for the tensile strain, where strain in the PDL model was usually higher except for some areas around the alveolar margin.

5.4 Discussion

All the models were tested with the same 100 N occlusal load. This is an arbitrary load value, but the primary aim was not to determine absolute strain values, rather to compare the effect of modelling the PDL. If absolute were required, then, since this is a linear analysis, the strains could be simply scaled from the values reported here. The results used were obtained from the outer surface of the cortical bone, the region furthest away from the PDL, and the key structural element of the mandible.

With the exception of a few locations, the difference plots (Figures 5.3, 5.5, 5.7, 5.9, and 5.11) generally showed that the strain is greater in the PDL model than in the no PDL model. However, the strain graphs (Figures 5.4, 5.6, 5.8, 5.10, and 5.12) showed that although strain is generally higher in the PDL model, the strain profiles for the two models are quite similar. The strain graphs for the rabbit model (Figure 5.10) showed several regions where the strain in the no PDL model was higher. However, the difference plots showed that, for most regions, strain was higher in the PDL model, highlighting the importance of considering strain throughout the mandible rather than just in a single cross-section.

The findings in this study are similar to those from the occlusal load applied to the human model in the previous study (Chapter 4). Not including a PDL generally increases the stiffness of the model leading to lower strains. This again agrees with the previous findings of Gröning *et al.* (2011a) and Marinescu *et al.* (2005). This confirms that the PDL appears to have a similar biomechanical role in all of these mandibles. However, the results here are not very conclusive as strains are quite similar for the no PDL and PDL models in all five specimens.

As for the previous human model (Chapter 4), the similarity between results for the no PDL and PDL models is probably due to the fact that only the molar regions were modelled, rather than a whole mandible. The boundary conditions applied (Figure 5.2) would restrict the deformation of the mandibular bone in this region compared to if a whole mandible was modelled, especially if a soft material is used to model the temporomandibular joint and thus allow displacements at the joint (*e.g.* Gröning *et al.*, 2011a, 2012b). In the models used in this study, sagittal bending caused

by the occlusal load would be the main source of strain, while additional sources of strain, such as transverse bending (wishboning) or torsion around the anterior-posterior axis, are not present. Therefore, the PDL would likely have less effect on the strains produced than in whole mandible models under wishboning and/or torsion. Therefore, finite element models of whole mandible may be better suited to investigating the role of the periodontal ligament on strains away from the alveolar bone since they allow for greater deformation. However, limiting the models to the molar region means higher resolutions scans can be used, compared to modelling the whole mandible, thus allowing for a more accurate representation of the trabecular bone. Therefore, these models are better for studying the local effects around the tooth socket in detail.

Chapter 6

Discussion

6.1 Introduction

The primary aim of this project was to investigate the effect of including the PDL in mandibular finite element models, in particular to determine how PDL affects the load transfer between the tooth and mandibular bone, and whether it is necessary to include details of its fibrous structure, rather than just representing it as a simple solid layer. This chapter provides a general discussion about the results obtained from the three studies in Chapters 3, 4 and 5, and how they relate to the overall aim of the research, and the current state of knowledge reported in the literature. This discussion is separated into four further sections. Sections 6.2 and 6.3 discuss the effect of the PDL on the strain distribution in the mandible with occlusal loads and orthodontic load respectively. Section 6.4 discusses general points about inclusion of PDL fibres in finite element models. Finally, Section 6.5 discusses some of the strengths and weaknesses of this study. A detailed description of the results has already been given along with each of the three studies (Chapter 3, 4 and 5), and so the discussion here focuses on the key results and how the results from the three studies relate to each other and the literature.

6.2 Occlusal Loading

An occlusal load was applied to the models in all three studies to simulate the effect of a typical bite force on the teeth. The simplified tooth model (in Chapter 3) and the human molar region model (in Chapter 4) are the first three-dimensional finite element models to investigate the effect of the periodontal ligament (PDL) fibres under an occlusal load. The human molar region model is also the first finite element model to include PDL fibres along with realistic, rather than simplified, tooth and bone geometry.

The simplified tooth model was used to develop and test the method for including the fibrous structure of the PDL in finite element models. This model was also used to compare the results from the model with no PDL layer at all, with a

homogenous solid PDL layer and with a fibrous PDL (Figures 3.6, 3.9-3.12). The results, especially the strain graphs in Figure 3.10, showed that inclusion of the PDL fibres affected the strain around the tooth socket, generally causing higher strain towards the cervical region and lower strains towards the apex compared to the solid PDL model.

The results from the simplified tooth models obviously could not reveal how the PDL affects strains elsewhere in the mandible, away from the tooth socket, so for the human (Chapter 4) and other species (Chapter 5) models strains were examined around the outside surface of the cortical bone. The human molar region model compared three different types of PDL: no PDL, solid PDL and fibrous PDL. These results showed that including a PDL, whether solid or fibrous, generally increases the strain compared to the model without a PDL (Figures 4.16 to 4.20). There was generally less difference between the solid and fibrous PDL models with most of the variation between these two being towards the superior side of the mandible around the alveolar process.

Since inclusion of PDL fibres in FE models is such a time consuming process, and because the results from the human model showed that the difference between solid PDL and no PDL models was similar to the difference in fibrous PDL and no PDL models, fibres were not included in the other species models (Chapter 5). Thus these models only compared models with a solid PDL to those with no PDL to determine whether the previous results were specific to the human molar region or if they might be true for other mammalian mandibles, with different tooth and bone morphologies. Broadly speaking, the results from the other species molar region models (Figures 5.3 to 5.12) agreed with those from the human models and showed that including the PDL increases the strain in the mandibular bone. This result shows that despite the different morphologies, the PDL has a similar effect in all of the species studied. Therefore, these findings are not specific to human molars and mandibular bone, but rather they show that in any finite element model of a mammalian mandible it is probably important to include the PDL.

As well as investigating different types of PDL, chapter 4 also investigated two different methods of modelling the trabecular tissue: either including the structure of the individual trabeculae, or representing the whole tissue as a homogenous bulk material. For practical purpose, most mandibular finite element models use the second method as scan resolution is not high enough to include the individual trabeculae (*e.g.* Tanne *et al.*, 1993; Koriath & Hannam, 1994; Ichim *et al.*, 2006, 2007; Gröning *et al.*, 2011b, 2012b). A sensitivity study by Gröning *et al.* (2012b) found that results were relatively

insensitive to changes in the Young's modulus of the trabecular tissue modelled as a bulk material. However, the results from this study suggest that strain may be affected by including the trabecular structure. This was seen to be the case regardless of how the PDL was modelled (Figures 4.13 to 4.15).

The results from the cat, cercocebus and rabbit models all showed both compressive and tensile strains to be higher throughout the mandible when the PDL was included. The pig, sheep and human models also generally showed this, although they did include noticeable regions where the opposite was true. This may be due to the differences in the tooth root morphology between the species. The cat and cercocebus teeth all have two very straight roots. The pig, sheep and human tooth roots are more complex. The human molar teeth also only have two roots but they are more curved than the cat or cercocebus. The sheep molars have two or three roots (three in this case on the loaded tooth) whilst the pig molars each have five roots. It is possible that the more complex tooth root morphology creates a more rigid structure. Therefore, if this is the case, including the PDL would have less effect in these species. Although the rabbit teeth each only have one root, these roots are highly curved. Additionally, these tooth roots take up a large proportion of the mandibular corpus, so it is understandable that including the PDL would have a noticeable effect, since this would create large holes in the mandibular corpus.

It is also important to consider the cross-sectional geometry of the mandible, as this influences its ability to resist loads. The cross sectional area moment of inertia (or second moment of inertia) is a measure of the distribution of material (bone in this case) around a particular axis (Van Eijden, 2000). Increasing the second moment of inertia about a particular axis increases the resistance to bending about that axis. Therefore, in the mandible, the further bone is located from the neutral axis, the better the bending resistance will be. For all six species, the mandible is deeper in the superior-inferior direction than in the buccolingual direction (see cross sections in Figures 4.15, 5.4, 5.6, 5.8, 5.10 and 5.12). This means that these mandibles are best suited to resisting sagittal bending loads than transverse bending or torsional loads. This is especially the case for the cercocebus (Figure 5.6) which appears to have a particularly high ratio of superior-inferior to buccolingual length. The cercocebus diet involves a lot of crushing of hard food items (Daegling *et al.*, 2011) and so the mandible is well suited to resist large sagittal bending loads. Visually, the cross-section of the pig mandible appears to be the most circular (Figure 5.8). This gives similar bending resistance in both directions and increased torsional rigidity compared to a more oval shape (Van Eijden, 2000). This

again makes sense since the pigs eat a diverse range of food requiring both biting and grinding motions (Langenbach *et al.*, 2002).

6.3 Orthodontic Loading

Orthodontic loads were applied to the simplified tooth models (Chapter 3) and the human molar region models (Chapter 4). In both cases there were noticeable differences between the results for the solid PDL and fibrous PDL models. The results from these studies can be considered with respect to hypotheses for the biomechanical cause of orthodontic tooth movement found in the literature. These hypotheses are discussed in Section 2.5 and three that focus on the strain in the alveolar bone are illustrated in Figure 3.1: they are the “pressure-tension” hypothesis (Schwartz, 1932), the “alveolar bending hypothesis” (Baumrind, 1969) and the “stretched fibre hypothesis” (Melsen, 2001).

Whether orthodontic tooth movement is triggered by strains in the alveolar bone or in the PDL remains the subject of much debate within the literature (*e.g.* Cattaneo *et al.*, 2005). In the case of PDL controlled orthodontic tooth movement, it is suggested that tooth displacement alters the vascularity and blood flow within the PDL, upsetting its homeostatic environment, which initiates biochemical and cellular activities that cause local bone adaptation. For alveolar bone controlled orthodontic tooth movement, it is suggested that alveolar bone adaptation is caused by strains in the alveolar bone through the same mechanisms that cause functional bone adaptation in other bones (Krishnan & Davidovitch, 2006).

For the simplified tooth models, strains in the alveolar bone from the orthodontic loads are shown in Figures 3.11 and 3.12. During orthodontic tooth movement, the tooth is moved in the direction of the applied load, *i.e.* from left to right in Figure 3.11, and from right to left in Figure 3.12. Generally, both figures show tension on the side that the tooth is moved towards (*i.e.* the distal side in Figure 3.11 and the lingual side in Figure 3.12) and compression on the opposite side. Strain was plotted from both the inside and outside surfaces of the alveolar bone, however, both figures show very little difference in strain between the two surfaces.

Assuming that tooth movement occurs under these conditions, the strain results do not match with the pressure-tension hypothesis which predicts compression on the side to which the tooth is moved and tension on the opposite side. This is essentially the

opposite of what is seen in these models. Strains on the inside surface of the alveolar bone match those predicted by the alveolar bending hypothesis. However, this hypothesis predicts bending of the alveolar bone, similar to a cantilever beam, such that tension and compression should be reversed on the outside surface of the alveolar bone. Again this is not seen with this model, as the strains are very similar on the two surfaces (Figures 3.11 and 3.12). Finally, strain in the fibrous PDL model is generally higher than those in the solid PDL model on the side that the tooth is moved away from (*i.e.* the mesial side in Figure 3.11 and the buccal side in Figure 3.12). This shows some agreement with the stretched fibre hypothesis which predicts high strains on this side due to stretching of the PDL fibres. However, this hypothesis predicts low strains on the opposite side whereas both Figures 3.11 and 3.12 show comparable strain magnitudes on both sides.

For the human molar region model, strains around both mesial and distal roots are shown in Figures 4.23 and 4.26. Therefore, these figures are most useful for examining the possible biomechanical cause of orthodontic tooth movement. Again, during orthodontic tooth movement, the tooth moves in the direction of the applied load, *i.e.* from left to right in both of these figures. Consequently, for the distomesial load (Figure 4.23) this means that bone would need to be added on the distal side and taken away from the mesial side around each root to allow the tooth to move in the mesiodistal direction. Similarly, for the buccolingual load (Figure 4.26) bone would need to be added to the buccal side and taken away from the lingual side of each root to allow the tooth to move in the buccolingual direction.

For Figure 4.26, the buccal side is primarily in tension and the lingual side is primarily in compression, although this pattern changes towards the apex of the tooth root, especially on the lingual side, due to the centre of rotation not being at the apex of the tooth but rather somewhere within the tooth root. Therefore, the results from this model suggest that for orthodontic tooth movement to occur, bone would need to be removed from areas in compression and added to areas in tension. For Figure 4.23, the distal side is primarily in tension and the mesial side is primarily in compression. Again, this varies a little towards the apex due to tipping of the tooth. Therefore, as with the buccolingual load, the results from this model also suggest that for orthodontic tooth movement to occur, bone would be removed from areas in compression and added to areas in tension.

These results can again be compared to the three hypotheses for the biomechanical cause of orthodontic tooth movement (Figure 3.1). The strain observed

here does not match with the alveolar bending hypothesis, which predicts tension on the inside surface of the alveolar bone on the side where bone is removed, and compression on the inside surface on the side where bone is added. The results here also do not match with the stretched fibre hypothesis. This predicts low strains on the side where bone is removed and high strains on the side where bone is added whereas here there is not much difference in the magnitude of strains on either side; and in fact for the buccolingual load (Figure 4.26), the highest strains are observed on the lingual side where bone would be removed. The results here most closely agree with the pressure-tension hypothesis, which predicts compression on the side where bone is removed and tension on the side where bone is added. However, this is not how bone adaptation is generally thought to occur in other bones where it is usually thought that compression causes bone formation and tension causes bone resorption (Currey, 1968; Melsen, 1999). Therefore, since the strains observed don't appear to match how strains usually cause bone remodelling, this provides some support to the suggestion that orthodontic tooth movement is controlled by the PDL rather than by the alveolar bone.

One of the main reasons authors give for orthodontic tooth movement being controlled by the PDL, rather than the alveolar bone, is that strain in the alveolar bone is thought to be far below that which would typically be required for mechanical adaptation of bone to occur (*e.g.* Chen *et al.*, 2014). According to Frost's Mechanostat theory, strains should generally be around 800 to 1500 microstrain during normal bone function (Frost, 1987). So, strains caused by orthodontic loads would need to be around this sort of magnitude to have an effect on bone adaptation. However, previous finite element studies have generally shown strains in the alveolar bone to be much lower than this (*e.g.* Middleton *et al.*, 1996a; Bourauel *et al.*, 1999; Jones *et al.*, 2001). The results from the single tooth model appear to support this suggestion, as the strains observed with the orthodontic loads are mostly less than 20 microstrain (Figures 3.11 and 3.12). However, in the human molar region model, especially in the case of the fibrous PDL, strains observed in the alveolar bone are reasonably high, up to 1200 microstrain (Figure 4.23), and so much closer to those that would normally be thought to cause bone adaptation.

A recent study by Dalstra *et al.* (2015) suggested that previous finite element studies have grossly underestimated the strain in the alveolar bone. Dalstra *et al.* (2015) suggested that the rough surface of the alveolar bone causes areas of stress concentration leading to high local strains capable of causing mechanical bone adaptation. So, this suggests that whilst none of the three hypotheses shown in Figure

3.1 could be fully confirmed, orthodontic tooth movement may still be mediated by the alveolar bone rather than the PDL. However, this hypothesis cannot be tested by the simplified tooth model since the surface of the alveolar bone is smooth, but the results from the human molar region model provide some support for this hypothesis. Alveolar bone strains are reasonably high in this model, and the strain profiles are not smooth but contain many spikes presumably caused by local variation in the alveolar bone geometry.

The results from the single tooth models (Chapter 3) and the human molar region models (Chapter 4) may appear contradictory, as the single tooth models seem to support the stretched fibre hypothesis, and the human molar region models seem to support the pressure-tension hypothesis. However, it is important to note that neither set of results fully support any of the three hypotheses. It is also worth noting that although some sensitivity analyses were conducted, none were conducted with orthodontic loads, examining the strains in the alveolar bone with different combinations of material properties. Therefore, it is possible that altering the material properties would alter the general pattern of strain in the alveolar bone and thus lead to different conclusions with respect to the biomechanical cause of orthodontic tooth movement.

Although the results from the orthodontic load studies are inconclusive, both sets of results show it is possible that bone adaptation in orthodontic tooth movement is controlled by strains in the alveolar bone, rather than by changes in the PDL. Strains in the single tooth model most closely matched the stretched fibre hypothesis, which is based on the mechanostat theory, and so is in keeping with how bone adaptation is generally thought to occur. Strains in the human molar region model, especially for the fibrous PDL, were reasonably high and close to those normally thought to cause bone remodelling. This suggests that simplified tooth models might underestimate strains in the alveolar bone. Therefore, the idea that orthodontic tooth movement is controlled by alveolar bone strains should not be discounted on the basis of these strains being too low. These are important results, and indicate that more research should be done to investigate the cause of orthodontic tooth movement, especially using models with accurate tooth, bone and PDL geometry.

6.4 Should PDL Fibres be Included in Finite Element Models?

Including the PDL layer in mandibular finite element models with realistic geometry (e.g. Chapter 4 and 5) is a time consuming process involving manual image segmentation (see Sections 4.2 and 5.2). Including the PDL fibres increases the time required even further and so it is important to consider whether or not this extra effort is necessary. The results from all three studies (Chapters 3, 4 and 5) suggest that including the PDL, compared to models without a PDL layer, does affect the strain both around the tooth socket and further away, and so it should be included in some way in mandibular finite element models. This agrees with the findings of previous studies (e.g. Gröning *et al.*, 2011a).

For the occlusal load (Section 6.2) results from the solid and fibrous PDL models were broadly similar, however, with the orthodontic load the results are quite different. For the simplified tooth model, the pattern of strain from the fibrous PDL model was noticeably different to that observed in the solid PDL model (Figures 3.11 and 3.12). In particular, compared to the solid PDL model, the fibrous PDL model had a more uniform strain distribution on the side that the tooth was moved away from and had higher strains around the apex. Neither of these two observations was then seen in the human molar region model. In this model, the strain patterns for the fibrous PDL and solid PDL were relatively similar, but the strain magnitudes were very different (Figures 4.21 to 4.26).

The results from Chapter 3 and 4 indicate that in some situations it may be important to consider inclusion of the fibrous structure of the PDL. If it is the strains around the mandible that are of interest, such as when investigating the functional morphology of the mandible, it may not be necessary to include the PDL fibres. However, if it is strains around the tooth socket that are of interest, such as when investigating orthodontic tooth movement, then it may be important to consider the fibrous structure of the PDL. Of course it should be remembered that only molar region models were used in this study. Therefore, the results may be different if PDL fibres were included in a whole mandible model, especially when considering strains around the mandible due to the occlusal load.

6.5 Strengths and Weaknesses of this Study

The main strength of this study was the high level of anatomical detail included in the molar region models. These models were created from high resolution micro-computed tomography (microCT) scans to capture the detailed geometry of all of the structures in the molar region. In particular, this allowed the detailed trabecular geometry to be included in the finite element models. The high resolution scans also allowed the space for the PDL to be visualised, which enabled the PDL geometry to be represented more accurately than in previous studies. Including the fibrous structure of the PDL further adds to the level of detail in these models, even though this was included in a very schematic way.

Although the models contained a high level of anatomical detail, they also had several limitations. Since only the molar region was modelled, this reduced the amount of deformation which could occur in these models compared to if a whole mandible was modelled. The boundary conditions applied probably over-constrained the model which has been shown to artificially stiffen finite element models (*e.g.* Marinescu *et al.*, 2005). To investigate mandibular functional morphology it would be better to include the whole mandible, ideally with soft constraints at the temporomandibular joint to allow for more realistic deformation of the bone (Gröning *et al.*, 2012b). Also, to simulate biting, only simplified occlusal loads were applied rather than any other loads which may occur during biting, such as shear loads. As well as the simplified loading, only isotropic material properties were used. However, previous validation studies have shown that meaningful results can still be obtained from isotropic models (Gröning *et al.*, 2009, 2012a, 2012b).

Chapter 7

Conclusions and Future Work

7.1 Conclusions

This thesis aimed to investigate different methods of representing the periodontal ligament (PDL) in mandibular finite element models and assess their effect under occlusal and orthodontic loads. This included the development of a method to model the fibrous structure of the PDL using link elements to represent the PDL fibres. The simplified single tooth model (Chapter 3) and the human molar region model (Chapter 4) represent the first three-dimensional finite element models in which the fibrous structure of the PDL has been investigated under an occlusal load simulating biting. Additionally, the human molar region model is the first model that combines PDL fibres and realistic tooth and bone geometry based on micro-computed tomography scans of a real human mandible.

Including the PDL in finite element models adds significantly to the time required to both create and solve the model. However, the results here indicate that it is important to include the PDL in mandibular finite element models when either occlusal or orthodontic loads are considered. Failure to include the PDL effectively fuses the teeth to the alveolar bone creating a much more rigid structure. This reduces the strains throughout the model not just in the area around the PDL. This agrees with the findings from previous studies (*e.g.* Marinescu *et al.*, 2005; Gröning *et al.*, 2011a, 2012b), although it is important to remember that these results relate to (mammalian) mandibles and should not be generalised to the normally much stiffer maxilla, without further research (Wood *et al.*, 2011; Gröning & Fagan, 2012). The maxilla is stiffer because of the bony palate between the two sides of the dental arch and because of its position within the skull where it is connected to the surrounding bone by sutures, which are strong fibrous joints that do not allow much movement unlike the synovial temporomandibular joint that articulates the mandible with the rest of the skull.

The results from applying an occlusal load to these models did not show much difference between the solid and fibrous PDLs in the cortical bone away from the tooth

socket. This suggests that for models used to investigate mandibular morphology, while it is important to include the PDL, it may not be necessary to include its fibrous structure. However, in this study only the molar region was modelled to achieve maximum scan resolution and thus accurate modelling of the geometry of the trabecular bone. In molar region models, the constraints applied are much closer to the loaded tooth than in a whole mandible model, where they would be applied around the temporomandibular joint (Gröning *et al.*, 2012b), and so deformation of the molar region is restricted. Therefore, it is possible that if a whole mandible was modelled this result may be different.

When an orthodontic load was applied, there were noticeable differences between the strains in the alveolar bone with the solid and fibrous PDL models. In particular, the results from the human molar region model (Chapter 4) showed that the magnitude of strain in the alveolar bone was greatly increased with the fibrous PDL compared to the solid PDL. This may be significant when considering the biomechanical stimuli for alveolar bone remodelling in orthodontic tooth movement as previous finite element studies have found the strains in the alveolar bone to be very low (*e.g.* Middleton *et al.*, 1996a; Bourauel *et al.*, 1999, 2000; Jones *et al.*, 2001), which has led some researchers to conclude that orthodontic tooth movement is regulated by the PDL and not the alveolar bone (*e.g.* Qian *et al.*, 2010; Chen *et al.*, 2014). Whether orthodontic tooth movement is triggered by strains in the alveolar bone or in the PDL remains an open question (*e.g.* Cattaneo *et al.*, 2005, 2009). The distribution of strains observed in these models did not agree with any current hypothesis for orthodontic tooth movement that suggests alveolar bone strains as the stimulus for alveolar bone remodelling. However, this was the first attempt to compare these hypotheses using a three-dimensional model including PDL fibres, and the results suggest that further research on the fibrous structure of the PDL and its biomechanical functions could be beneficial.

7.2 Future Work

This research has highlighted the importance of the PDL fibres and their effect on strain in the mandibular bone, especially in the tooth socket. These strains are particularly important for orthodontic tooth movement and so further work investigating the fibrous structure of the PDL may help shed light on the biomechanical mechanisms underlying

bone remodelling in orthodontic tooth movement. In particular, further research is required to learn more about the PDL and its organization, so that it could be included more accurately in future finite element models.

Firstly, the PDL fibres were included in these studies (Chapters 3 and 4) by creating link elements connecting nodes on the interface between the alveolar bone and PDL with nodes on the interface between the tooth root and PDL. In real PDL these fibres do not stop at these surfaces, but rather they insert deeper into the tooth root and alveolar bone where they are known as Sharpey's fibres (Kuroiwa *et al.*, 1994; Ho *et al.*, 2007). Future finite element models could attempt to include these Sharpey's fibres along with the principal fibres of the PDL. Including Sharpey's fibres could alter the strains in the tooth root and tooth socket as the force would be transferred into the root and socket rather than just to the surface. This may prevent local strain concentrations from developing such as those seen in the simplified tooth model (Figure 3.9).

Histological studies could be performed to further investigate the structure and orientation of the PDL fibres, especially of the Sharpey's fibres. For example, do the oblique fibres of the PDL remain at an oblique angle to the bone/cementum surface after insertion or does their orientation change? This would affect how strains are transferred to the surrounding bone. Synchrotron radiation based microtomography allows for higher resolution scans than conventional micro-computed tomography (microCT) and could, therefore, be used to provide a detailed three-dimensional view of the PDL fibre orientations at the insertion sites (Dalstra *et al.*, 2015).

Only limited validation was performed in this study by comparing tooth displacement in the model to those previously reported in the literature. However, the resulting strains were not compared to experimental ones. None of the previous finite element models including the fibrous structure of the PDL have been validated against experimental strains either. Validating these models would be useful in determining how best to include the PDL in future models. Strains within the tooth socket cannot be measured without cutting a section through the socket, which would alter the strains observed. Consequently, the validation for these models could be done only by comparing the surface strains in the model to those recorded though *in vitro* loading experiments. Digital speckle pattern interferometry provides a full-field view of the surface strains in a given area (*e.g.* Gröning *et al.*, 2009, 2012a). Therefore, this could be used to validate the models under an occlusal load and then an orthodontic load could be applied to these validated models.

Another limitation of this study is the lack of information available about the material properties of the PDL fibres. Many studies have investigated the material properties of the PDL as a whole, but there is currently very little information available on the properties of the fibres themselves, which is key if they are to be included as a separate structure in finite element models. Research has been done on the material properties of collagen fibres in general (Gautieri *et al.*, 2012), but not specifically those in the PDL. Van Driel *et al.* (2000) loaded a tooth for several hours and recorded the tooth displacement. They found an instantaneous tooth displacement within the first few seconds followed by a creep displacement over several hours. They suggested that one possible explanation for this was that over time interstitial fluid was pushed out of the PDL and so the load support was taken up by the solid component, *i.e.* the PDL fibres. If this is true, then if displacement was allowed to reach equilibrium it would be the PDL fibres which were completely carrying the load. So, a similar experiment to that done by Van Driel *et al.* (2000) could be performed, increasing the load after equilibrium is reached, thus loading the PDL fibres to assess their material properties.

Additional research would be very important for improving our understanding of the forces acting on the alveolar bone. Unwanted alveolar bone resorption causes problems during orthodontic treatment, the loosening and eventually loss of dental implants, and leads to tooth loss, especially in the elderly. Increased understanding of the physiological strains occurring in this region will help to improve the management and outcome of dental treatments, and thus improve the quality of life for the patients involved.

Appendix I

List of Publications

Peer-Reviewed Journal Articles

McCormack, S. W., Witzel, U., Watson, P. J., Fagan, M. J. and Gröning, F. (2014). The Biomechanical Function of Periodontal Ligament Fibres in Orthodontic Tooth Movement. *PLoS ONE* 9, 7, e102387.

Conference Presentations

McCormack, S. W., Gröning, F., Witzel, U. and Fagan, M. J. (2013). *The Influence of Fibrous Periodontal Ligament on Tooth Movement and Load Transfer: A 3D Finite Element Study*. 19th Congress of the European Society of Biomechanics, 25-28 August, Patras, Greece.

References

- Al-Sukhun, J., Kelleway, J. and Helenius, M. (2007). Development of a three-dimensional finite element model of a human mandible containing endosseous dental implants. I. Mathematical validation and experimental verification. *Journal of Biomedical Materials Research Part A* 80A, 234-246.
- Ashman, R. B. and Van Buskirk, W. C. (1987). The elastic properties of a human mandible. *Adv. Dent. Res.* 1, 1, 64-67.
- Atmaram, G. H. and Mohammed, H. (1981). Estimation of Physiologic Stresses with a Natural Tooth Considering Fibrous PDL Structure. *J. Dent. Res.* 60, 5, 873-877.
- Baumrind, S. (1969). A reconsideration of the propriety of the “pressure-tension” hypothesis. *American Journal of Orthodontics* 55, 12-22.
- Benazzi, S., Kullmer, O., Grosse, I. R. and Weber, G. W. (2012). Brief Communication: Comparing Loading Scenarios in Lower First molar Supporting Bone Structures Using 3D Finite Element Analysis. *Am. J. Phys. Anthropol.* 147, 128-134.
- Berkovitz, B. K. B. (1990). The structure of the periodontal ligament: an update. *European Journal of Orthodontics* 12, 51-76.
- Borák, L., Florian, Z., Bartáková, S., Prachár, P., Murakami, N., Ona, M., Igarashi, Y. and Wakabayashi, N. (2011). Bilinear elastic property of the periodontal ligament for simulation using a finite element mandible model. *Dental Materials Journal* 30, 4, 448-454.
- Boryor, A., Geiger, M., Hohmann, A., Wunderlich, A., Sander, C., Sander, F.M. and Sander, F. G. (2008). Stress distribution and displacement analysis during an intermaxillary disjunction – A three-dimensional FEM study of a human skull. *J. Biomech.* 41, 376-382.
- Bourauel, C., Freudenreich, D., Vollmer, D., Kobe, D., Drescher, D. and Jäger, A. (1999). Simulation of Orthodontic Tooth Movements – A Comparison of Numerical Models. *J. Orofac. Orthop.* 60, 136-151.
- Bourauel, C., Vollmer, D. and Jäger, A. (2000). Application of Bone Remodeling Theories in the Simulation of Orthodontic Tooth Movements. *J. Orofac. Orthop.* 61, 266-279.
- Bousdras, V. A., Cunningham, J. L., Ferguson-Pell, M., Bamber, M. A., Sindet-Pedersen, S., Blunn, G. and Goodship, A. E. (2006). A novel approach to bite force measurements in a porcine model in vivo. *Int. J. Oral Maxillofac. Surg.* 35, 663-667.
- Burr, D. B., Robling, A. G. and Turner, C. H. (2002). Effects of biomechanical stress on bones in animals. *Bone* 30, 781-786.
- Cattaneo, P. M., Dalstra, M. and Melsen, B. (2005). The Finite Element Method: a Tool to Study Orthodontic Tooth Movement. *J. Dent. Res.* 84, 5, 428-433.

- Cattaneo, P. M., Dalstra, M. and Melsen, B. (2008). Moment-to-force ratio, center of rotation, and force level: A finite element study predicting their interdependency for simulated orthodontic loading regimens. *Am. J. Orthod. Dentofacial Orthop.* 133, 681-689.
- Cattaneo, P. M., Dalstra, M. and Melsen, B. (2009). Strains in periodontal ligament and alveolar bone associated with orthodontic tooth movement analyzed by finite element. *Orthod. Craniofac. Res.* 12, 120-128.
- Chakkalakal, D. A. (1989). Mechanoelectric transduction in bone. *J. Mater. Res.* 4, 1034-1036.
- Chen, X. and Chen, H. (1998). The influence of alveolar structures on the torsional strain field in a gorilla corporeal cross-section. *Journal of Human Evolution* 35, 611-633.
- Chen, C. S. and Ingber, D. E. (1999). Tensegrity and mechanoregulation: from skeleton to cytoskeleton. *Osteoarthritis and Cartilage* 7, 81-94.
- Chen, J., Li, W., Swain, M., Darendeliler, M. A. and Li, Q. (2014). A Periodontal Ligament Driven Remodeling Algorithm for Orthodontic Tooth Movement. *J. Biomech.* 47, 1689-1695.
- Clerehugh, V., Tugnait, A. and Genco, R. J. (2009). *Periodontology at a Glance*. Singapore: Wiley-Blackwell.
- Coleman, M.N. and Colbert, M.W. (2007). Technical note: CT thresholding protocols for taking measurements on three-dimensional models. *Am. J. Phys. Anthropol.* 133, 723-725.
- Cook, S. D., Weinstein, A. M. and Klawitter, J. J. (1982). A three-dimensional finite element analysis of a porous rooted Co-Cr-Mo alloy dental implant. *Journal of Dental Research* 61, 25-29.
- Currey, J. D. (1968). The Adaptation of Bones to Stress. *J. Theoret. Biol.* 20, 91-106.
- Currey, J. D. (1984). What Should Bones Be Designed to Do? *Calcif. Tissue Int.* 36, S7-S10.
- Currey, J. D. (2002). *Bones: structure and mechanics*. Princeton: Princeton University Press.
- Currey, J. D. (1989). Strain rate dependence of the mechanical properties of reindeer antler and the cumulative damage model of bone fracture. *J. Biomech.* 22, 469-475.
- Daegling, D. J. and Hylander, W. L. (1997). Occlusal forces and mandibular bone strain: Is the primate jaw "overdesigned"? *Journal of Human Evolution* 33, 705-717.
- Daegling, D. J. and Hylander, W. L. (1998). Biomechanics of torsion in the human mandible. *Am. J. Phys. Anthropol.* 105, 73-87.

- Daegling, D. J. and Hylander, W. L. (2000). Experimental Observation, Theoretical Models, and Biomechanical Inference in the Study of Mandibular Form. *Am. J. Phys. Anthropol.* 112, 541-551.
- Daegling, D. J., Ravosa, M. J., Johnson, K. R. and Hylander, W. L. (1992). Influence of teeth, alveoli, and periodontal ligaments on torsional rigidity in human mandibles. *Am. J. Phys. Anthropol.* 89, 59-72.
- Daegling, D. J., Hotzman, J. L., and Rapoff, A. J. (2008). Effects of Dental Alveoli on the Biomechanical Behavior of the Mandibular Corpus. In Vinyard, C. J., Ravosa, M. J. and Wall, C. E. (eds.). *Primate Craniofacial Function and Biology*. New York: Springer. 127–148.
- Daegling DJ, McGraw WS, Ungar PS, Pampush JD, Vick AE, Bitty EA (2011) Hard-Object Feeding in Sooty Mangabeys (*Cercocebus atys*) and Interpretation of Early Hominin Feeding Ecology. *PLoS ONE* 6(8): e23095.
- Dalstra, M., Cattaneo, P. M., Laursen, M. G., Beckmann, F. and Melsen, B. (2015). Multi-level synchrotron radiation-based microtomography of the dental alveolus and its consequences for orthodontics. *Journal of Biomechanics* 48, 801-806.
- De Abreu, R. A. M., Pereira, M. D., Furtado, F., Prado, G. P. R., Mestriner Jr., W. and Ferreira, L. M. (2014). Masticatory efficiency and bite force in individuals with normal occlusion. *Archives of Oral Biology* 59, 1065-1074.
- Dorow, C., Krstin, N. and Sander, F. G. (2002). Experiments to Determine the Material Properties of the Periodontal Ligament. *J. Orofac. Orthop.* 63, 94-104.
- Dorow, C., Krstin, N. and Sander, F. G. (2003). Determination of the Mechanical Properties of the Periodontal Ligament in a Uniaxial Tensional Experiment. *J. Orofac. Orthop.* 64, 100-107.
- Duncan, R. L. and Turner, C. H. (1995). Mechanotransduction and the functional response of bone to mechanical strain. *Calcif. Tissue Int.* 57, 344-358.
- Fajardo, R.J., Ryan, T.M. and Kappelman, J. (2002). Assessing the accuracy of high-resolution X-ray computed tomography of primate trabecular bone by comparisons with histological sections. *Am. J. Phys. Anthropol.* 118, 1-10.
- Fajardo, R.J., Müller, R., Ketcham, R.A. and Colbert, M. (2007). Nonhuman anthropoid primate femoral neck trabecular architecture and its relationship to locomotor mode. *Anat. Rec.* 290, 422-436.
- Fanuscu, M. I. and Chang, T-L. (2004). Three-dimensional morphometric analysis of human cadaver bone: microstructural data from maxilla and mandible. *Clin. Oral Implants Res.* 15, 213-218.
- Farah, J. W., Craig, R. G. and Silarskie, D. L. (1973). Photoelastic and finite element stress analysis of a restored axisymmetric first molar. *Journal of Biomechanics* 6, 511-520.

- Farah, J. W., Craig, R. G. and Meroueh, K. A. F. (1989). Finite element analysis of three- and four-unit bridges. *Journal of Oral Rehabilitation* 16, 603-611.
- Fill, T. S., Carey, J. P., Toogood, R. W. and Major, P. W. (2011). Experimentally Determined Mechanical Properties of, and Models for, the Periodontal Ligament: Critical Review of Current Literature. *J. Dent. Biomech.* 10, 2011, 1-10.
- Fill, T. S., Toogood, R. W., Major, P. W. and Carey, J. P. (2012). Analytically determined mechanical properties of, and models for the periodontal ligament: Critical review of literature. *J. Biomech.* 45, 9-16.
- Frost, H. M. (1964). *The Laws of Bone Structure*. Springfield, Illinois: Thomas.
- Frost, H. M. (1987). Bone “Mass” and the “Mechanostat”: A Proposal. *Anat. Rec.* 219, 1-9.
- Frost, H. M. (1997). Why Do Marathon Runners Have Less Bone Than Weight Lifters? A Vital-Biomechanical View and Explanation. *Bone* 20, 3, 183-189.
- Gautieri, A., Vesentini, S., Redaelli, A. and Buehler, M. J. (2012). Viscoelastic properties of model segments of collagen molecules. *Matrix Biology* 31, 141-149.
- Giesen, E. B. W. and Van Eijden, T. M. G. J. (2000). The three-dimensional cancellous bone architecture of the human mandibular condyle. *J. Dent. Res.* 79, 957-963.
- Goel, V. K., Khera, S. C., Gurusami, S. and Chen, R. C. S. (1992). Effect of cavity depth on stresses in a restored tooth. *Journal of Prosthetic Dentistry* 67, 174-183.
- Gröning, F. (2013). Zusammenhänge zwischen der Morphologie des Kronenfortsatzes und der Funktion des Schläfenmuskels: ein Beispiel für den Einsatz der Finite-Elemente-Analyse in der Paläoanthropologie. In: Pastoors, A., Aufferman, B. (eds.). *Pleistocene foragers: their culture and environment. Festschrift in honour of Gerd-Christian Weniger for his sixtieth birthday*. Mettmann: Wissenschaftliche Schriften des Neanderthal Museums 6, 213-224.
- Gröning, F. and Fagan, M. J. (2012). Comment on “The effects of modelling simplifications on craniofacial finite element models: The alveoli (tooth sockets) and periodontal ligaments” (volume 44, issue 10, pages 1831–1838). *J. Biomech.* 45, 1749-1750.
- Gröning, F., Liu, J., Fagan, M. J. and O’Higgins, P. (2009). Validating a voxel-based finite element model of a human mandible using digital speckle pattern interferometry. *J. Biomech.* 42, 1224-1229.
- Gröning, F., Fagan, M. J. and O’Higgins, P. (2011a). The effects of the periodontal ligament on mandibular stiffness: a study combining finite element analysis and geometric morphometrics. *Journal of Biomechanics* 44, 1304-1312.
- Gröning, F., Liu, J., Fagan, M. J. and O’Higgins, P. (2011b). Why Do Humans Have Chins? Testing the Mechanical Significance of Modern Human Symphyseal Morphology With Finite Element Analysis. *Am. J. Phys. Anthropol.* 144, 593-606.

- Gröning, F., Bright, J. A., Fagan, M. J. and O'Higgins, P. (2012a). Improving the validation of finite element models with quantitative full-field strain comparisons. *J. Biomech.* 45, 1498-1506.
- Gröning, F., Fagan, M. and O'Higgins, P. (2012b). Modeling the Human Mandible Under Masticatory Loads: Which Input Variables are Important? *Anat. Rec.* 295, 853-863.
- Grosse, I. R., Wood, S. A., Strait, D. S., Dumont, E. R. and Ross, C. F. (2012). Response to the Comment by Gröning and Fagan on "The effects of modelling simplifications on craniofacial finite element models: The alveoli (tooth sockets) and periodontal ligaments" (volume 44, issue 10, pages 1831–1838). *J. Biomech.* 45, 1750-1751.
- Hall, B. K. (2005). *Bones and Cartilage: Developmental and Evolutionary Skeletal Biology*. San Diego: Elsevier Academic Press.
- Henneman, S., Von Den Hoff, J. W. and Maltha, J. C. (2008). Mechanobiology of tooth movement. *European Journal of Orthodontics* 30, 299-306.
- Herring, S. W. (1993). Functional Morphology of Mammalian Mastication. *Amer. Zool.* 33, 289-299.
- Hert, J., Liskova, M. and Landrgot, B. (1969). Influence of the long-term, continuous bending on the bone. *Folia Morphol. (Praha)* 17, 389-399.
- Ho, S. P., Marshall, S. J., Ryder, M. I. and Marshall, G. W. (2007). The tooth attachment mechanism defined by structure, chemical composition and mechanical properties of collagen fibers in the periodontium. *Biomaterials* 28, 5238-5245.
- Hohmann, A., Kober, C., Young, P., Dorow, C., Geiger, M., Boryor, A., Sander, F. M., Sander, C. and Sander, F. G. (2011). Influence of different modeling strategies for the periodontal ligament on finite element simulation results. *Am. J. Orthod. Dentofacial. Orthop.* 139, 775-783.
- Hollins, C. (2008). *Levison's Textbook for Dental Nurses (10th edition)*. Oxford: Wiley-Blackwell.
- Huiskes, R. (2000). If bone is the answer, then what is the question? *J. Anat.* 197, 145-156.
- Hung, C. T., Allen, F. D., Pollack, S. R. and Brighton, C. T. (1996). What is the role of the convective current density in the real-time calcium response of cultured bone cells to fluid flow. *J. Biomech.* 29, 1403-1409.
- Hylander, W. L. (1984). Stress and strain in the mandibular symphysis of primates: a test of competing hypotheses. *Am. J. Phys. Anthropol.* 64, 1-46.
- Hylander, W. L. (1985). Mandibular function and biomechanical stress and scaling. *Am Zool.* 25, 315-330.

- Ichim, I., Swain, M. V. and Kieser, J. A. (2006). Mandibular stiffness in humans: numerical predictions. *J. Biomech.* 39, 1903-1913.
- Ichim, I., Kieser, J. A. and Swain, M. V. (2007). Functional significance of strain distribution in the human mandible under masticatory load: Numerical predictions. *Archives of Oral Biology* 52, 465-473.
- Jones, M. L., Hickman, J., Middleton, J., Knox, J. and Volp, C. (2001). A Validated Finite Element Method Study of Orthodontic Tooth Movement in the Human Subject. *Journal of Orthodontics* 28, 29-38.
- Kato, H. (1982). The function of tooth supporting structures. Part II. The dynamics of molars in function and at rest. *J. Jpn. Prosthodont. Soc.* 26, 133-147.
- Katona, T. R. and Qian, H. (2001). A mechanism of noncontinuous supraosseous tooth eruption. *Am. J. Orthod. Dentofacial Orthop.* 120, 263-271.
- Ko, C. C., Chu, C. S., Chung, K. H. and Lee, M. C. (1992). Effects of posts on dentin stress distribution in pulpless teeth. *Journal of Prosthetic Dentistry* 68, 421-427.
- Kohnke, P. (ed.). (2009). *Theory Reference for the Mechanical APDL and Mechanical Applications*. Canonsburg, PA, USA: ANSYS, Inc.
- Komatsu, K., Shibata, T. and Shimada, A. (2007). Analysis of contribution of collagen fibre component in viscoelastic behaviour of periodontal ligament using enzyme probe. *Journal of Biomechanics* 40, 2700-2706.
- Korioth, T. W. and Hannam, A. G. (1994). Deformation of the Human Mandible During Simulated Tooth Clenching. *J. Dent. Res.* 73, 1, 56-66.
- Korioth, T. W., Romilly, D.P. and Hannam, A. G. (1992). Three-dimensional finite-element stress analysis of the dentate human mandible. *Am. J. Phys. Anthropol.* 88, 69-96.
- Krishnan, V. and Davidovitch, Z. (2006). Cellular, molecular, and tissue-level reactions to orthodontic force. *Am. J. Orthod. Dentofacial Orthop.* 129, 469e.1-469e.32)
- Kuroiwa, M., Chihara, K. and Higashi, S. (1994). Electron microscopic studies on Sharpey's fibers in the alveolar bone of rat molars. *Journal of Anatomy* 69, 6, 776-782.
- Langenbach, G. E. J., Zhang, F., Herring, S. W. and Hannam, A. G. (2002). Modelling the masticatory biomechanics of a pig. *Journal of Anatomy* 201, 5, 383-393.
- Lanyon, L. E. (1992). The success and failure of the adaptive response to functional loading-bearing in averting bone fracture. *Bone* 13, S17-S21.
- Lanyon, L. E. and Rubin, C. T. (1984) Static vs dynamic loads as an influence on bone remodelling. *J. Biomech.* 17, 897-905.
- Lanyon, L. E., Goodship, A. E., Pye, C. J. and Macfie, J. H. (1982) Mechanically adaptive bone remodelling. *J. Biomech.* 15, 141-154.

- Lee, T. C. and Taylor, D. (1999). Bone Remodelling: Should We Cry Wolff? *Ir. J. Med. Sc.* 168, 2, 102-105.
- Limbert, G., Middleton, J., Laizans, J., Dobelis, M. and Knets, I. (2003). A Transversely Isotropic Hyperelastic Constitutive Model of the PDL. Analytical and Computational Aspects. *Computer Methods in Biomechanics and Biomedical Engineering*, 6, 5-6, 337-345.
- Liskova, M. and Hert, J. (1971). Reaction of bone to mechanical stimuli. *Folia Morphol. (Praha)* 19, 301-317.
- Mac Donald, B. J. (2007). *Practical Stress Analysis with Finite Elements*. Dublin: Glasnevin Publishing.
- Marinescu, R., Daegling, D. J. and Rapoff, A. J. (2005). Finite-Element Modeling of the Anthropoid Mandible: The Effects of Altered Boundary Conditions. *Anat. Rec.* 283A, 300-309.
- McCulloch, C. A. G., Lekic, P. and McKee, M. D. (2000). Role of physical forces in regulating the form and function of the periodontal ligament. *Periodontology* 24, 56-72.
- Melsen, B. (1999). Biological reaction of alveolar bone to orthodontic tooth movement. *Angle Orthod.* 69, 151-158.
- Melsen, B. (2001). Tissue reaction to orthodontic tooth movement – a new paradigm. *European Journal of Orthodontics* 23, 671-681.
- Meyer, B. N., Chen, J. and Katona, T. R. (2010). Does the center of resistance depend on the direction of tooth movement? *Am. J. Orthod. Dentofacial Orthop.* 137, 354-361.
- Middleton, J., Jones, M. and Wilson, A. (1996a). The role of the periodontal ligament in bone modeling: The initial development of a time-dependent finite element model. *Am. J. Orthod. Dentofac. Orthop.* 109, 155-162.
- Middleton, J., Jones, M. L., Hickman, J., Danios, C. and Volp, C. (1996b). Three dimensional modelling of teeth when subjected to orthodontic loading: numerical and experimental validation. *10th Conference of the European Society of Biomechanics* Abstract 273.
- Misch, C. E., Qu, Z. and Bidez, M. W. (1999). Mechanical Properties of Trabecular Bone in the Human Mandible: Implications for Dental Implant Treatment Planning and Surgical Placement. *J. Oral Maxillofac. Surg.* 57, 700-706.
- Mühlemann, H. R. (1967). Tooth mobility: a review of clinical aspects and research findings. *J. Periodontol.* 38, 686-713.

- Naveh, G. R. S., Shahar, R., Brumfeld, V. and Weiner, S. (2012a). Tooth movements are guided by specific contact areas between the tooth root and the jaw bone: A dynamic 3D microCT study of the rat molar. *Journal of Structural Biology* 177, 477-483.
- Naveh, G. R. S., Chattah, N. L. T., Zaslansky, P., Shahar, R. and Weiner, S. (2012b). Tooth-PDL-bone complex: Response to compressive loads encountered during mastication – A review. *Archives of Oral Biology* 57, 1575-1584.
- O'Connor, C. F., Franciscus, R. G. and Holton, N. E. (2005). Bite Force Production Capability and Efficiency in Neandertals and Modern Humans. *Am. J. Phys. Anthropol.* 127, 129-151.
- Parfitt, G. J. (1960). Measurement of the Physiological Mobility of Individual Teeth in an Axial Direction. *J. Dent. Res.* 39, 608-618.
- Picton, D. C. A. (1963). Vertical movement of cheek teeth during biting. *Arch. Oral Biol.* 8, 109-118.
- Pietrzak, G., Curnier, A., Botsis, J., Scherrer, S., Wiskott, A. and Belser, U. (2002). A Nonlinear Elastic Model of the Periodontal Ligament and its Numerical Calibration for the Study of Tooth Mobility. *Computer Methods in Biomechanics and Biomedical Engineering* 5, 2, 91-100.
- Poppe, M., Bourauel, C. and Jäger, A. (2002). Determination of the Elasticity Parameters of the Human Periodontal Ligament and the Location of the Center of Resistance of Single-rooted Teeth. *J. Orofac. Orthop.* 63, 358-370.
- Provatidis, C. G. (2000). A comparative FEM-study of tooth mobility using isotropic and anisotropic models of the periodontal ligament. *Medical Engineering and Physics* 22, 359-370.
- Qian, H., Chen, J. and Katona, T. R. (2001). The influence of PDL principal fibers in a 3-dimensional analysis of orthodontic tooth movement. *Am. J. Orthod. Dentofacial Orthop.* 120, 272-279.
- Qian, Y., Liu, Z. and Fan, Y. (2010). Numerical simulation of canine bodily movement. *Int. J. Numer. Meth. Biomed. Engng.* 26, 157-163.
- Qin, Y-X., McLeod, K. J., Guilak, F. Rubin, C. T. and Chiang, F-P. (1996). Correlation of bony ingrowth to the distribution of stress and strain parameters surrounding a porous-coated implant. *J. Orthop. Res.* 14, 862-870.
- Ralph, W. J. and Thomas, C. D. L. (1998). Tooth support in the human mandible. *J. Oral Rehabilitation* 15, 5, 499-503.
- Ramos, A., Ballu, A., Mesnard, M., Talaia, P. and Simões, J. A. (2011). Numerical and experimental models of the mandible. *Experimental Mechanics* 51, 1053-1059.
- Rees, J. S. (2001). An investigation into the importance of the periodontal ligament and alveolar bone as supporting structures in finite element studies. *Journal of Oral Rehabilitation* 28, 425-432.

- Rees, J. S. and Jacobsen, P. H. (1997). Elastic modulus of the periodontal ligament. *Biomaterials* 18, 995-999.
- Reich, K. M., Gay, C. V. and Frangos, J. A. (1990). Fluid shear stress as a mediator of osteoblast cyclic adenosine monophosphate production. *J. Cell Physiol.* 143, 100-104.
- Reina, J. M., García-Aznar, J. M., Domínguez, J. and Doblaré, M. (2007). Numerical estimation of bone density and elastic constants distribution in a human mandible. *Journal of Biomechanics* 40, 828-836.
- Robling, A. G., Hinant, F. M., Burr, D. B. And Turner, C. H. (2002). Improved bone structure and strength after long-term mechanical loading is greatest if loading is separated into short bouts. *J. Bone Miner. Res.* 17, 1545-1554.
- Rubin, C. T. and Lanyon, L. E. (1984). Regulation of bone formation by applied dynamic loads. *J. Bone Joint Surg. Am.* 66, 397-402.
- Ruff, C., Holt, B. and Trinkaus, E. (2006). Who's Afraid of the Big Bad Wolff?: "Wolff's Law" and Bone Functional Adaptation. *Am. J. Phys Anthropol.* 129, 484-498.
- Ryan, T. M. and Ketcham, R. A. (2002a). Femoral head trabecular bone structure in two omomyid primates. *J. Hum. Evol.* 42, 241-263.
- Ryan, T. M. and Ketcham, R. A. (2002b). The three-dimensional structure of trabecular bone in the femoral head of strepsirrhine primates. *J. Hum. Evol.* 43, 1-26.
- Scherf, H. and Tilgner, R. (2009). A new high-resolution computed tomography (CT) segmentation method for trabecular bone architectural analysis. *Am. J. Phys. Anthropol.* 140, 39-51.
- Schroeder, H. E. (2000). *Orale Strukturbiologie*. Stuttgart: Thieme.
- Schwartz, A. M. (1932). Tissue changes incidental to orthodontic tooth movement. *Int. J. Orthodontia* 18, 331-352.
- Schwartz-Dabney, C. L. and Dechow, P. C. (2003). Variations in Cortical Material Properties Throughout the Human Dentate Mandible. *Am. J. Phys. Anthropol.* 120, 252-277.
- Sloan, P. (1979). Collagen fibre architecture in the periodontal ligament. *Journal of the Royal Society of Medicine* 72, 188-191.
- Spoor, C.F., Zonneveld, F.W. and Macho, G.A. (1993). Linear measurements of cortical bone and dental enamel by computed tomography: Applications and problems. *Am. J. Phys. Anthropol.* 91, 469-484.
- Takahashi, N., Kitagami, T. and Komori, T. (1980). Behaviour of teeth under various loading conditions with finite element method. *Journal of Oral Rehabilitation* 7, 453-461.

- Tanne, K. and Sakuda, M. (1983). Initial stress induced in the periodontal tissue at the time of the application of various types of orthodontic force: three dimensional analysis by means of the F.E.M. *J. Osaka Univ. Dent. School* 23, 143-171.
- Tanne, K., Lu, Y. C., Tanaka, E. and Sakuda, M. (1993). Biomechanical changes of the mandible from orthopaedic chin cup force studied in a three-dimensional finite element model. *Eur. J. Orthod.* 15, 527-533.
- Thresher, R. W. and Saito, G. E. (1973). The stress analysis of human teeth. *Journal of Biomechanics* 6, 443-449.
- Toms, S. R. and Eberhardt, A. W. (2003). A nonlinear finite element analysis of the periodontal ligament under orthodontic tooth loading. *Am. J. Orthod. Dentofacial Orthop.* 123, 657-665.
- Toms, S. R., Lemons, J. E., Bartolucci, A. A. and Eberhardt, A. W. (2002a). Nonlinear stress-strain behaviour of periodontal ligament under orthodontic loading. *Am. J. Orthod. Dentofacial Orthop.* 122, 174-179.
- Toms, S. R., Dakin, G. J., Lemons, J. E. and Eberhardt, A. W. (2002b). Quasi-linear viscoelastic behavior of the human periodontal ligament. *Journal of Biomechanics* 35, 1411-1415.
- Tsubota, K., Suzuki, Y., Yamada, T., Hojo, M., Makinouchi, A. and Adachi, T. (2009). Computer simulation of trabecular remodeling in human proximal femur using large-scale voxel FE models: Approach to understanding Wolff's law. *Journal of Biomechanics* 42, 1088-1094.
- Turner, C. H. (1998). Three rules for bone adaptation to mechanical stimuli. *Bone* 23, 399-497.
- Turner, C. H. (1999). Toward a Mathematical Description of Bone Biology: The Principle of Cellular Accommodation. *Calcif. Tissue Int.* 65, 466-471.
- Turner, C. H. and Pavalko, F. M. (1998). Mechanotransduction and functional response of the skeleton to physical stress: The mechanisms and mechanics of bone adaptation. *J. Orthop. Sci.* 3, 346-355.
- Turner, C. H., Forwood, M. R. and Otter, M. W. (1994). Mechanotransduction in bone: do bone cells act as sensors of fluid flow. *FASEB J.* 8, 875-878.
- Van Driel, W. D., Van Leeuwen, E. J., Von Den Hoff, J. W., Maltha, J. C. and Kuijpers-Jagtman, A. M. (2000). Time-dependent mechanical behaviour of the periodontal ligament. *Proc. Instn. Mech. Engrs. Part H* 214, 497-504.
- Van Eijden, T. M. G. J. (2000). Biomechanics of the Mandible. *Crit. Rev. Oral. Biol. Med.* 11, 1, 123-136.
- Warden, S. J., Hurst, J. A., Sanders, M. S., Turner, C. H., Burr, D. B. and Li., J. (2005). Bone adaptation to a mechanical loading program significantly increases skeletal fatigue resistance. *J. Bone Miner. Res.* 20, 809-816.

- Watson, P. J., Gröning, F., Curtis, N., Fitton, L., Herrel, A., McCormack, S. W. and Fagan, M. J. (2014). Masticatory biomechanics in the rabbit: a multi-body dynamics analysis. *Journal of the Royal Society Interface* 11, 20140564.
- Wills, D. J., Picton, D. C. A. and Davies, W. I. R. (1976). A study of the fluid systems of the periodontium in macaque monkeys. *Archs. Oral Biol.* 21, 3, 175-185.
- Wilson, A. (1991). Linear and non-linear analysis of orthodontic tooth movement. PhD Thesis, University of Wales.
- Witzel, U., Jackowski, J. and Jöhren, P. (1998). Analyse der Spannungsverteilung im spongiösen Sinus-Augmentat nach sekundärer Implantation mit Hilfe der Methode der finiten Elemente (FEM). *Target* 1.98, 10-11.
- Wolff, J. (1892). *Das Gesetz der Transformation der Knochen*. Berlin: Hirschwald.
- Wolff, J. (1986). *The Law of Bone Remodelling*. Berlin: Springer.
- Wood, S. A., Strait, D. S., Dumont, E. R., Ross, C. F. and Grosse, I. R. (2011). The effects of modeling simplifications on craniofacial finite element models: The alveoli (tooth sockets) and periodontal ligaments. *Journal of Biomechanics* 44, 1831-1838.
- Wright, K. W. J. (1975). *On the mechanical behaviour of human tooth structures*. PhD Thesis, Brunel University.
- Yaşar, F. and Akgünlü, F. (2005). Fractal dimension and lacunarity analysis of dental radiographs. *Dentomaxillofacial Radiology* 34, 261-267.
- Yettram, A. L., Wright, K. W. J. and Pickard, H. M. (1976). Finite element stress analysis of the crowns of normal and restored teeth. *Journal of Dental Research* 55, 1004-1011.
- Zhao, L., Patel, P. K., Widera, G. E. O., Han, H. and Harris, G. F. (2001). Medical imaging genesis for finite element-based mandibular surgical planning in the pediatric subject. In: *Engineering in Medicine and Biology Society, 2001*. Proceedings of the 23rd Annual International Conference of the IEEE, 2509-2512.
- Zhurov, A. I., Limbert, G., Aeschlimann, D. P. and Middleton, J. (2007). A constitutive model for the periodontal ligament as a compressible transversely isotropic visco-hyperelastic tissue. *Computer Methods in Biomechanics and Biomedical Engineering*, 10, 3, 223-235.